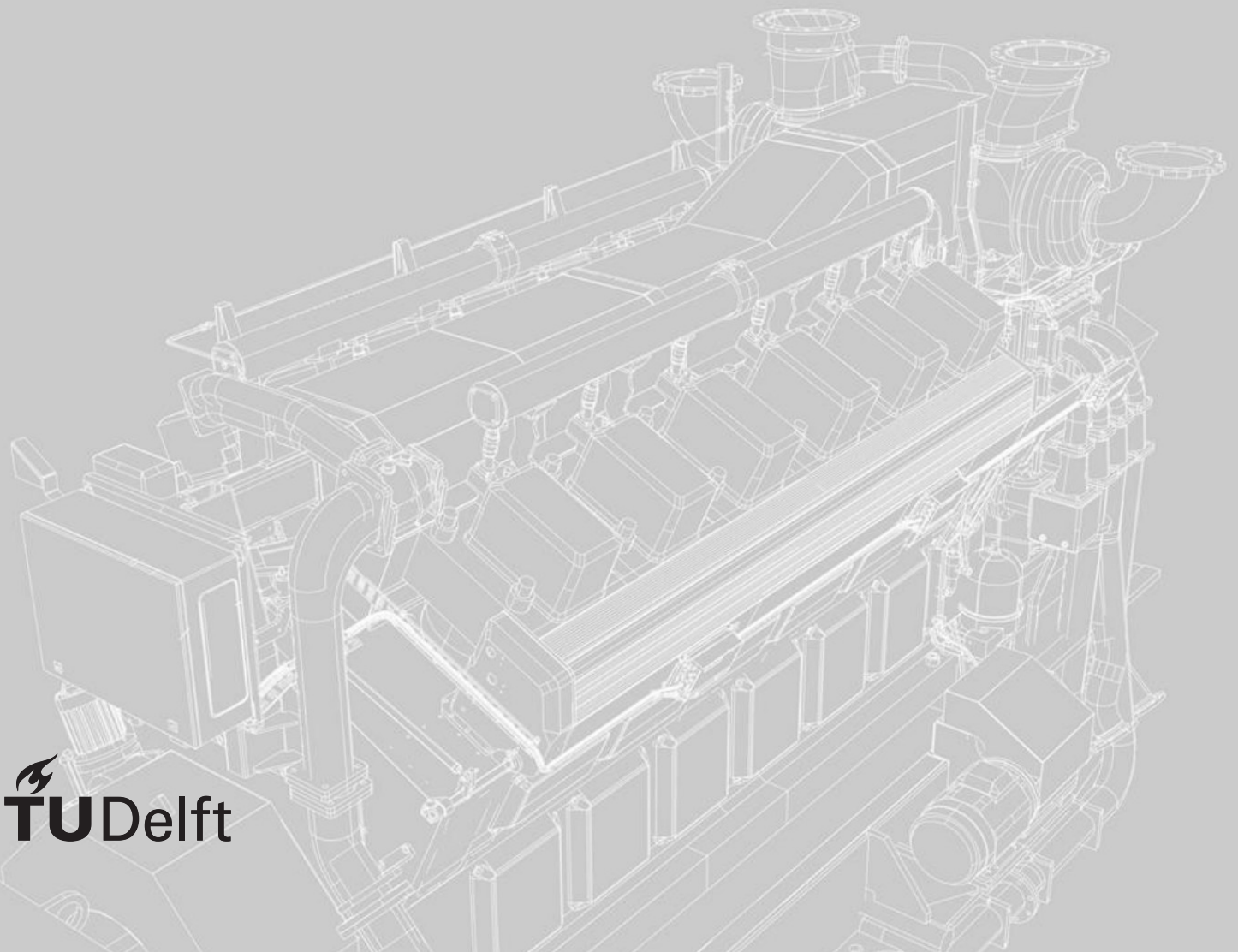


# HYBRID ELECTRIC TURBOCHARGING

Improving the loading capability and  
efficiency of a dual fuel engine

J.A. Westhoeve

Delft University of Technology  
SDPO.18.033.m





# Hybrid Electric Turbocharging

Improving the loading capability and efficiency  
of a dual fuel engine

by

J.A. Westhoeve

to obtain the degree of Master of Science  
at the Delft University of Technology,  
to be defended publicly on Wednesday August 22, 2018 at 9:30 AM.

Student number:	4371968	
TU Delft number:	SDPO.18.033.m	
IHC MTI number:	AO156	
Project duration:	May 24, 2017 – August 22, 2018	
Thesis committee:	Ir. K. Visser, Rear-Admiral (ME) ret., Ir. B.T.W. Mestemaker, Dr.ir. M. Godjevac, Prof.dr.ir. S.A. Klein,	TU Delft, Chairman and Daily Supervisor IHC MTI, Daily Supervisor TU Delft, Internal TU Delft, External

An electronic version of this thesis is available at <http://repository.tudelft.nl/>.





# Abstract

Emission regulations applied to marine industry for amongst others the propulsion system of a vessel are becoming more strict due to governmental agreements to lower the greenhouse gas emissions. Engine manufacturers are enhancing their engine designs to reduce the engine fuel consumption, which is commonly done by implementing a turbocharger to downsize the engine. One large drawback which comes with a turbocharged engine is the low torque development for the low to mid engine speed range due to limitations set to prevent unstable turbocharger phenomena. Moreover, the engine is not able to follow the power request almost instantaneously due to a time delay between the engine and turbocharger response. Formula One engineers close this gap by introducing an integrated electric machine into the turbocharger structure (hybrid electric turbocharger) to, first, take power out from the turbocharger to increase the system efficiency, and second by assisting the turbocharger to improve the engine power delivery response.

However the understanding of the effects of a hybrid electric turbocharger on both the system efficiency as well as the engine loading capability is lacking. One turbocharger limit, the compressor surge, is not concerned in most literature what rises the need for further research up to which extent the engine can be assisted with the hybrid electric turbocharger. In this work, the effect of taking power from the turbocharger to increase the system efficiency, called turbocompounding, is investigated. Turbocharger assistance is investigated for both steady state as well as dynamic operation. The effect of assisting the turbocharger for steady state operation is investigated to increase the engine's operating envelope. Dynamic operation comprises the investigating up to which extent the assisting mode improves the dual fuel engine's loading capability for four types of engine loading. These types of engine loading are: one instant load step, three consecutive load steps from 0 - 100% load, a load ramp and, last, a sinusoidal engine loading.

This has been done with a simulation based study wherein a mean value dual fuel engine model is composed based on merging two available mean value engine models, after which it is verified and validated. Thereafter power take in/out together with an air excess ratio control strategy is included by means of adding/taking torque to/from the turbocharger shaft and limiting it with eight boundary controllers to avoid impractical situations.

With turbocompounding the system efficiency can be increased at the expense of a deteriorated gas exchange and increased thermal loading of the engine. The maximum quantity of recovered energy to be obtained, requires a hybrid electric turbocharger which replaces a waste gated turbocharger instead of a non waste gated single stage turbocharger. Taking power from the turbocharger lowers the power available for the compressor which leads to reduced inlet receiver pressure and corresponding lowering of the air excess ratio and deterioration of the scavenging process.

Assisting the turbocharger for steady state operation leads to a smaller operating envelope due to the limitation of compressor surge. Combining turbocharger assistance with gas exchange bypass valves, to avoid compressor surge, results in a rise of the low speed torque output up to an almost constant engine torque output. The system efficiency can be improved for the low speed region when the turbocharger is assisted in combination with the gas exchange valves.

The load step capability, found by limiting the minimum air excess ratio during the load step event, cannot be increased with turbocharger assistance which starts to speed up the turbocharger immediately after the load step is applied to the engine. However, the recovery time needed before a second load step can be taken, is reduced with turbocharger assistance compared to the baseline engine. When the turbocharger assistance starts to speed up the turbocharger a couple of seconds before the load is applied, the load step capability can be improved. A load ramp can be taken in a shorter period of time with turbocharger assistance enabled. For cyclic loading, the hybrid electric turbocharger operates in turbocompounding mode for the lower load frequencies, and assistance is used for the higher load frequencies. With turbocharger assistance the air excess ratio does follow the sinusoidal engine load while the air excess ratio of the non-assisted engine always lags due to the turbocharger lag.

Further research should be done with regard to a hybrid electric turbocharger for the natural gas combustion of the dual fuel engine. Using the engine speed drop should be implemented as limitation for the loading capability determination instead of the minimum allowable air excess ratio applied in this thesis.



# Preface

Mechanical systems and especially internal combustion engines applied in agricultural machines have always been my field of interest from childhood on. In 2013, I was thinking ahead what I wanted to do after finishing the bachelor Mechanical Engineering at Rotterdam University of Applied Sciences (HBO), what was planned to be in 2014. Searching for an interesting study that provided internal combustion engine related topics, the Diesel A and B courses offered at TU Delft caught my attention. Next step on the road of life was to go ahead with the master Mechanical Engineering, specialisation Mechanical Systems and Integration which is the equivalent of marine engineering.

November 2015, after a tough bridging program, I attended my first lectures of this master program which were given by Ir. P. de Vos about engine room systems and Ir. K. Visser about diesel engines. From that moment on, an incredible experience started in which I learned a lot about marine engineering and especially prime movers. The obligatory courses of this master program were in line with my field of interest, and the large number of elective courses brought me a variety of interesting topics. Two amazing Vulcanus study tours to marine engineering related companies in Finland and Germany in which I especially enjoyed the visits to engine manufactures.

With this thesis, I complete a topic related to the core of this experience at the TU Delft: integrating an electric machine in the turbocharger of a dual fuel marine engine to increase the system efficiency and improve the loading capability.

My special thank is for IHC MTI B.V., where I spent the last one and a half year working on both my research assignment as well as my graduation project. I am very grateful to my daily supervisors Ir. Klaas Visser (TU Delft) and Ir. Benny Mestemaker (IHC MTI B.V.) who helped me with technical support and progress meetings. I also thank the committee members Dr.ir. M. Godjevac and Prof.dr.ir. S.A. Klein for having found time to be part of the thesis committee. Next to thank is the whole marine engineering team of the TU Delft and in particular to Harsh, Mike and Ioana for their support with the basics of the engine model. I would like to thank my fellow students at IHC MTI B.V. for, firstly their support and assistance how to continue when I came to a standstill. And secondly for the social moments such as the coffee breaks and trips, which were useful to get some distraction. Finally, I cannot thank my family enough for being a constant source of motivation and moral support.

*Jan Westhoeve  
August 2018*



# Contents

<b>1</b>	<b>Introduction</b>	<b>3</b>
1.1	Background . . . . .	3
1.2	Motivation for research . . . . .	3
1.3	Research objective . . . . .	4
1.4	Project boundaries . . . . .	4
1.5	Thesis outline . . . . .	4
<b>2</b>	<b>Dual Fuel Engine</b>	<b>7</b>
2.1	Introduction . . . . .	7
2.2	Working principle of a four-stroke dual fuel engine . . . . .	7
2.2.1	Gas exchange of a dual fuel engine . . . . .	9
2.2.2	Advanced turbocharger configuration . . . . .	11
2.2.3	Energy balance of a large dual-fuel engine . . . . .	12
2.2.4	Operating envelope of a dual-fuel engine . . . . .	13
2.3	Loading capability of a dual fuel engine . . . . .	15
2.3.1	Effect of air-fuel composition on loading capability . . . . .	16
2.3.2	Load acceptance of a dual-fuel engine . . . . .	18
2.3.3	Gas exchange during transient operation . . . . .	20
2.4	Conclusions. . . . .	22
<b>3</b>	<b>Hybrid Electric Turbocharging</b>	<b>23</b>
3.1	Introduction . . . . .	23
3.2	History of turbocharging . . . . .	23
3.3	Turbocompounding to improve overall plant efficiency. . . . .	24
3.3.1	Efficiency increase realised with electrical turbocompounding . . . . .	25
3.3.2	Assisting turbocharger to improve overall plant efficiency . . . . .	26
3.3.3	Effect of turbocompounding on engine conditions . . . . .	26
3.4	Hybrid electric turbocharger to improve dynamic loading capability . . . . .	27
3.4.1	Hybrid electric turbocharging to improve transient load capability . . . . .	27
3.4.2	Hybrid electric turbocharging to improve loading capability. . . . .	28
3.5	Operating envelope with hybrid electric turbocharging. . . . .	29
3.6	Conclusions. . . . .	31
<b>4</b>	<b>Model Approach</b>	<b>33</b>
4.1	Introduction . . . . .	33
4.2	Model overview . . . . .	33
4.3	Modelling terminology . . . . .	34
4.4	Engine model classification. . . . .	35
4.4.1	Difference between analytical and empirical engine models. . . . .	35
4.4.2	Available analytical engine models. . . . .	35
4.4.3	Selection of appropriate mean-value engine model . . . . .	36
4.5	Model build-up . . . . .	37
4.5.1	Dual fuel engine . . . . .	37
4.5.2	Basic elements of B model . . . . .	37
4.5.3	Characterization of cylinder process . . . . .	38
4.5.4	Advanced Miller timing . . . . .	40
4.5.5	Turbocharger fundamentals . . . . .	40

4.6	Dual-fuel model verification . . . . .	41
4.7	Matching of the engine model . . . . .	42
4.7.1	Matching parameter groups . . . . .	42
4.7.2	Matching assumptions. . . . .	42
4.7.3	Matching approach . . . . .	42
4.7.4	In-cylinder process matching . . . . .	43
4.7.5	Turbocharger matching . . . . .	44
4.7.6	Inlet/outlet piping matching. . . . .	44
4.7.7	Matching of other parts . . . . .	45
4.7.8	Matching results dual fuel engine model. . . . .	45
4.8	Model validation . . . . .	47
4.9	Control strategy electric machine . . . . .	48
4.9.1	Main controller: air excess ratio . . . . .	48
4.9.2	Boundary controllers to operate within boundaries . . . . .	48
4.9.3	Implementation of an anti-windup . . . . .	49
4.9.4	Overview control strategy . . . . .	49
4.9.5	Air excess ratio estimation . . . . .	51
4.9.6	Compressor mass flow estimation . . . . .	51
4.10	Conclusions. . . . .	52
<b>5</b>	<b>Static Analysis</b>	<b>53</b>
5.1	Introduction . . . . .	53
5.2	Operating envelope baseline Wärtsilä 6L34DF . . . . .	54
5.3	Effect of turbocompounding on system. . . . .	55
5.3.1	Turbocompounding: System power output . . . . .	56
5.3.2	Turbocompounding: Gas exchange . . . . .	56
5.3.3	Turbocompounding: System efficiency . . . . .	58
5.3.4	Turbocompounding: Fuel consumption . . . . .	59
5.3.5	Turbocompounding: Thermal loading engine . . . . .	59
5.3.6	Effect of set point on system power output and efficiency . . . . .	61
5.4	Turbocompounding for three turbocharger matching conditions. . . . .	62
5.5	Sensitivity analysis . . . . .	64
5.5.1	Sensitivity to controller parameter sweep . . . . .	65
5.5.2	Sensitivity to cylinder parameters . . . . .	65
5.5.3	Sensitivity of compressor and turbine parameters . . . . .	67
5.6	Approach of Operating Curve Shaping . . . . .	69
5.7	Compressor surge limit reduces operating envelope . . . . .	70
5.8	Operating curve shaping with EAT and Blow-off Valve . . . . .	71
5.9	Operating curve shaping with EAT and Bypass Valve . . . . .	74
5.10	Conclusions. . . . .	76
<b>6</b>	<b>Dynamic Analysis</b>	<b>77</b>
6.1	Introduction . . . . .	77
6.2	Loading capability: Three consecutive load steps . . . . .	78
6.2.1	Engine load . . . . .	78
6.2.2	Air excess ratio . . . . .	79
6.2.3	Turbocharger speed . . . . .	79
6.2.4	Fuel mass flow . . . . .	80
6.2.5	Electric machine torque . . . . .	80
6.2.6	Inlet receiver pressure . . . . .	81
6.2.7	Quantification of consecutive load steps. . . . .	81
6.3	Loading capability: Instant load step . . . . .	82
6.3.1	Load step capability as function of acceptable air excess ratio . . . . .	82
6.3.2	Load step capability with variable inlet valve closure. . . . .	82
6.3.3	Load step capability with and without ETC . . . . .	83
6.3.4	Load step capability with preboost. . . . .	83
6.4	Loading capability: load ramp . . . . .	84
6.4.1	Load ramp without electrical assistance . . . . .	84
6.4.2	Load ramp with electrical assistance . . . . .	85

---

6.5	Loading capability: sinusoidal load . . . . .	86
6.5.1	Power electric machine . . . . .	87
6.5.2	Turbocharger speed . . . . .	88
6.5.3	Air excess ratio . . . . .	89
6.6	Conclusions. . . . .	90
<b>7</b>	<b>Proposal for Future Research</b>	<b>91</b>
<b>8</b>	<b>Conclusions and Recommendations</b>	<b>93</b>
8.1	Conclusions. . . . .	93
8.2	Recommendations . . . . .	94
	<b>Bibliography</b>	<b>97</b>
<b>A</b>	<b>Diesel B parameters</b>	<b>103</b>
<b>B</b>	<b>Compressor map visualisation</b>	<b>105</b>
<b>C</b>	<b>Derivation of compressor mass flow and air excess ratio estimation</b>	<b>109</b>
<b>D</b>	<b>Figures STA12V280 &amp; STA12V280WG</b>	<b>113</b>



# Nomenclature

## Abbreviations

aBDC	After Bottom Dead Center
AFR	Air to fuel ratio
bBDC	Before Bottom Dead Center
BDC	Bottom Dead Center
BEP	Best Efficiency Point
BMEP	Break Mean Effective Pressure
BPV	Bypass Valve
CH <sub>4</sub>	Methane
CI	Compression Ignition
CO	Carbon Monoxide
CO <sub>2</sub>	Carbon Dioxide
CSD	Cutter Suction Dredger
CVT	Continuous Variable Transmission
DI	Direct Injection
E	Estimated engine data
EAT	Electric Assisted Turbocharging
EVC	Outlet valve closure
EVO	Outlet valve opens
F	Factory Acceptance Test engine data
FGT	Fixed Geometry Turbocharger
HC	Hydrocarbon
HFO	Heavy Fuel Oil
ICE	Internal Combustion Engine
IHC	Industriële Handels Combinatie
ISG	Integrated Starter Generator
IVC	Inlet valve closure
IVO	Inlet valve opens
LNG	Liquefied Natural Gas
MARPOL	Marine Pollution
MDF	Marine Diesel Fuel
NG	Natural Gas
PG	Product Guide
PM	Particular Matter
pt	Physics theory
SA	Sensitivity Analysis
SCR	Selective Catalytic Reduction
SFC	Specific Fuel Consumption
SI	Spark Ignition
SL	Smoke Limit
SO <sub>x</sub>	Sulphur Oxide
STP	Standard Temperature and Pressure (273.15 K and 1E5 Pa)
T	Test bench engine data
TDC	Top Dead Center
TSHD	Trailing Suction Hopper Dredger
VGT	Variable Geometry Turbocharger
VIC	Variable Inlet valve Closing
VOI	Variable of Interest
WHRS	Waste Heat Recovery System

**Subscripts**

<i>amb</i>	Ambient conditions
<i>b</i>	brake
<i>ca</i>	Charge air
<i>com</i>	Compressor
<i>cyl</i>	over cylinder
<i>des</i>	Desired value
<i>EC</i>	Outlet closure
<i>EM</i>	Electric Machine
<i>eng</i>	engine
<i>EO</i>	Outlet opens
<i>exh, valve</i>	Exhaust valve
<i>FI</i>	Fuel injection
<i>fresh</i>	Fresh air
<i>gen</i>	Generator
<i>IC</i>	Inlet closure
<i>IC, eff</i>	Effective Inlet closure
<i>IO</i>	Inlet valve opens
<i>ir</i>	Inlet receiver
<i>max</i>	Maximum acceptable value
<i>nom</i>	Nominal value variable
<i>or</i>	Outlet receiver
<i>sys</i>	System
<i>TC</i>	Turbocharger
<i>tur</i>	Turbine

**Greek Symbol**

$\eta$	Efficiency	[-]
$\kappa$	Heat capacity ratio	[-]
$\lambda$	Air excess ratio	[-]
$\mu$	Non-dimensional mass flow	[-]
$\nu$	Non-dimensional rotorspeed	[-]
$\omega$	Angular velocity	[rad/s]
$\pi$	Pressure ratio	[-]
$\psi$	Enthalpy coefficient	[-]
$\tau$	Temperature ratio	[-]
$\varphi$	Flow coefficient	[-]

**Roman symbol**

$\alpha$	Crank angle	[deg]
$J$	Mass moment of inertia	[kg · m <sup>2</sup> ]
$M$	Torque	[Nm]
$Ma$	Mach number	[-]
$n$	Speed	[rpm]
$p$	Pressure	[Pa]
$T$	Temperature	[K]
$w$	Work	[ $\frac{J}{kg}$ ]

**Superscripts**

*	Normalised relative to nominal value
---	--------------------------------------

# Introduction

## 1.1. Background

With the growth in global economy, greater demands have been placed on harbours and commercial waterways around the world due to the increase in global sea transport and the size of marine vessels. Dredging is required for land reclamation, replenishment and for increasing water widths and depths to ensure safe access for ships (Hiranandani, 2014). This dredging equipment needs to excavate large volumes of sediment in waterways and coastal areas. The floating dredge equipment requires medium-speed engines which needs to be highly reliable, efficient and proven, but also have to comply with the emission legislation which become more stringent. Until now, most seagoing vessels are powered with heavy fuel oil (HFO) because of its low costs and availability compared with cleaner marine fuels such as marine diesel fuel (MDF). HFO is still widely used regardless of its technical problems as well as its negative impact on the marine environment. HFO contains high levels of asphalt, carbon residues, sulphur and metallic compounds. The combustion of HFO leads to significant amounts of air pollutants such as nitric oxides (NO<sub>x</sub>), sulphate oxides (SO<sub>x</sub>), carbon monoxide (CO), particulate matter (PM) and the greenhouse gas carbon dioxide (CO<sub>2</sub>) (Banawan et al., 2010). The environmental impact of the emitted exhaust gasses is the fifth largest contributor to air pollution and carbon emissions. Therefore the public concerns have increased regarding the environmental impact of these emissions (Marra, 2011). Most of the dredging ships/equipment operate in port regions which often are close to highly populated areas, therefore, the urgency of reducing air emissions is greater than for traditional transportation vessels. Sometimes limitations to air emissions are agreed in dredging contracts.

As a consequence, environmental legislation has been introduced in different sectors in order to reduce exhaust emissions from fossil fuels related combustion processes. MARPOL annex VI has been introduced by International Maritime Organization (IMO) for controlling the emission of the above mentioned emissions (IMO, 2014). An initial strategy is adopted by IMO's Marine Environment Protection Committee (MEPC) to reduce the CO<sub>2</sub> emissions from shipping by at least 50% by 2050 which is in line with the Paris agreement to lower or even phase out the greenhouse gas emissions as soon as possible. One way to deal with emissions is to use costly secondary methods (end-of-pipe solutions) such as scrubbers for reducing the (SO<sub>x</sub>) emission and Selective Catalytic Reduction (SCR) for reducing the emission of (NO<sub>x</sub>) (Winnes et al., 2016). Another option is to use non-conventional fuels such as natural gas. The use of natural gas as marine fuel has large environmental benefits through an average reduction of (SO<sub>x</sub>), (NO<sub>x</sub>), (CO<sub>2</sub>) and (PM) pollutants by an amount of about 98%, 86%, 11% and 96% (Banawan et al., 2010; Kumar et al., 2011).

## 1.2. Motivation for research

The last five years a noticeable transition is going on to switch from conventional marine diesel engines, running on marine diesel fuel (MDF) or heavy fuel oil (HFO), to liquefied natural gas (LNG). In 2010, Royal IHC stepped into this transition by initiating investigations into the potential of LNG as marine fuel for powering some of the new-build dredgers. The currently installed dual-fuel engines in new-build dredgers at Royal IHC's shipyards have a dual fuel methodology which involves the capability to run either on a liquid fuel type or on natural gas which still needs a small quantity of liquid fuel to be injected for ignition purpose. An important downside of gas engines is their lower load acceptance capability compared with conventional marine diesel engines. The loading acceptance of a gas engine operating in part load is relatively low due to combustion instabilities caused by unbalanced fuel air mixtures. The dual fuel engines have to switch back within a second

from mainly gas to solely diesel fuel to prevent engine stall due to these combustion limitations. The imbalance in air and fuel can be traced back to the turbocharger which does not immediately deliver the desired level of boost pressure when the load drops or increases.

However, Royal IHC would like to investigate methods to prevent this switch-over during a load step. Decreasing the impact of the load step on the engine can be done by using a hybrid drive line which consists of an electric motor in the drive train to assist the engine running on gaseous fuel in a direct way. Installing a fully diesel electric drive system is another solution in which the engine drives a generator and an electric motor drives the power consumers. This leads to lower load steps because dredge pumps can be soft started due to no mechanical connection between engine and power consumer. This electrification increases the complexity of the drive system and could lower the overall efficiency because of extra energy conversions. The latter one is the case when, based on the operational profile, a diesel direct drive line would be the best topology, but a diesel electric drive line is chosen due to loading capability constraints.

Another option is to solve this problem in its source: using a turbocharger with an integrated electrical machine to control the amount of air going into the cylinder with respect to the available fuel. The electric machine can be used as power take in (PTI) or power take out (PTO) to control the right amount of air in the combustion chamber. This advanced charge air system is considered as an interesting topology, and therefore research will be further done into its potential regarding to the system efficiency and loading capability.

### 1.3. Research objective

The research objective to be answered in this thesis is:

*Investigate the potential of an hybrid electric turbocharger for enhancing the loading capability of a dual-fuel engine and its potential as waste heat recovery system.*

This will be done by stepwise approaching the following research activities:

- Adapt an existing mean-value engine model which comprises solely diesel combustion into a dual-fuel (diesel/natural gas) model which can predict the engine dynamics within the entire operating envelope accurate enough compared with test bench measurements.
- Integrate a power take out into the turbocharger model in order to investigate the potential of turbo-compounding.
- Analyse the effect of recovering energy from the exhaust gasses on the total power plant efficiency.
- Analyse the engine's static behaviour improvement possibility to shape the operating envelope.
- Analyse the engine's dynamic behaviour for multiple loading functions at varying engine load points.
- Sensitivity analysis of the dual fuel engine with integrated turbocompound system to study the effect of varying input parameters on the system efficiency gain.

### 1.4. Project boundaries

This research is limited to the topologies in which one turbocharger can both assist the engine during loading events and can recover energy which otherwise would be lost to environment.

The following boundaries are used in this research:

- No investigation is done into the type of electrical machine and energy storage.
- No validation of the whole system will be done due to the lack of test bench data.
- The available semi-empirical gas engine model is used, however it is not improved to a generic gas combustion model.
- No financial related analysis is performed in order to determine the return on investment. However, in Chapter 5 the system efficiency gain will be discussed. These results could be used as input for estimating the fuel consumption savings for a certain vessel.

### 1.5. Thesis outline

The first chapter is used as introduction to the origin of the research objective. The second chapter is intended as an explanation based on literature of the dual fuel engine with regard to its working principle and the origin of the loading capability for both the diesel as well as the gas mode. The third chapter is meant to give an

---

overview of hybrid electric turbocharger applications discussed in literature. This chapter shows an overview of increased system efficiency, loading capability as well as constraints which should be taken into account. The modelling approach used in this thesis is shown in Chapter 4. It starts with the modelling terminology, following with the dual fuel model selection, system build-up, verification and validation of the engine model and the control strategy integrated in the system. The obtained results for turbocompounding and turbocharger assisting mode are divided into two chapters: first the steady state and secondly the dynamic results. Chapter 5 shows the obtained static results such as system efficiency increase, effect on loading capability and increasing the operating envelope. A sensitivity analysis is performed to find what the effect of several system parameters is on the system efficiency. The dynamic results are shown in Chapter 6 which includes four types of engine loading applied to the system with turbocharger assistance. Chapter 7 is meant to propose a system topology which is interesting to investigate in future. The discussed topology is composed based on knowledge gathered in this research. Resting Chapter 8, which contains the conclusions drawn up based on the obtained results, and secondly recommendations to continue with this topic.



# 2

## Dual Fuel Engine

### 2.1. Introduction

In this chapter the working principles of a dual fuel engine will be given. The dual fuel operating principle is not a well-known technology compared to the internal combustion engine (ICE) running on the Diesel cycle mainly used in maritime industry. First the deviation of a dual fuel engine with respect to the in-cylinder processes will be given, whereafter the gas exchange of fresh air and exhaust gasses will be discussed. In the second part of this chapter, the loading capacity of a dual fuel engine to its in-cylinder process will be discussed to relate operational limitations of the engine to parametric quantities.

### 2.2. Working principle of a four-stroke dual fuel engine

The dual fuel engine is a prime mover that converts chemical energy from two types of fuel into thermal energy by means of a combustion reaction. The thermal energy of this combustion reaction is converted into mechanical energy which becomes partly available as work at the output shaft for other power consumers and partly is lost due to various losses. The dual-fuel engine is a four-stroke internal combustion engine (ICE) where the combustion reaction takes place in the combustion chamber between the available fuel and air where the latter one acts as a working medium which contains the oxidizer. The engine cycle is comprised of four processes: gas air mixture inlet, compression, expansion and gas exhaust, as can be seen in Figure 2.1.

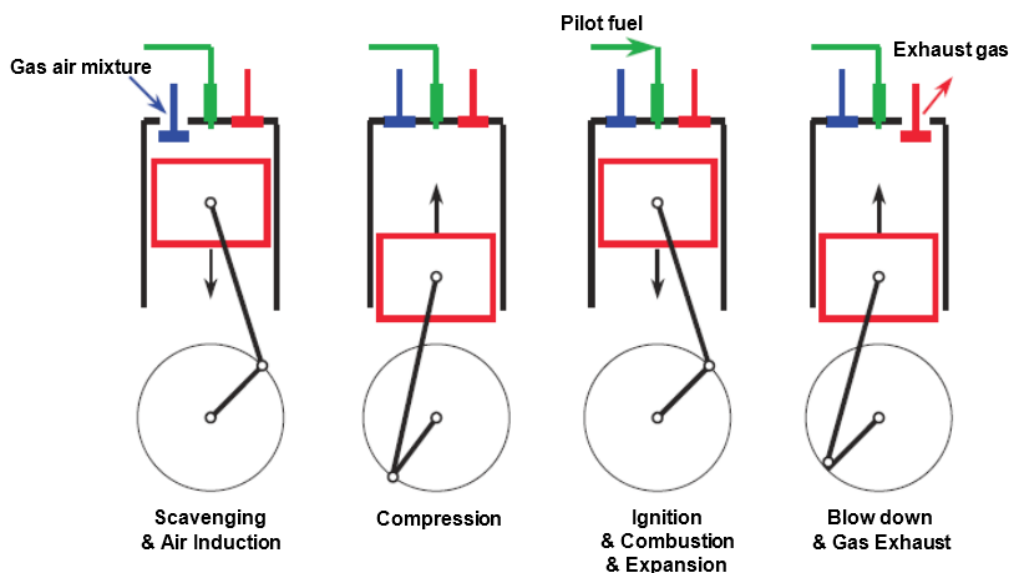


Figure 2.1: Operation principle of a 4-stroke port injected, pilot ignited gas engine, adapted from Stapersma (2010a)

Charge air is swallowed into the combustion chamber during the induction stroke when the inlet valve is opened and the piston moves downwards. The amount of charge air can be increased by raising the air flow density by means of a compressor which is located in the inlet circuit, as can be seen in Figure 2.2. After increasing the charge air density, it is cooled down in the charge air cooler after which the charge air is available in the inlet receiver for inducing into the in-cylinder process. Raising the charge air pressure above the ambient pressure enables the designer to use scavenging during the valve overlap period if a positive pressure difference is available between inlet and outlet ( $p_{ir} > p_{or}$ ). Charge air flows from the inlet port through the combustion chamber in which the piston is (near) top dead center (TDC) via the outlet port into the outlet receiver. This scavenging flow clears the combustion chamber by dispelling remained exhaust gasses from the previous cycle, besides this flow is used to cool down certain engine components (mainly the exhaust valve) due to the lower temperature of this scavenge flow compared to the temperature of the cylinder components (Stapersma, 2010a). In an engine running on the Diesel cycle, liquid fuel is directly injected near the end of the compression stroke in a high pressure and temperature environment. The injected fuel evaporates and self-ignition takes place, known as compression ignition (CI). Developing an ICE for running on gaseous fuel is not one straightforward path with only a few standardized adjustments compared with a conventional four-stroke diesel engine. Every gas engine manufacturer has created its own way of making its engine able to run on gaseous fuels like natural gas (NG). These engines differ mainly in how the gaseous fuel is introduced in the combustion process and how the combustion reaction is initiated.

(Georgescu et al., 2016b) have identified nine distinct gas engine types which differ in the way how the gaseous fuel is injected and ignited. The goal is similar for all the different methods, to burn a combination of natural gas as main fuel and a pilot fuel as ignition source for the gas mode. However, their exhaust emissions and operational behaviour are complete different from each other. Gas admission can be done by either direct into the combustion chamber such as with diesel fuel or indirectly by injecting it into the fresh air path where it is mixed with fresh air. The latter method can be divided in injecting the gaseous fuel before the turbocharger into the fresh air path, known as homogeneous charging, or it can be injected in the inlet port of each individual cylinder which is known as port injection. The main difference between indirect and direct gas admission is the presence of a premixed charge during the induction and compression stroke. Port injection is a widely applied method to admit the gas into the modern engines (Georgescu et al., 2016b). Gas is injected by nozzles in the inlet ports. This allows scavenging while avoiding methane slip because the timing of gas injection is controllable. The compromise is the imperfect gas air mixture homogeneity compared with homogeneous charging (Georgescu et al., 2016b). The required conversions for changing a conventional diesel engine into a dual fuel engine are much less radical than placing a gas injector into the cylinder head. For the implementation of port injectors, only small air intake manifold modifications are required. Although, no radical modification is necessary, engine manufacturers optimize their engines for using gas as main fuel with for instance optimized piston crowns for better air gas mixtures due to the enhanced swirl-like motion (Cho and He, 2007).

Table 2.1: Properties of methane compared to diesel fuel, adapted from (Burel et al., 2013; Hegab et al., 2017; Zulkifli et al., 2015)

	Methane	Diesel fuel
Formula	$CH_4$	avg. $C_{12}H_{23}$
Molecular weight	16	200 (approx.)
Density gas (gas at STP) [ $kg/m^3$ ]	0.717	-
Density gas (liquid) [ $kg/m^3$ ]	415	810 - 890
Freezing point [K]	91	233 - 272
Boiling point [K]	111	461 - 616
Lower heating value MJ/kg	50.0	40.8
Flash point [K]	85	347
Auto ignition temperature [K]	813 - 833	483 - 589
Stoichiometric air excess ratio	17.2	14.7

The utilisation of natural gas in diesel engines suffers from the poor ignition characteristics due to the high auto-ignition temperature compared with conventional diesel fuel (Burel et al., 2013; Hegab et al., 2017). The major part of natural gas consists of methane, the remainder parts are various concentrations of heavier hydrocarbons (Hegab et al., 2017). The difference in auto-ignition temperature for natural gas (mainly methane) and diesel fuel can be seen in Table 2.1. Because of the large difference in auto-ignition temperature only changing the main fuel is not enough to alter the engine from running on a liquid fuel to a gaseous fuel type. The

relative high compression ratio of CI engines results in high pressure and temperature above the auto-ignition temperature of the pilot fuel where it spontaneously ignites without an external source of ignition. Typical cylinder charge conditions prior to ignition are pressure and temperature levels up to about 700 K and 3 MPa (Korakianitis et al., 2011). The auto-ignition temperature of diesel fuel lays about 300 K higher than for natural gas, as can be seen in Table 2.1. Therefore an ignition source is necessary for initiating the combustion process (Nwafor, 2002). Natural gas is drawn into the cylinder during the intake stroke and is, therefore, present in the combustion chamber during the compression stroke, while a small quantity of diesel fuel is injected when the piston reaches almost top dead center (TDC). The conditions in the combustion chamber leads to the auto-ignition of this pilot diesel fuel which is the ignition source for the primary fuel, the premixed charge. The moment of ignition can be chosen by adjusting the injection timing. The main advantage of using diesel fuel as pilot fuel for ignition is the possibility to run the engine on a mixture of diesel and natural gas or only on a liquid fuel type. This dual-fuel capability gives the operator the flexibility to power the ship with only a liquid fuel when natural gas is not available in the region of operation.

### 2.2.1. Gas exchange of a dual fuel engine

The power density of engines has been increasing where the addition of the turbocharger plays a major role. Turbocharging is a well-known method to increase the power density of the engine by increasing the air density. The turbocharger is a device which recovers waste heat from the exhaust gasses, transports it via a shaft to the compressor side for compressing ambient air up to a certain pressure level. The density of fresh air induced during the induction stroke even further increases due to lowering the compressed air temperature in the intercooler. The turbocharger and engine have both their own characteristic which matches only optimal for a certain design point which will be further elaborated in Section 2.3.3.

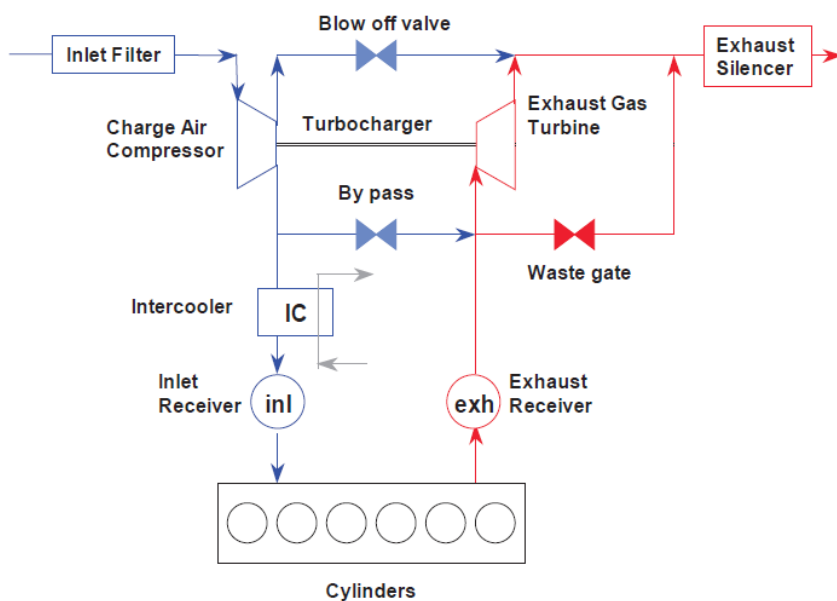


Figure 2.2: Gas exchange lay-out of engine, adapted from Stapersma (2010a)

The addition of three valves to the gas paths before and after the cylinder process and using variable inlet valve timing enables the control of fresh air into the cylinder:

- The waste gate is a widely applied technology to control the flow of exhaust gas through the turbine. This manner of flow control is in most cases part of the turbine inlet design and bypasses exhaust gas from the turbine inlet directly to the turbine outlet without extracting mechanical energy. Reducing the turbine power, and therefore the compressor power, lowers the air mass flow into the cylinder. The air fuel ratio in the cylinder reduces up to the desired level to have a more efficient combustion process.
- The by-pass valve is meant to direct compressed air from the intake to the outlet receiver without entering the cylinder process. In certain operational points, the resistive effect of the cylinder on the turbocharger flow, forces the turbocharger conditions into less efficient areas of its performance area. The by-pass valve is mainly used to avoid compressor surge owing to the increased mass flow through the compressor. The effect of a by-pass valve on the air fuel ratio in the cylinder process is limited, therefore

knock cannot be avoided with this type of air control (Georgescu et al., 2016a). The BPV not only prevents compressor surge, but also enables the mass flow through the compressor to be increased. This is a result of changed operating conditions of the compressor which, for nominal load, could lead to a more favourable situation wherein the compressor efficiency increases, and finally leads to a higher mass flow and increased pressure ratio (Meier and Czerwinski, 1989).

- The blow off valve is the third valve that is applied in engines for regulating the gas exchange. It is a valve between the inlet receiver and exhaust silencer or environment used to direct a part of the charge air to the to the environment instead of the cylinder process. The reduced mass flow to the (resistive) cylinder process leads to a lower inlet receiver's pressure which moves the operational conditions away from the surge line into the stable region of the compressor map (Stapersma, 2010b).
- Another way of controlling the air fuel ratio inside the engine core is to adjust the valve timing in order to control the quantity of fresh air. A couple of dual fuel engines feature advanced Miller timing as well as variable inlet valve closing (VIC). Advanced Miller timing comprises closure the inlet valve before the piston reaches bottom dead center (BDC) (Hermann and Prenninger, 2007). Less charge air is induced during this relatively short duration of the induction stroke. Stopping the cylinder gas exchange before the piston reaches bottom dead center (BDC) leads to a lowered compression ratio of the air charge in the cylinder. This will cause an overall temperature reduction in the combustion chamber and an associated NOx emission reduction, which is the main driver for applying Miller timing in engines. Next to lower peak temperatures in the cylinder, it also lowers the tendency to knock because of the reduced temperature at the end of the compression stroke. Decreasing the compression ratio while keeping the expansion ratio at a higher value increases the engine efficiency because the required work for the compression process is reduced (Cho and He, 2007). Variable inlet valve closing plays a role for part load operation where the charge air temperatures lowers to a certain degree where combustion becomes critical in terms of ignition quality. Early closing of the inlet valve results in a reduced volumetric efficiency due to the reduced in-cylinder volume when the inlet valve closes. Therefore the charge air pressure has to increase in order to provide the in-cylinder process with sufficient fresh air (Cui et al., 2013). Increasing the charge air pressure is achievable with modern turbochargers for nominal conditions. However for part load operation, no sufficient boost pressure is delivered by the turbocharger and, therefore, insufficient fresh air is available for the combustion process (Codan et al., 2010). At part load operation the variable inlet valve timing extends the opening duration, increasing the amount of trapped charge air and compression ratio. The pressure and temperature at the end of the compression stroke are raised, therefore ignition quality is improved. The given options used in dual fuel engine industry enables the control of air excess ratio for the in-cylinder process.

### Thermal overloading of engine due to back pressure

The turbine has a resistive effect on the exhaust mass flow which results in an increased outlet receiver pressure level. A certain pressure level in the outlet receiver is needed to overcome the hydraulic pressure losses in the exhaust pipint in order to discharge the burned gasses from the in-cylinder volume into atmosphere, known as back pressure. When the pressure level in the outlet receiver increases, the engine has to put more work into the expulsion process to expel the exhaust mass flow out of the cylinder volume into the outlet receiver, known as pumping losses. Putting more work into the expulsion stroke while the load on the engine does not change, means that more fuel must be injected to avoid engine stall.

An increased outlet receiver pressure lowers the pressure ratio ( $\Pi_{cyl}$ ) over the inlet to outlet valves, therefore it negatively influences the scavenging process because of the reduced fresh air mass flow during the valve overlap period. Extreme situations could occur when the back pressure rises up to a level where the engine starts to smoke due to incomplete combustion (Sapra et al., 2017). Sapra et al. (2017) concluded that for his engine situation, where back pressure was added due to a water column on the exhaust outlet, that shortening the valve overlap period avoided the occurrence of negative scavenging. The valve overlap period is used to force scavenge air from the inlet through the cylinder to the outlet receiver. Negative scavenging can occur when the outlet receiver pressure ( $p_{or}$ ) is higher than the inlet receiver pressure ( $p_{ir}$ ). The period of time that both inlet and outlet valve are opened can be adjusted in order to prevent negative scavenging. Sapra et al. (2017) has developed a methodology that can be applied for defining the maximum acceptable back pressure levels of marine diesel engines. One large deviation in his research is the additional back pressure due to an underwater exhaust after the turbine, while the application of a hybrid electric turbocharger leads to a back pressure increase before the expansion process in the turbine. The pressure ratio over the turbine is expected to be increased instead of decreased like in Sapra et al. (2017) his research. The similarity of these two back pressure cases is the increased work needed for the expulsion of exhaust gasses from the cylinder volume to

the outlet receiver. (Sapra et al., 2017) used the exhaust valve and outlet receiver temperature as indicators for thermal overloading of the engine. Another boundary that can be used for defining thermal overloading is the air excess ratio ( $\lambda$ ) because a low value means lowering the amount of fresh air to the injected fuel which can lead to high outlet receiver temperatures and engine smoking.

### 2.2.2. Advanced turbocharger configuration

At part load operation, there is a large mismatch between the operational conditions of the engine and those required by the turbocharger in order to provide boost pressure. If the turbocharger is matched for full load operation, it suffers from worse boost pressure build-up for lower loads, as mentioned in 2.3.3.

$$\frac{d\omega_{TC}}{dt} = \frac{M_T - M_C}{J_{TC}} \quad (2.1)$$

where  $M_T$  and  $M_C$  denote the torque developed by the turbine and consumed by the compressor, whereas  $J_{TC}$  denotes the mass moment of inertia turbocharger rotor.

The most obvious technique for gaining faster turbocharger speed-up is to lower the mass moment of inertia of the turbocharger's rotor. Rakopoulos and Giakoumis (2009) has estimated a fifth power relationship between the disk diameter and the inertia of the rotor. By reducing the rotor inertia, faster acceleration of the turbocharger shaft is established resulting in a faster build-up of boost pressure and increased air mass flow rate values, as can be seen in Figure 2.3. The fuel supply during load steps and transient operation needs to be less limited resulting in an raised torque development per cycle.

Giakoumis (2016) states three ways to lower the turbocharger mass moment of inertia. Firstly, the rotor mass can be lowered by employing lighter materials such as ceramics. The change from metal to ceramic rotor reduced the response time in boost pressure by 30% and therefore the engine speed response was enhanced. The second way is to achieve a turbocharger inertia reduction is to install multiple smaller turbochargers instead of using one large single turbocharger. The flow requirements are divided over the number of installed parallel turbochargers at the same time, hence the rotor diameter decreases compared with the single unit. Two, or even more, turbochargers are already installed in V-type engine configurations, each turbocharger is coupled to the exhaust manifold and intake air receiver of one cylinder bank (Giakoumis, 2016). These multiple turbochargers can be switched on and off, depending on the operational conditions of the engine. Loonstijn (2016) has done an extensive research into the implementation of sequential (multiple parallel placed) turbocharging for a fast naval vessel. The latter method is to install a smaller turbocharger with a lower mass moment of inertia. Since the exhaust flow requirements do not change, it leads to an increased rotational speed because the turbine nozzle area is reduced, while the exhaust mass flow stays the same. An important risk of raising the rotational speed is to over boost the engine at higher engine loads and speeds resulting in overloading the engine. A measure to avoid over-boosting is to implement a waste gate valve which bypasses gradually exhaust gasses directly in the exhaust pipe instead of expanding it in the turbine. Nowadays, the waste-gate valve is a common component that is integrated in the turbocharger housing (Giakoumis, 2016; Rose et al., 2011).

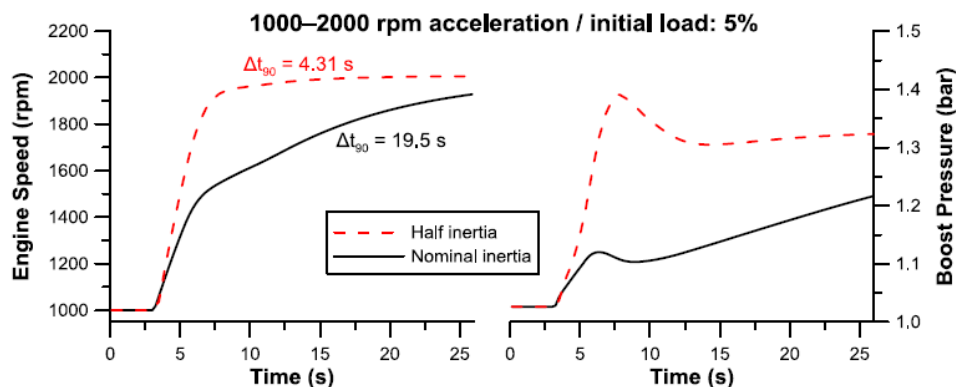


Figure 2.3: Effect of turbocharger mass moment of inertia on engine speed response ( $\Delta t_{90}$ ) corresponds to the time needed to reach 90% of the final demanded speed, from Giakoumis (2016)

Increased rotor acceleration is only possible when the developed turbine torque ( $M_T$ ) is improved at part load engine operation. Fixed geometry turbochargers (FGT) are matched to have peak efficiency at a certain engine condition, however outside this operation point, the boosting efficiency of the FGT decreases, as shown in

Figure 2.4. The variable geometry turbocharger (VGT) can be seen as a band of FGTs each covering a specific operational region, it contains a mechanism to adjust the cross sectional area of the volute by varying blades inside the turbine housing (Figure 2.4). The reduction of the nozzle's area increases the exhaust manifold pressure and temperature which means that the exhaust gas enthalpy is increased resulting in higher kinetic energy available to the turbine rotor (Giakoumis, 2016).

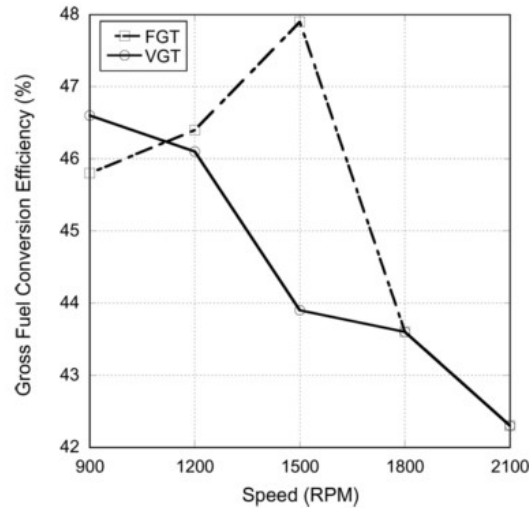


Figure 2.4: Gross fuel conversion efficiency vs. speed at part load operation, from Jacobs et al. (2008)

The engine torque build-up performance can be improved over the entire speed range compared with a fixed-geometry unit. However, the VGT still relies on the build-up of exhaust gas energy which is insufficient available at off design conditions (Rose et al., 2011). However, implementing of a VGT in combination with a marine diesel engine running on HFO is not clearly discussed in literature. Heim (2002) gives as main reason the fouling of the adjustable vanes during the long periods in which marine engines run at steady state. The fouling could stuck the mechanism to adjust the vanes. Although the benefits and potential enhancement for the lower speed range of a marine diesel engine, the VGT is still not popular in marine industry compared with the automotive and land-based applications.

### 2.2.3. Energy balance of a large dual-fuel engine

As in every thermodynamic cycle, also the dual fuel engine is not able to convert the total chemical energy from the fuel into useful work. A large part of the fuel energy is lost to environment due to heat losses such as the charge air cooler, the engine jacket cooling water, radiation, lubrication heat and the remaining heat in the exhaust gasses after the turbine.

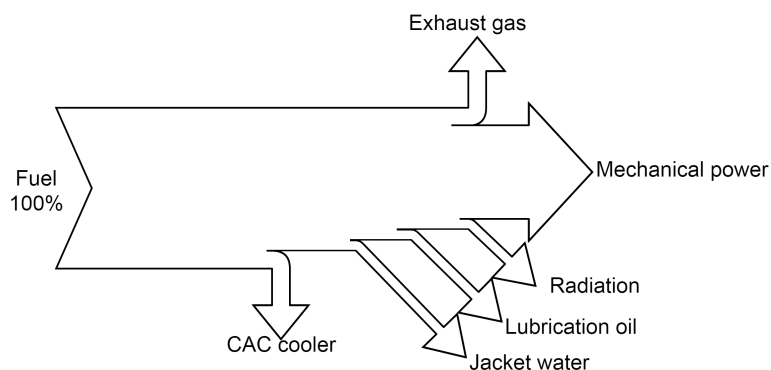


Figure 2.5: Sankey diagram dual-fuel engine

Table 2.2: Energy flows of the Wärtsilä 6L34DF for two combustion modes at 100% load and speed, drawn up with data from Wärtsilä Engines (2012)

Table 2.3: Energy flows for diesel mode

	kW	%
Fuel input	6887	100
Mechanical power	3000	43.6
Exhaust flow	1934	28
Charge air HT	933	13.6
Charge air LT	179	2.6
Jacket water	425	6.2
Lubrication oil	261	3.8
Radiation	121	1.8
Unknown	34	0.4
Total	6887	100

Table 2.4: Energy flows in gas mode

	kW	%
Fuel input	6225	100
Mechanical power	3000	48.2
Exhaust flow	1577	25.3
Charge air HT	601	9.7
Charge air LT	171	2.8
Jacket water	372	6.0
Lubrication oil	260	4.2
Radiation	120	1.9
Unknown	115	1.9
Total	6225	100

As can be seen in Figure 2.5, the conversion from chemical energy to useful work results in a loss of about half of the fuel energy introduced into the system. Fuel costs could be decreased when the engine efficiency is further increased. This can be done by lowering the quantity of waste heat. Apart from the exhaust gas, the major heat flows are the cooling water from the charge air coolers and the jacket water cooler. These cooling water flows have a relative high quantity, but unfortunately due to the relative small temperature difference it has a low exergy compared with the heat available in the exhaust gasses which has a considerable temperature difference between the source and the environment. The available quantity of cooling water considerably exceeds the heating loads of a typical vessel. A large part has to be dumped into sea via the sea water heat exchanger when no waste heat recovery system is installed (Singh and Pedersen, 2016).

Improving the efficiency is possible when the engine's output is increased without deteriorating fuel consumption. The effect of friction losses of the bearings, piston skirts and cam shaft will relatively decrease when the engine's output increase for the same engine. Turbocharging is a manner to rise the engine output. Using a larger compression ratio is a useless manner because of structural limitations due to the higher peak pressure level and increased engine friction losses (Klimstra and Hattar, 2006). A noticeable reduction of the heat loss to the jacket water cooling is hard to achieve because of the almost adiabatic cylinder process. Engines with a large bore, like the Wärtsilä 6L34DF, have a low cylinder area to volume ratio, hence a relative small wall area for transferring heat from the cylinder process to the jacketed cooling water (Klimstra and Hattar, 2006).

The main idea of a waste heat recovery system is to increase the system's useful energy output without injecting more fuel. Therefore only the quantity of heat wasted is not sufficient for selecting a waste heat recovery system. Another important factor is the quality of heat, called exergy, which increases the higher the temperature at which the waste heat flow is available. Singh and Pedersen (2016) consider the exhaust gasses as the waste heat flow with the highest potential to recover energy because of the high temperature and mass flow.

As can be seen in Figure 2.5, the three main waste heat sources are the exhaust gasses, the charge air coolers and the jacket water cooling. Up to about 30% of the fuel's energy is lost to environment via the exhaust. These energy losses rises the question if it is possible to recover energy from these exhaust gasses in order to increase the engine efficiency. Various waste heat recovery systems are discussed in literature to recover energy from marine waste heat flows, which will be further discussed in Section 3.3.

#### 2.2.4. Operating envelope of a dual-fuel engine

The diesel engine is generally known as a constant torque drive over the whole engine's speed range (Klein Woud and Stapersma, 2008). However the implementation of a turbocharger to increase the power density, changes the constant torque behaviour for the lower to mid speed range. Figure 2.6 shows the operating envelope of a one-stage turbocharged engine. The dropped torque output for the lower engine speed range is caused by the compressor operating conditions.

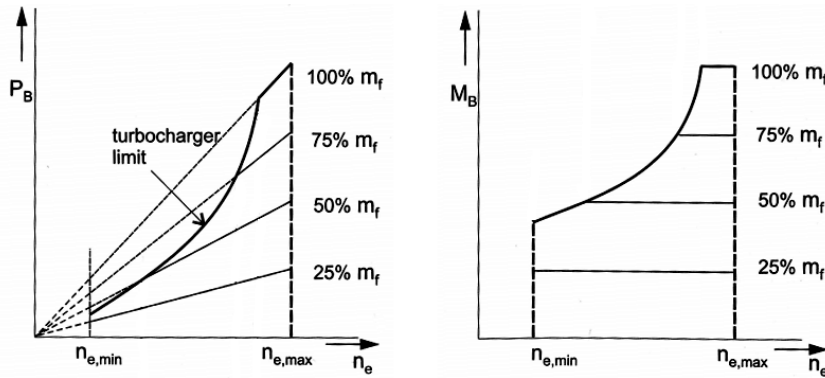


Figure 2.6: Drive characteristic of a one-stage turbocharged engine, adapted from (Klein Woud and Stapersma, 2008)

Every compressor has a limited operating range, see Figure 2.7 due to various phenomena related to flow and mechanical conditions. The maximum rotational speed must not be exceeded due to large centrifugal forces, the mechanical limitation. Flow related limitations are the surge line, the choke and blocking limits. For very low turbocharger speeds, the compressor does not deliver mass flow to the inlet receiver, its behaviour represents a blocking orifice. This boundary, the blocking limit, represents the maximum negative pressure ratio over the compressor. The choke limit comprises the maximum air mass flow through the narrowest part of the compressor because it reaches sonic conditions (Guzzella and Onder, 2010). The maximum speed and choke limit usually do not pose any problems in the matching process. The surge limit, however, is an important limitation which limits the boost pressure output for operational conditions wherein a relative low compressor mass flow is established.

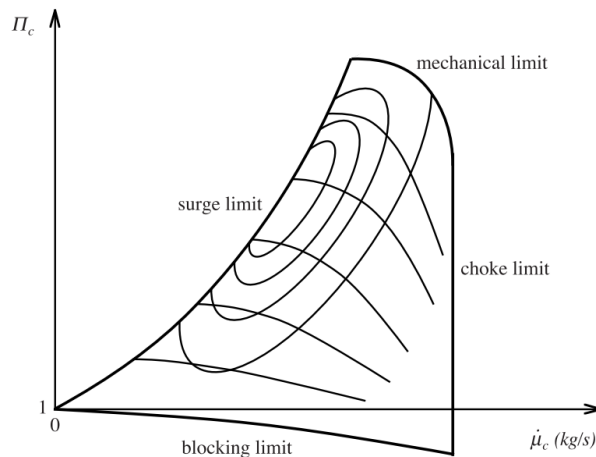


Figure 2.7: Boundaries of operation of a compressor, from Guzzella and Onder (2010)

Surge is defined as the operating point at which centrifugal compressor reaches its maximum head capability and minimum flow limits (Ghanbariannaeni and Ghazanfarihashemi, 2012). The compressor of a turbocharger consists of a rotating impeller which increases the kinetic energy of the fluid and the plenum converts the kinetic energy into potential energy in form of a pressure rise. When the pressure level in the plenum increases above the pressure level that is created by the rotating impeller, the flow tends to reverse. Surge is a very complex phenomenon in which the total centrifugal compressor stage stalls. When surge occurs, the flow patterns in the compressor become unstable which occurs for low mass flows at high pressure ratios, as can be seen in Figure 2.7. The mass flow starts to fluctuate and can even reverse through the compressor stage with accompanying pressure fluctuations. Compressor surge must always be avoided because of its violent nature (Semlitsch and Mihăescu, 2016).

Compressor surge is not a limiting factor for steady state operation at lower engine speeds, but also during transient operation. When the load is suddenly dropped, the enthalpy level of the exhaust gases drops due to the lowered fuel rack setting. The power developed by the turbine drops, therefore the compressor output pressure level drops as well. The pressure level in the inlet manifold is still at a relative high level, which could

lead to back flow from the inlet receiver through the compressor to the inlet. Lowering the pressure level in the inlet manifold is a measure to prevent compressor surge. This can be done with a blow off valve between the inlet manifold and environment. Another measure is to open the bypass valve between the inlet and outlet manifold in order to blow off the surplus of pressure.

The matching process of the turbocharger is important for getting the desired engine torque speed characteristics with the lowest possible BSFC (Terdich et al., 2013). The turbocharger has to cope with various operational conditions as discussed before. Preferably a wide operating envelope is needed wherein the turbocharger delivers a stable pressurized mass flow to the engine. With one-stage turbo charging a wide compressor map cannot be reached due to the lack of turbine power to drive the compressor, therefore advanced turbocharging topologies are developed. One example to improve low-speed torque output is a sequentially turbocharged diesel engine which comprises multiple turbochargers. One turbocharger delivers boost pressure for low engine speed range, and for higher engine speeds one or more turbochargers are added in order to maintain boost pressure for higher exhaust mass flows. As can be seen in Figure 2.8, the torque output of the sequentially turbocharged diesel engine is improved.

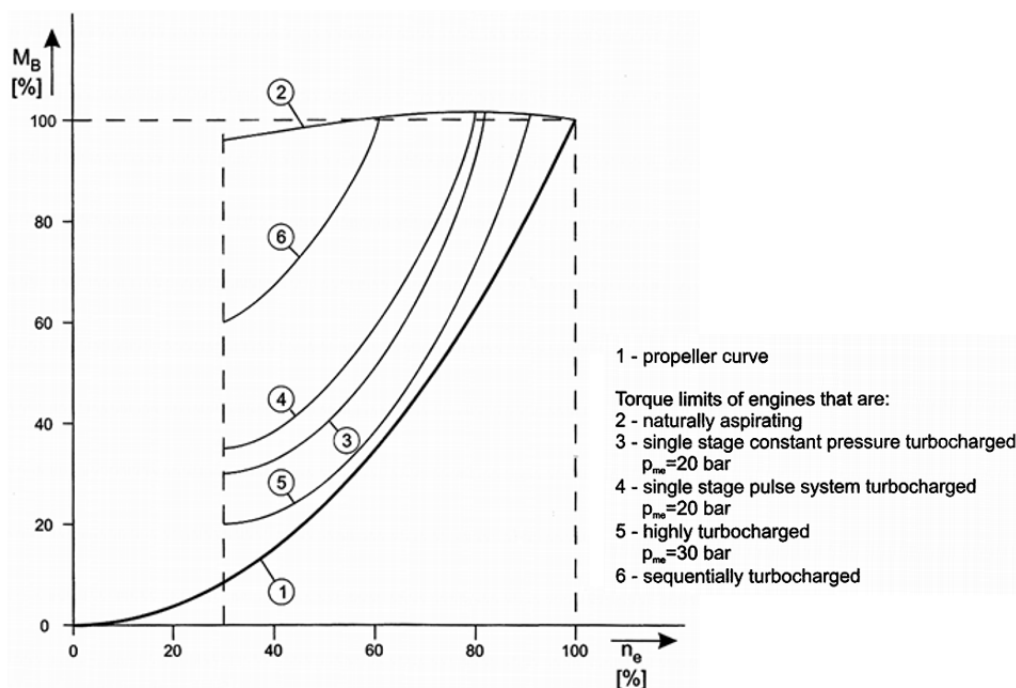


Figure 2.8: Torque capacity of different types of diesel engines, from Klein Woud and Stapersma (2008)

### 2.3. Loading capability of a dual fuel engine

The loading capability of an engine is an important characteristic for preventing engine stall owing to the varying load from, for example, the dredge system. The load step acceptance is the ability of the engine to cope with a sudden increase of load.

Most classification societies approve the roles by IACS with regard to load acceptance. This classification states that the engine input load may be split into more than two intermittent load steps (0 - x - y - 100%) depending on the system conditions if this is possible. The split of the load steps depends on the nominal BMEP and can be calculated according to the following equation:

$$0\% - [800/BMEP]\% - [800/BMEP + \frac{1}{2}(100 - 800/BMEP)]\% - 100\% \quad (2.2)$$

As an example, the W6L34DF dual fuel marine engine with a BMEP of 22 bar the consecutive load steps are: 0 - 38 - 68 - 100%. However in practice, mostly 0 - 33 - 66 - 100% is used. If the applied load cannot be split into three steps, two equally distributed steps (0 - 50 - 100%) must be used as load acceptance requirement (Christer Wik, 2010). IACS defines next to engine input requirements also requirements for the engine output states. After applying the defined load, as described before, the engine speed variation has to be within 10% of the rated engine speed and the engine speed has to recover within 5s to its nominal speed, as is visualized in Figure 2.9.

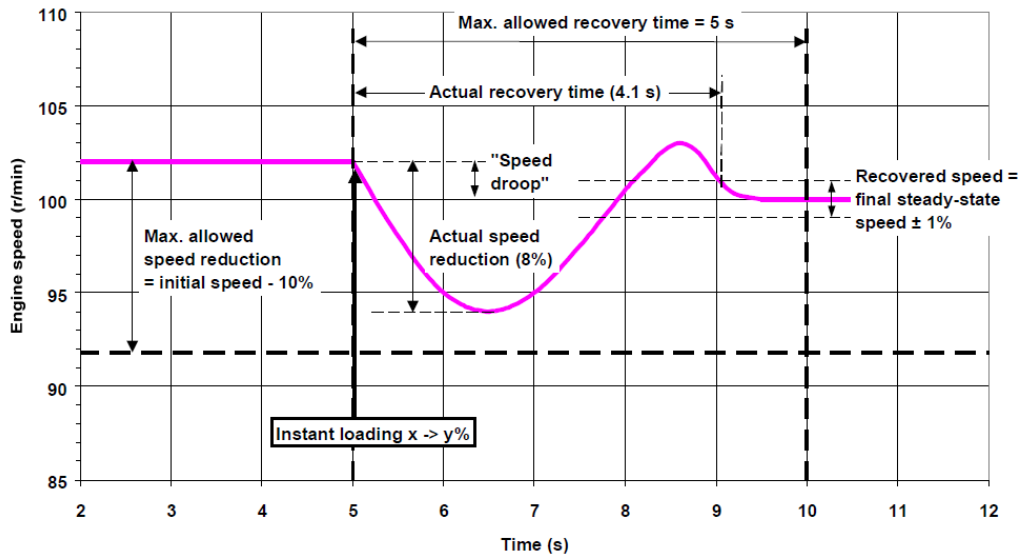


Figure 2.9: General demands for loading capability, from Christer Wik (2010)

CIMAC WG17 'Gas Engines' use a two-step model for the engine's transient response behaviour after a sudden increase of load. The first step is the response of the speed governor when a sudden load is applied to the engine. The second step is the recovery time needed to speed up the turbocharger and to reach a new stable operation point. When a stable operation point is reached, the next load step could be applied to the engine (CIMAC WG17 'Gas Engines', 2011).

### 2.3.1. Effect of air-fuel composition on loading capability

The tendency of an air-fuel mixture to ignite spontaneously depends strongly upon the reactivity of the fuel itself, the air excess ratio ( $\lambda$ ) and the pressure and temperature conditions in the cylinder. The air excess ratio ( $\lambda$ ) is an important parameter in the combustion process of natural gas for obtaining a proper combustion. Lambda is a critical parameter for the operation of a lean-burn gas engine (Cho and He, 2007). The operational range of a gas engine, with regard to the air excess ratio ( $\lambda$ ), is much narrower compared with the same engine running on diesel fuel, as can be seen in Figure 2.10.

When the applied load on the engine goes beyond the maximum power output, the torque output of the engine drops. The available quantity of combustion air decreases while the fuel rack still provides maximum fuel injection resulting in too much fuel present in the cylinder for having a complete combustion. This smoke limit is the only limitation with regard to the diesel fuel injection for obtaining a complete combustion. However, the air fuel equivalence ratio for the combustion process of natural gas is limited on both sides. If the engine load increases up to such an extent, knocking could occur due to a lowering air excess ratio. Knocking is the spontaneous ignition of the gas/air mixture in the cylinder that does not start off correctly with regard to the desired ignition timing. Diesel fuel has excellent autoignition requirements compared with natural gas because of the difference in autoignition properties, as described in Section 2.2. Knock has next to the previous given important parameters also a very close relation to the residence time. The longer an air fuel mixture is exposed to a certain level of temperature and pressure, the higher the tendency to have knock (Claudio Christen, 2013).

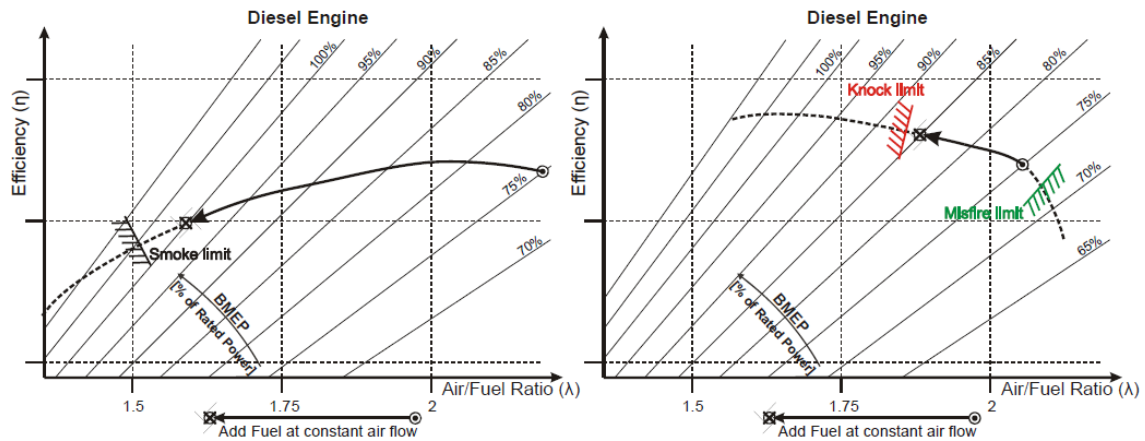


Figure 2.10: Injecting additional fuel at constant air flow (High base load of 75% rated BMEP) (CIMAC WG17 ‘Gas Engines’, 2011)

Where knocking limits the combustion process for lower air excess ratios, misfire leads to improper combustion for higher air excess ratios. The air fuel mixture becomes lean when  $\lambda$  increases. The chemical reaction between fuel and air slows down leading to a lower flame development and an increased ignition delay (Zulkifli et al., 2015). Misfire occurs when too much air in relation to the amount of fuel is present inside the combustion chamber. Flame propagation through the whole combustion chamber is not possible any more because of the absence of sufficient premixed air-fuel mixture to combust or due to insufficient ignition energy (Cho and He, 2007). Slow flame propagation results in a slow heat release, incomplete combustion and high hydrocarbon (HC) emissions due to expelling unburned fuel into atmosphere. Moving the operating conditions of the combustion process into these two regions (knock and misfire) have to be avoided. The occurrence of incorrect ignition is not only affected by the air excess ratio. It depends on the temperature, pressure, composition of air gas mixture but also has a close relation to the laminar flame speed (Zulkifli et al., 2015).

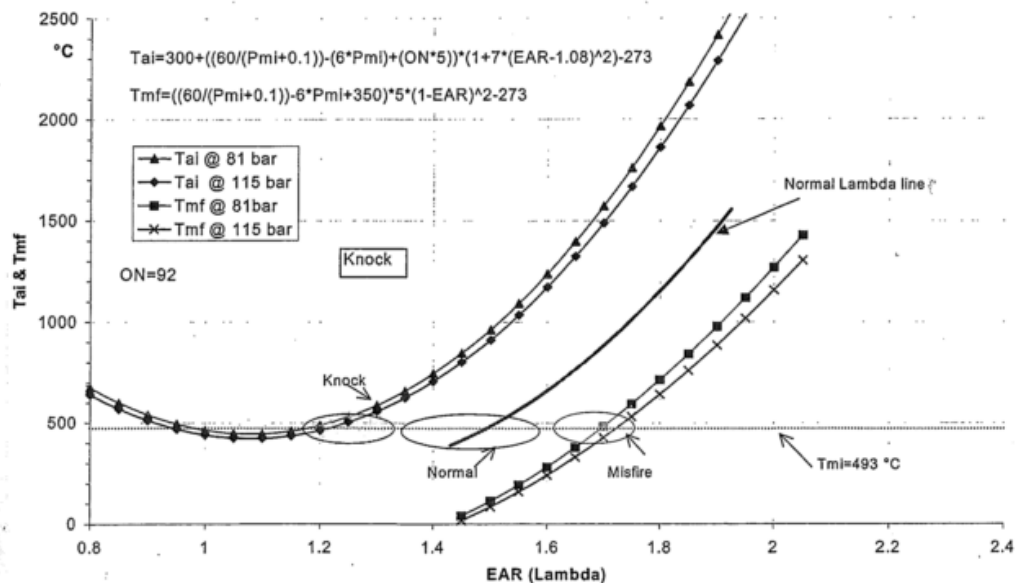


Figure 2.11: Autoignition and misfire temperature vs Lambda, from Daugas and Chen (2000)

The tendency of knock limit and misfire are difficult processes to describe. Daugas and Chen (2000) have studied the knocking and misfiring behaviour of a spark-ignited gas engine. They found an empirical correlation between the mixture pressure, octane number and Lambda. These empirical relations for knock and misfire have been chosen by Georgescu et al. (2016a) for its simplicity and easy integration in mean-value gas engine simulation models. The knocking and misfire regions as function of  $\lambda$  and the autoignition and misfiring temperatures are depicted in Figure 2.11. The operational range lays between the knocking and misfiring regions.

### 2.3.2. Load acceptance of a dual-fuel engine

A gas engine can handle very limited load steps compared with a diesel engine due to knocking and misfiring, as explained in Section 2.2. The air fuel ratio must be controlled very accurately when load steps are applied on the engine such as engaging a dredge pump. However, the load acceptance in gas mode is restricted in the low load region by the turbocharging ability to provide boost pressure similar to the turbo lag behaviour of a diesel engine. The reduced air fuel ratio during rapid output increase in a diesel engine leads to soot generation from incomplete combustion. (Rakopoulos and Giakoumis, 2009) However the diesel engine can still withstand the increased load where a gas engine fails due to knock. That is why gas engines have poorer transient response compared with diesel engines. The air supply plays an important role for the engine response during transients. When a certain load is suddenly applied to the engine, the turbocharger has to spool up which takes some time until sufficient power can be extracted from the exhaust gas to drive the compressor resulting in providing boost pressure. The slow reaction of the turbocharger after the start of a transient event leads to a relative low AFR during the early cycles of a transient event. The combustion is negatively influenced resulting in slow engine torque and speed response. The turbocharger and engine have both their own characteristic which matches only optimal for a certain design point. In most cases, the turbocharger is matched with the gas engine exhaust gas flow and intake air flow conditions for full load operation. However, their characteristics do not match optimally at other operational conditions such as part load. A relative large turbocharger matched for full load operation suffers from worse transient performance because of the rotor's inertia which needs to spin-up before boost pressure is provided to the cylinder.

As an example, the maximum instant load step for a large bore port injected gas engine is shown in Figure 2.12 for both operating in gas mode as well as operating in diesel mode. The low load acceptance in gas mode is clearly shown, although the engine type and operating conditions are not known.

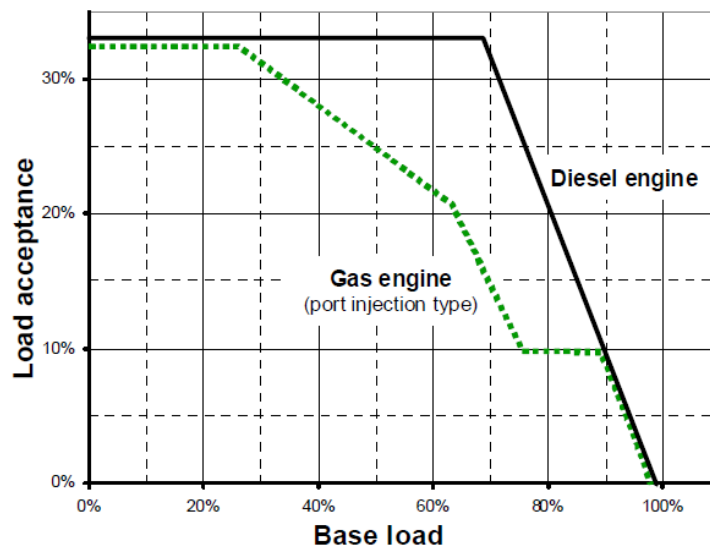


Figure 2.12: Maximum load acceptance for a port injected gas engine (CIMAC WG17 'Gas Engines', 2011)

Another loading type is the increase of load over a period of time, the load ramp. As an example, the load increase from 0 - 100% for the Wärtsilä 6L34DF is shown in Figure 6.14. The time needed to increase the engine loading is large for the engine running in gas mode compared to the emergency diesel mode.

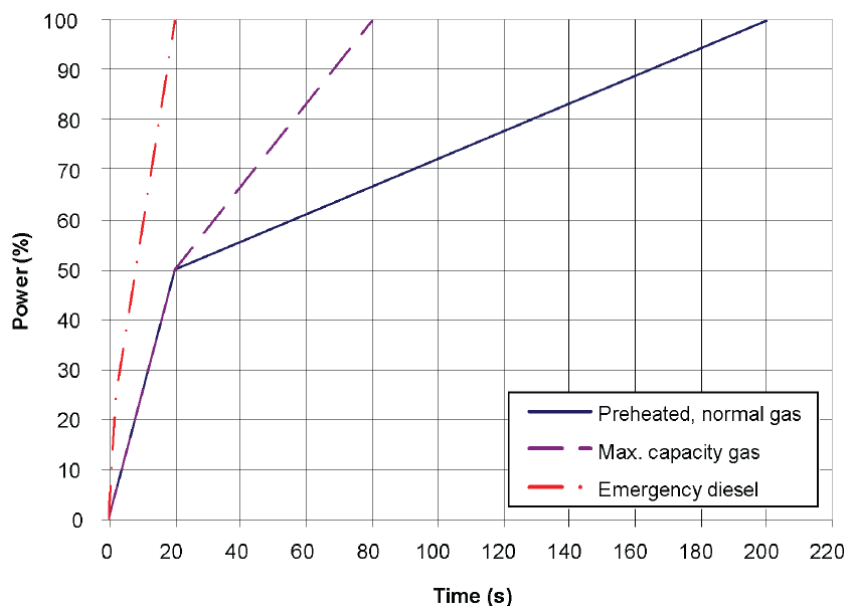


Figure 2.13: Maximum load ramp Wärtsilä 6L34DF for diesel and gas mode, from Wärtsilä Engines (2012)

The efficiency of dual-fuel engines has been rising from 35% in the year 1990 to 46% in 2005. In the year 1990, a break mean effective pressure (BMEP) of 12 bar was the limit for stationary gas engines. However, it is already risen to a BMEP of 20 bar in 2005 and, at the time of writing, the Wärtsilä 31DF engine has been introduced which has a BMEP of 27 bar. The change to much leaner air gas mixtures has made it possible to raise the BMEP (Klimstra and Hattar, 2006). Unfortunately, the increased BMEP comes with a higher tendency to knock. Inducing a leaner air gas mixture can be used to compensate the increased risk of engine knock (Klimstra and Hattar, 2006). The need for a proper quantity of fresh air has become an important condition to create the work needed to cope with the engine load. However the turbo lag behaviour is an undesirable aspect during dynamic engine operation which affects the air fuel mixture condition. The compressor is not able to deliver the right amount of fresh air needed in the combustion process related to the quantity of injected fuel. Knock limits the power build up of the gas engine, with as a result engine stall. Figure 2.14 shows the load step response for a standby Diesel engine and two gas engines. The recovery time for both gas engines is obviously longer than for the diesel engine. The high BMEP gas engine stalls for a 0 – 40% load step due to, probably, the fuel controller limits its output to prevent the occurrence of engine knock. This can be avoided when the operational point moves from the knocking region into the stable combustion region by supplying additional boost pressure (increasing the air excess ratio), as can be seen in Figure 2.11.

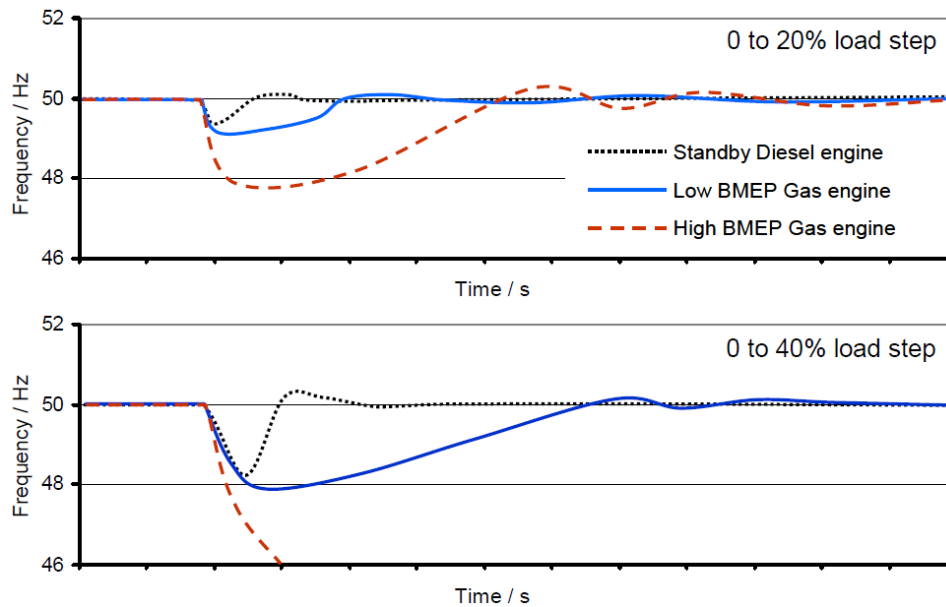


Figure 2.14: Load step response example of typical Standby Diesel and Mixture-charged Gas engines CIMAC WG17 'Gas Engines' (2011)

### 2.3.3. Gas exchange during transient operation

Where most marine engines operate the greatest part of the time at steady-state operation at sea, engines powering dredging systems have to deal with highly varying loads. The transient response of a turbocharged engine is mostly affected by the dynamic response of the turbocharger. When a load or speed increase event is initiated, the fuel rack almost immediately increase the provided fuel per cycle. On the contrary, the in-cylinder process does not receive the right amount of fresh air because of the mechanical inertia of the turbocharger, the thermal and fluid inertia in the ducts between the compressor and cylinder (Rakopoulos and Giakoumis, 2009). The mismatch, between fuel and fresh air, in the cylinder rises the probability to reach the smoke limit for the dual-fuel engine in diesel mode and diesel engines as well. But in gas mode, the air excess ratio ( $\lambda$ ) is important to prevent knocking or misfire phenomena in the combustion process. These combustion limitations cannot be totally prevented when the turbocharger boost pressure build-up is improved. The torque delivered by the engine cannot be increased beyond the limit due to these limiting combustion conditions. Lowering the time between the start of a transient event up to at which the turbocharger starts to deliver boost pressure improves the engine response and lowers the soot emission (Rakopoulos and Giakoumis, 2009).

Turbocharger sizing is a very important matching process which depends on the desired engine performance requirements. The operational conditions used for the matching process between the turbocharger and the engine determines up to which extend boost threshold plays an important role for the operating envelope of the engine. The combination of a particular turbocharger, piping arrangement and engine type determines to which sense the system can cope with dynamic loads. The dual-fuel engine under investigation in this thesis, the Wärtsilä 6L34DF, is presumable matched for nominal condition, maximum power at nominal speed. Part load operation is, therefore, highly influenced by the worse boost pressure provided at part load operation, probably the result of a remarkable boost threshold. This can however not be verified at this moment. The transient response of the Wärtsilä 6L34DF could be negatively influenced by a constant pressure turbocharger system. The kinetic energy available in the exhaust gas blow-down pulses is maybe not utilized to increase the pressure in the outlet receiver. The larger the outlet receiver, the longer it takes to pressure the outlet receiver after applying a load or speed increase event on the engine. However this cannot be verified as well.

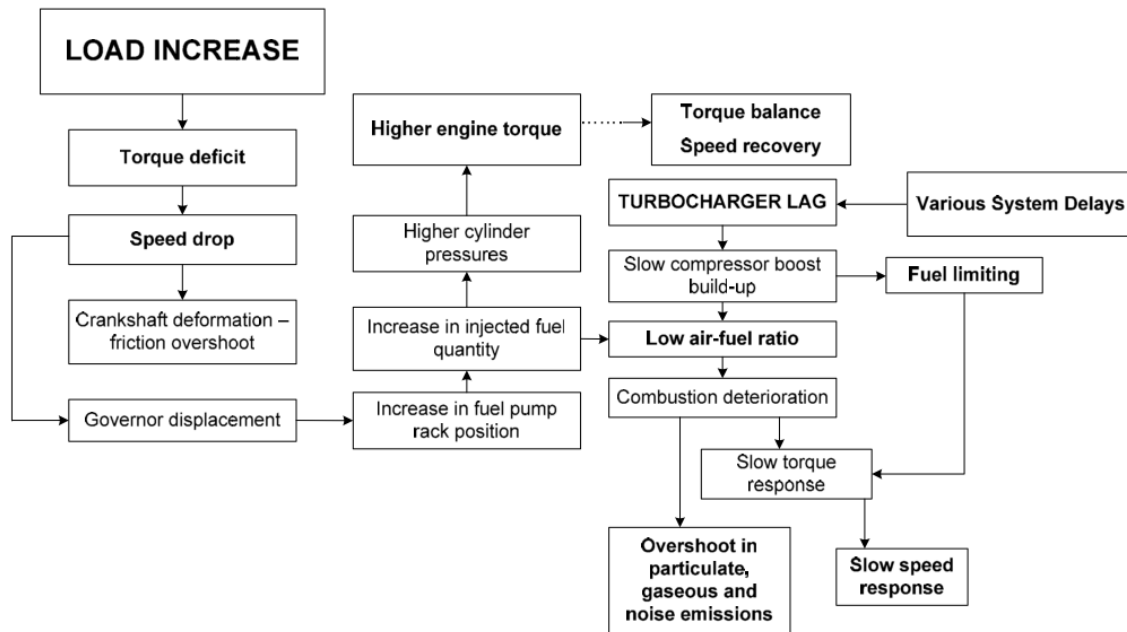


Figure 2.15: Series of events after a step load increase of a turbocharged diesel engine, from Rakopoulos and Giakoumis (2009)

The consecutive steps that happens after the engine load is increases, are shown in a causality diagram (Figure 2.15). The turbocharger starts producing a positive pressure ratio over the compressor only when sufficient exhaust gas energy is available in the exhaust gas flow. Below a certain operational point, no boost is provided to the inlet receiver anymore, in literature commonly given as: boost threshold. Boost threshold is the lowest engine power and speed combination at which the turbocharger starts to produce boost pressure when full throttle is applied. A lower engine speed than the boost threshold results in insufficient exhaust gas energy to drive the turbocharger in order to produce above-atmospheric pressure levels in the intake receiver. Therefore the torque output for a naturally aspirated engine and a turbocharged engine are almost the same below this boost threshold. Selecting a turbocharger with the lowest boost threshold does not lead to the best performance possible for the engine. It is a trade-off between high torque at low engine speeds and maximum power at full speed. The back pressure increases inevitably when a relative small turbocharger is chosen at higher engine speeds and loads.

Turbo lag is the additional time delay above boost threshold, when full fuel is injected and the turbocharger needs to accelerate to deliver positive pressure to the engine. The difference between boost threshold and turbo lag is the time needed after boost pressure starts to develop and at which the turbocharger reaches steady state operation. Turbo lag decreases as engine speeds rises due to the increased exhaust mass flow, and therefore available energy for the turbine.

Providing boost pressure is disconnected from the boost threshold when a turbo compound topology is applied for providing torque to the compressor, and turbo lag is reduced due to the increased shaft acceleration as a result of the provided additional torque on top of the delivered torque from the turbine. The turbo compound topology could both improves the boost pressure build up of the compressor as well as the acceleration of the turbocharger shaft.

## 2.4. Conclusions

The dual fuel engine differs with the diesel engine because natural gas is used as main fuel while a small diesel quantity is injected as ignition source. Moreover the dual-fuel engines are able to run on solely liquid type fuel such as marine diesel fuel or heavy fuel oil. The exhaust gas waste heat flow accounts to 25 - 30% of the fuel energy which is lost to environment. This waste heat source could be used to recover energy due to a high temperature difference with environment compared with other waste heat flows. The operating envelope of a dual fuel engine is limited on the left side due to the limitation of compressor surge, comparable to the operating envelope of the diesel engine. The natural gas combustion is limited on both sides of the air excess ratio range. For rich air fuel mixtures the engine is prone to knocking and on the lean side the engine is prone to misfire. The loading capability of the dual fuel engine for natural gas combustion is lower than for diesel mode. The low to mid speed range torque development is limited due to the mismatch of the engine turbocharger combination for other operating points than the nominal point, for which the engine and turbocharger are matched.

# Hybrid Electric Turbocharging

## 3.1. Introduction

This chapter comprises the literature study related to this hybrid electric turbocharger. The study is carried out to gain insight up to which extent the turbocharger integrated electric machine both system's efficiency as well as the dynamic behaviour of the engine can improve or not. The first part of this chapter comprises the gain in system efficiency, often described in literature as turbocompounding. The second part is related to the gain in static and dynamic loading capability when the e-machine assists the turbocharger, often described as: electrically assisted turbo charging. The steady state engine torque output is called: torque curve shaping. The implementation of an electric machine to the turbocharger's shaft is not possible without operational limitations which has to be included in the electric machine controller, these will be covered in this chapter as well.

## 3.2. History of turbocharging

The invention of a high-speed device to boost an internal combustion engine with waste heat from the exhaust gasses goes back to the beginning of the previous century when Alfred Büchi received a patent for his thoughts about turbocharging. Turbochargers are a well-known method to increase the power density and efficiency of internal combustion engines. However, out of the matching point, there is a mismatch between the low-speed (engine) and high-speed (turbocharger) devices. As explained in Section 2.2.4, the matching process between these two devices determines the operating envelope. Obtaining the highest efficiency at full load and speed possible for a one-stage turbocharged engine, could lead to the lack of sufficient low-speed torque. This gap of power to drive the compressor can be filled by the integration of an electric machine on the turbocharger shaft, named hybrid electric turbocharging. Next to the turbine, an electric machine can add power to the turbocharger shaft to drive the compressor, as can be seen in Figure 3.1. For cases where insufficient exhaust energy is available for the turbine, the electric machine can speed up the compressor in order to boost the engine. Another feature is the possibility to extract excess power from the turbine with a power take out, such as a generator. The harnessed energy can either be supplied to other power consumers or can be stored in an energy storage such as a battery or super capacitor.

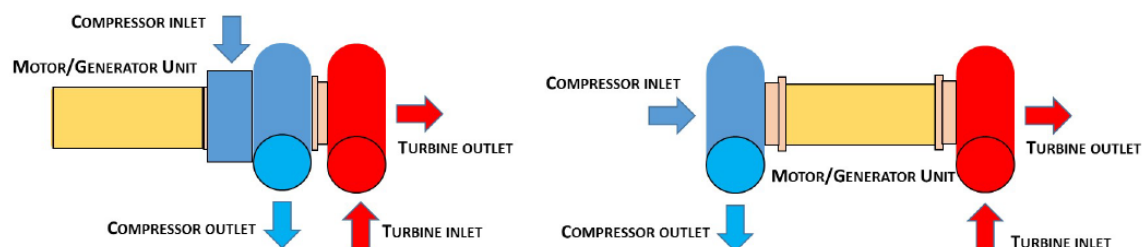


Figure 3.1: Schematic of a turbocharger with a motor/generator unit side of compressor (left) or between compressor and turbine (right) as used in F1, adapted from Boretti (2017)

The single application of this hybrid electric turbocharger can be found in racing sport, namely the Formula One. From 2014 on, the Formula One cars are equipped with the hybrid electric turbocharger to improve the

lateral acceleration by assisting the turbocharger via the electric machine when the driver wants to accelerate like as just after a turn. For other parts of the track, excess exhaust energy can be recovered with the electric machine and is stored in an energy storage for the next electric assistance event.

### 3.3. Turbocompounding to improve overall plant efficiency

While a marine dual-fuel engine has a high efficiency, still a considerable amount of waste heat is lost to the environment, as explained in Section 2.2.3. Various waste heat recovery topologies are described in literature, however certain systems are only limited to onshore applications due to practical reasons like dimensions, weights, operational conditions. Singh and Pedersen (2016) specify which features a waste heat recovery system needs to have in order to successfully harness energy from waste heat in marine applications:

- High efficiency for harnessing the waste heat;
- High power density to power large power demands;
- Able to handle transient heat source and sink properties;
- Adaptable to changing vessel operation profile;
- Easiness of integrating the WHRS with other power systems aboard;
- Reliable in operation;
- Small footprint due to space and weight limitations;
- Safe in operation and handling aboard.

The heat flows, which have even a relative low quality, can be recovered with bottoming thermodynamic cycles such as a Steam Rankine Cycle or an Organic Rankine Cycle. Organic Rankine cycles applies the principle of the Steam Rankine Cycle, but uses an organic working fluid that has a lower boiling point than water in the Steam Rankine Cycle (Chen et al., 2010). In the past, several WHRS are investigated within the department of Maritime and Transport Technology of Delft University of Technology. The implementation of a Steam Rankine cycle is investigated by both Boonen (2009) and de Ruyck (2010). Thimmanoor (2018) has adapted their SRC model in order to investigate the potential of organic fluids in stead of steam as a working fluid. The main advantage of bottoming cycles for harnessing exhaust gas energy, is the almost negligible impact on the engine performance. While, expanding the exhaust gasses in a power turbine or turbo compound increases the back pressure on the engine, a heat exchanger after the turbine has less impact on the resistance of the exhaust elements. van Fulpen (2016) investigated the integration of an adsorption chiller to make use of the low quality heat flows. The cooling water from a diesel engine was used in his research to provide energy to a refrigeration cycle. The previous mentioned WHRS can harness energy from multiple heat sources, the turbocompound system does only extract energy from the exhaust gasses. Turbocompounding comprises the implementation of a turbine in the exhaust piping to recover waste heat energy via expansion instead of wasting it via a waste gate

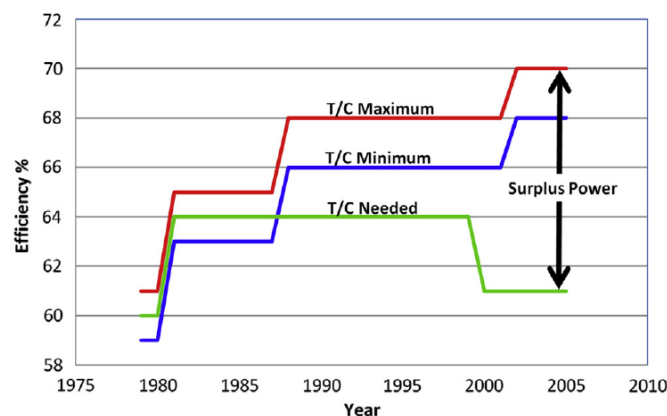


Figure 3.2: Turbocharger improvements in surplus efficiency for new generation turbochargers. Singh and Pedersen (2016)

Within the research of this thesis, only the high quality waste heat flow from the exhaust gasses is considered as heat source for harnessing energy with a turbo compound system. The recovered energy can fed to the engine's crankshaft/flywheel by means of a mechanical connection with gears or belts, a hydraulic connection, or can

be converted into electrical energy to be directed to the drive line or to other electrical energy consumers. A conventional turbocharger is, in essence, a WHRS that recovers energy from the exhaust gas flow and turns it into mechanical power for driving the compressor. The efficiency of fixed geometry turbochargers around their optimal operation point is improved such, that the work extractable from the exhaust flow exceeds the power requirement of the compressor. Figure 3.2 shows the trend of increasing surplus energy recoverable from the exhaust gases. A common method for controlling the amount of exhaust flow into the turbine is done by regulating this flow with a waste gate. As explained in Section 2.2.1, this waste gate bypasses the surplus of exhaust flow around the turbocharger to prevent engine over-boosting. However, bypassing a part of the exhaust gases with the waste gate reduces the system's efficiency potential (Heim, 2002).

Turbocompounding is a broad concept, because various topologies can be composed with a turbine as waste heat recovery device. An additional turbine stage can be located in series downstream the turbocharger turbine, in literature commonly referred to as low-pressure turbocompounding, or the turbine can be placed in parallel with the turbocharger turbine, which is called high-pressure turbocompounding. Aghaali and Ångström (2015); Teo et al. (2015) give a thorough review of various turbocompounding topologies from high to low pressure and mechanical to electrical turbocompounding configurations. The scope of this research is high-pressure turbocompounding with an electric machine integrated in the turbocharger unit. Therefore the other turbocompounding topologies are not covered in this chapter.

### 3.3.1. Efficiency increase realised with electrical turbocompounding

Hermann and Prenninger (2007) states that the most promising application of a hybrid electric turbocharger can be found in maritime applications because these engines operate at constant high load for extended periods of time. The implementation of a hybrid electric turbocharger is a new development in maritime industry. The only marine application of this hybrid electric turbocharger is done by Mitsubishi Heavy Industries (Ito, 2012; Yoshihisa, 2007, 2012) in a seagoing vessel. The main purpose was to recover electricity from the surplus energy in the exhaust gases. World's first marine related hybrid electric turbocharger was implemented onboard the Shin Koho, a bulk carrier powered by a 20.090 kW MAN 7S65ME-C two-stroke diesel engine. Modifications to a conventional turbocharger were done by connecting a permanent magnet synchronous generator at the inlet side of the compressor, as can be seen in Figure 3.3. The hybridization of the turbocharger has resulted in a 313mm longer and 4600kg heavier turbocharger unit compared with the conventional one. The maximum designed power output is 754 kW at a speed of about 9000 rpm that accounts for an additional power output potential of 3.75%. However, no quantitative results of efficiency gains are published. (Yoshihisa, 2012) only publish that the quantity of produced electrical power was sufficient for supplying the entire electrical demand of 420kW of the ship during normal cruising. No information is available why Mitsubishi Heavy Industries have not equipped more vessels with the hybrid electric turbocharger. Their next step was to investigate the assisting mode, but no consecutive literature is found that shows results with a hybrid electric turbocharger on the two-stroke marine diesel engine's loading capability.

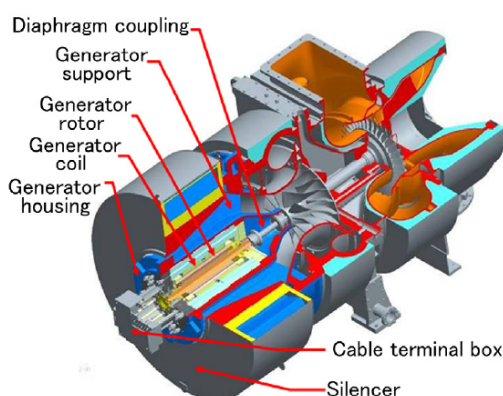


Figure 3.3: Cross-sectional view of the MET83MAG hybrid turbocharger, from (Yoshihisa, 2012)

Electric turbochargers have been investigated for the automotive industry as waste heat recovery method for reducing the fuel consumption. Table 3.1 gives an overview of literature wherein a hybrid electric turbocharger is applied as turbocompounding device. Very limited results are published with regard to increased engine efficiency when turbocompounding is applied. No extensive turbocompounding results are published for, for example, engine speed ranges, varying loads, changes in turbocharger topologies, engine parameters such as valve timing or turbocompounding control strategies.

Table 3.1: Overview of turbocompounding with an hybrid electric turbocharger in literature

Researcher	Type of research	Application	Engine	E-machine specs	Efficiency increase
Rusman (2018)	Simulation	Marine	Diesel four-stroke 5000 kW at 1000 rpm	200 kW	3 %
Shiraishi and Krishnan (2014)	Measurements	Marine	Diesel two-stroke 5000kW	252 kW	Not mentioned
Yoshihisa (2012)	Measurements	Marine	Diesel four-stroke 2.0 liter	550 kW 10000 rpm	Not mentioned
Pasini et al. (2016)	Simulation	Automotive	Diesel four-stroke 51 kW at 4000 rpm	7 kW 140.000 rpm	6 %
Bumby et al. (2006)	Simulation	City bus	Diesel four-stroke 363 kW	7.5 kW 130.000 rpm	6.4 %
Sendyka and Soczowka (2006)	Simulation	Automotive	Diesel four-stroke 346 kW at 2200 rpm	Not mentioned	5 to 11 %
Boretti (2017)	Simulation	Automotive	Gasoline SI engine 2.0 liter	Not mentioned	4 to 5 %
Arsie et al. (2015)	Simulation	Automotive	Gasoline SI engine 1.4 liter	1 kW	5 %
Dimitriou et al. (2017)	Simulation	Automotive	Gasoline SI engine 2.0 liter	5 %	Not mentioned
Zhang et al. (2017)	Simulation	Automotive	Gasoline SI engine 2.0 liter 175 kW at 5500 rpm	200 kW	3 %

### 3.3.2. Assisting turbocharger to improve overall plant efficiency

Literature from Mitsubishi Heavy Industries, Ltd does not show the effects of turbocharger assistance on the engine's loading capability for large marine engines, however an article is published for a small automotive diesel engine by Yasuaki (2006). They found, based on a simulation study, an increased engine efficiency for low engine speeds by assisting the turbocharger. As can be seen in Figure 3.4, the engine thermal efficiency is increased up to 12% by assisting the turbocharger with 2 kW. No detailed information about the engine is available, besides that they used a 2.0 liter diesel engine in their simulation study. Yasuaki (2006) states that assisting the turbocharger improved the fuel efficiency by 8% for 1 kW assist, and 12% for 2 kW assist. However, no information is available if the energy consumed by the electric machine is involved in this fuel economy calculation. No other research is found which conclude or contradict this gain in engine efficiency by assisting the turbocharger.

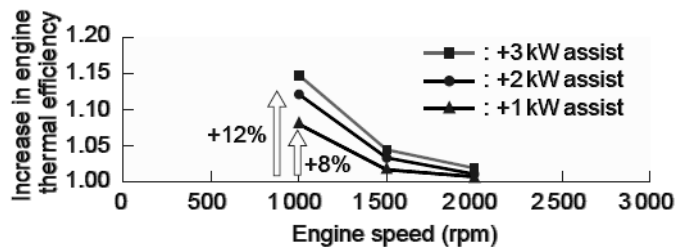


Figure 3.4: The hybrid electric turbo enhances the thermal efficiency, adapted from Yasuaki (2006)

### 3.3.3. Effect of turbocompounding on engine conditions

The power from the turbocharger's turbine could exceed the power required for driving the compressor at nominal engine power and speed due to the increased turbine efficiency level, as already shown in Figure 3.2. Therefore the surplus power from the turbine can be extracted from the turbocharger shaft to increase the system power output. As energy is drawn from the turbocharger, its speed will lower until a new equilibrium is established. The mass flow through the turbine will first drop due to the higher resistive effect of the turbine on the exhaust gas flow. The higher exhaust mass flow ( $m_{exh}$ ) from the engine into outlet receiver and a lower out-flow to the turbine leads to an increased outlet receiver pressure ( $p_{ir}$ ). The increased outlet receiver pressure ( $p_{or}$ ) is required to force the exhaust mass flow from the outlet receiver through the turbine into the environment, which is called back pressure. An increased outlet receiver pressure ( $p_{or}$ ) means a rise in the pressure ratio over the turbine ( $\pi_T$ ) with as result more power generated by the turbine. However, the engine needs to put more work into the expulsion stroke to expel the burned gasses from the combustion chamber into the exhaust manifold, known as pumping losses. Additional to the increased pumping work, the scavenging mass flow ( $\dot{m}_{sc}$ ) is lowered due to the lower pressure gradient over the intake and exhaust valve ( $\Delta p_{ir-or}$ ). However,

the exergy lost due to expansion process between the cylinder when the exhaust valve opens and the outlet receiver, can be reduced with a higher outlet receiver pressure ( $p_{or}$ ) (Aghaali and Ångström, 2015). As mentioned before an effective integration of the turbocompounding concept is only achieved when the generator power exceeds the deteriorated engine power owing to the increased back pressure (Hermann and Prenninger, 2007). While the engine efficiency decreases due to the increased back pressure, the additional power output due to turbocompounding could lead to an overall engine efficiency increase (Aghaali and Ångström, 2015; Hountalas et al., 2007).

### 3.4. Hybrid electric turbocharger to improve dynamic loading capability

The benefit of an integrated electric machine in the turbocharger is the possibility to assist the turbocharger during load step events by improving the speed up of the turbocharger compared with no assistance. Increasing the acceleration of the turbocharger leads to a shorter time frame needed to build up boost pressure in the inlet receiver. Improved turbocharger acceleration can only be achieved if the following equation is met:

$$\frac{M_T + M_{EM} - M_C}{J_{TC} + J_{EM}} > \frac{M_T - M_C}{J_{TC}} \quad (3.1)$$

where  $M_T$ ,  $M_{EM}$  and  $M_C$  denote the torque developed by the turbine, the applied torque during assisting mode and the torque consumed by the compressor, whereas  $J_{TC}$  and  $J_{EM}$  denote the mass moment of inertia of the turbocharger rotor and the electric machine that provide the torque for the assisting mode. Adding inertia to the turbocharger shaft due to the electric machine could even lower the system of the engine due to a lower turbocharger shaft acceleration for dynamic operation. Deterioration of the fuel economy could occur when the electric machine is not used, and the developed torque of the turbine ( $M_T$ ) has to accelerate the turbocharger shaft which leads to a lower turbocharger shaft acceleration compared with the case wherein the electric machine is used together with the turbine Tavcar et al. (2011). The inertia of the electrical machine should therefore be as low as possible to ensure that the torque developed by the turbine ( $M_T$ ) can accelerate the turbocharger shaft. Otherwise electrical energy has to be provided to the electrical machine in order to counterbalance the deterioration of the shaft acceleration. The influence of inertia on loading capability will be further investigated in Chapter 6. Katrasnik et al. (2005) concludes that the added shaft inertia of the electric machine should not exceed 33 - 50% of the turbocharger's inertia to efficiently assist the turbocharger. The shaft acceleration of the free running electric machine should be approximately an order of magnitude larger than the turbocharger without any electrical machine (Katrasnik et al., 2005).

#### 3.4.1. Hybrid electric turbocharging to improve transient load capability

As long as Equation (3.1) is met, it leads to an enhanced boost pressure build up compared with no assistance (baseline). Yasuaki (2006) have done test bench experiments with a hybrid turbocharger, which replaces the variable geometry turbocharger (VGT), mounted on a 2L direct injected intercooled diesel engine. The hybrid turbocharger was controlled with a constant torque input until a turbocharger speed of 120.000 rpm was reached and constant power was provided at higher turbocharger speeds. Figure 3.5 shows the transient response of the turbocharger speed with the hybrid turbo and with the baseline VGT. A transient load increase was applied to the engine and both turbocharger responses were measured. As can be seen, the assisted turbo spools up more quickly and the boost pressure build up response is faster compared with the VGT configuration (Yasuaki, 2006). However, only a transient load increase is applied to the engine, no investigations were done for a sudden load step comparable with clutching in a dredge pump in dredging application or a sudden generator load rise. Moreover, no measurements are shown in relation to combustion parameters such as the air excess ratio ( $\lambda$ ).

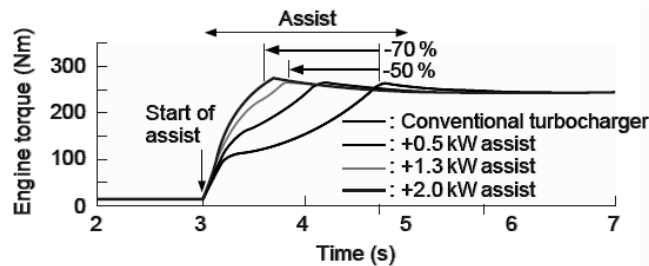


Figure 3.5: Hybrid turbo improves the overall response to develop engine torque, adapted from Yasuaki (2006)

### 3.4.2. Hybrid electric turbocharging to improve loading capability

Assisting the turbocharger improves the ability of the diesel engine to cope with load steps where a conventional turbocharged diesel engine stalls.

Katrasnik et al. (2003) has performed a simulation based investigation for the load acceptance of a six-cylinder 6.87 turbocharged MAND0826 LOH 15 automotive diesel engine which develops 162 kW at 2400 rpm. A sudden load step from 31 to 93 kW was applied to a generator driven by this engine at a speed of 1500 rpm. Next to the turbocharged diesel engine, two cases with electrical assistance to the turbocharger shaft are investigated. Three asynchronous electric motors, EM1, EM2 and EM3, were investigated to assist the turbocharger to improve its dynamic response. EM1 has an angular acceleration of  $833 \text{ rad/s}^2$ , however it was rejected because Equation (3.1) was not fulfilled. EM2 has an angular acceleration of  $3333 \text{ rad/s}^2$  and EM3 an angular acceleration of  $6667 \text{ rad/s}^2$ .

The applied load and developed engine power for the non assisted and two assisted cases (EM2 and EM3) are shown in Figure 3.6. The non assisted turbocharged engine stalled due to the limitation of injected fuel. A pneumatic controlled regulator was used to prevent excess fuel injection during dynamic operation such as accelerating or sudden load increase. A faster raise of boost pressure was obtained with the two assisted cases due to the larger quantities of fuel that was introduced in the cylinder compared with the non assisted case. As can be seen in Equation (3.1), the time needed to develop the engine power is the shortest for the case with electric motor EM3 which has a higher angular acceleration compared with the case with electric motor EM2. The power and speed figures shows an increased loading acceptance when the turbocharger is assisted, however no results are shown for other engine parameters such as the air excess ratio ( $\lambda$ ) and thermal loading indicators ( $T_{or}$  &  $T_{ex, valve}$ ).

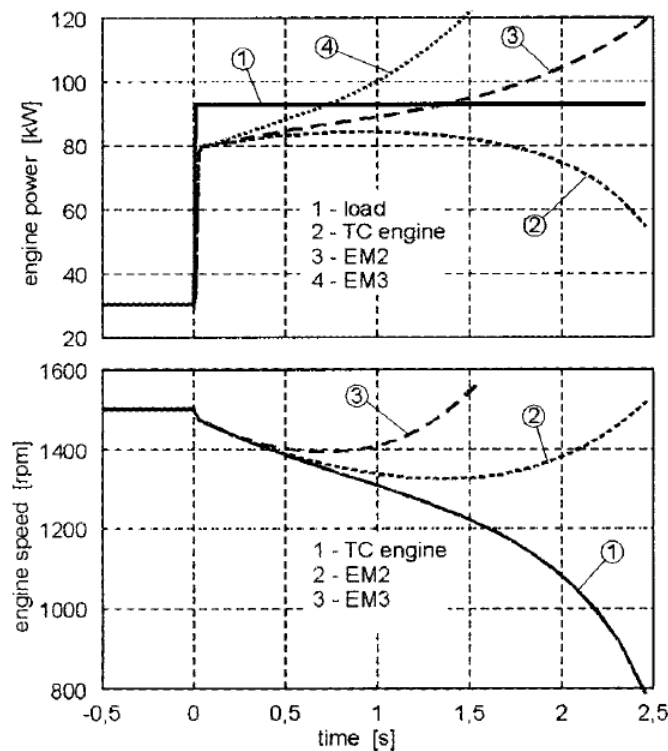


Figure 3.6: Load step acceptance for a turbocharged and electrically assisted turbocharger engine, from Katrašnik et al. (2005)

Katrašnik et al. (2005) has simulated the response of another Diesel engine rated at 131 kW 1500 rpm running a generator for a "sudden" load increase from 0 to 97 kW. The duration over which the load was increased is not mentioned. A comparison study has been done for three cases: an integrated starter/generator on flywheel (ISG) and two different types of electrical machines connected to turbocharger shaft (EMG, EM2). The "EM2" is an asynchronous electric motor with a maximum angular acceleration of  $3333 \text{ rad/s}^2$ , the "EMG" is labelled as a "high performance electric motor" with an angular acceleration of  $19860 \text{ rad/s}^2$ . The turbocharger assistance "EMG" has an angular acceleration which is about three times higher than the "EM2" assistance case. The engine speed is shown in Figure 3.7a. Both the non assisted MAN engine and the EM2 assisted case stall for the sudden load step. The EMG turbocharger assistance case and the combination of a hybrid electric tur-

bocharger and integrated starter/generator cases (ISG, ISG + EMG) enable the diesel engine to cope with the the load step. As can be seen in Figure 3.7a, the lowest engine speed drop is achieved with the case wherein both an electric motor is coupled to the flywheel, and the turbocharger is assisted with the "EMG" electric motor. Supporting the engine via a flywheel mounted electric machine is a direct measure to assist the diesel engine, power can be directly added where the power is required. For the assisted turbocharger, the engine response just after the load rise is the same as the conventional engine till the moment in time when Equation (3.1) is fulfilled. For the EMG assisting case, an increased turbocharger angular acceleration (Figure 3.7d) results in a faster development of engine power (Figure 3.7b) compared with the baseline engine (MAN), as shown in Figure 3.7b. As shown in Figure 3.7c there is no difference in the air excess ratio ( $\lambda$ ) drop just after the load step was applied. The lowest air excess ratio reached is the same for all assisting measures, but the turbocharger assisting measures reduce the recovery time compared to the ISG case, and therefore lowers the duration in which the engine operates with incomplete combustion and corresponding production of particular matter (PM) and associated visible black smoke. Ktrašnik et al. (2005) conclude that the best topology to handle load rises is to combine a flywheel mounted electric machine and an electrically assisted turbocharger. This topology combines both direct power addition to increase the power delivered to the drive train and indirect to increase the turbocharger angular acceleration which leads to a faster development of engine power compared to the non assisted case.

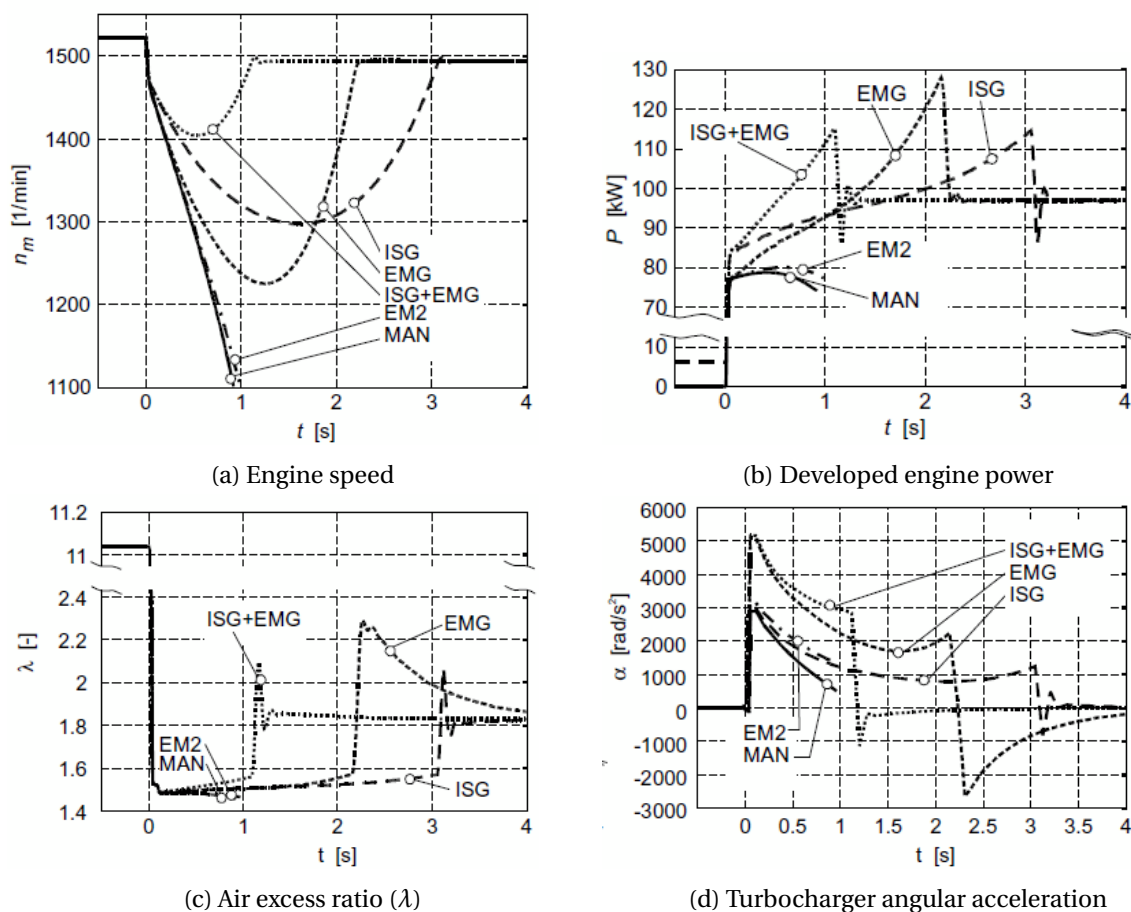


Figure 3.7: AC generator input power increase from 0 to 97 kW, from (Ktrašnik et al., 2005)

### 3.5. Operating envelope with hybrid electric turbocharging

Assisting the turbocharger is not limited to only dynamic operation. The steady state engine performance, often called the engine operating envelope, can be improved as well with a hybrid electric turbocharger, however compressor surge limits this potential. The surge region (left area of turbocharger limit in Figure 2.6) is of specific interest for the low to mid engine speed range because the operational conditions of a hybrid turbocharger in assisting mode (low air mass flow rate and high pressure ratio) may limit the power/torque output of the engine (Tavcar et al., 2011). However a simulation based research conducted by Burke (2016); Tavcar et al. (2011) conclude that the potential of assisting the turbocharger is constrained by the compressor

map width, shown in Figure 3.8. The compressor map is incomplete, only the constant speed lines (grey) are shown as function of reduced mass flow and pressure ratio. When the surge line shown in Section 2.2.4 with respect to the constant speed lines is used for Figure 3.8, it becomes clear that the operating condition of the compressor with assistance leads to operating in the unstable surge region. No other literature is found which visualises the operating conditions in the compressor map for the hybrid electric turbocharger with enabled assistance.

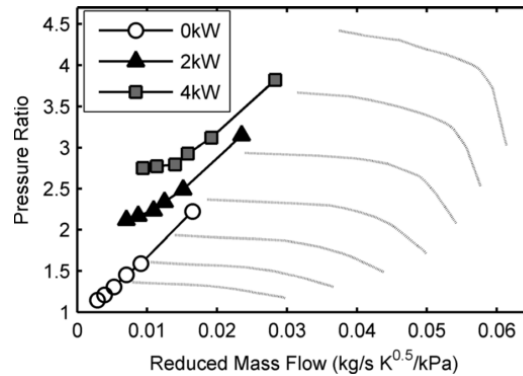


Figure 3.8: E-turbo operating showing surge problem due to compressor map width, from (Burke, 2016)

Next to the occurrence of compressor surge at low engine speeds, Tavcar et al. (2011) states as well that at higher engine speeds the provided additional power is limited by the maximum in-cylinder pressure and thermal overloading such as the exhaust gas temperature and the temperatures of the liner, piston, cylinder head, valves as well as the maximum turbocharger speed. These constraints should be implemented into the electric machine controller in order to obtain realistic results.

However, in literature multiple simulation studies show an enlarged operating envelope by electrically assisting the turbocharger. Zellbeck et al. (1999) showed, based on simulation results, the raised BMEP of a small diesel engine at lower engine speeds by electrically assisting the variable geometry turbocharger. The compressor and turbine model are based on characteristics obtained from measurements. The implementation of compressor surge is not mentioned in their research. No additional gas exchange valves such as the bypass or blow off valve are used.

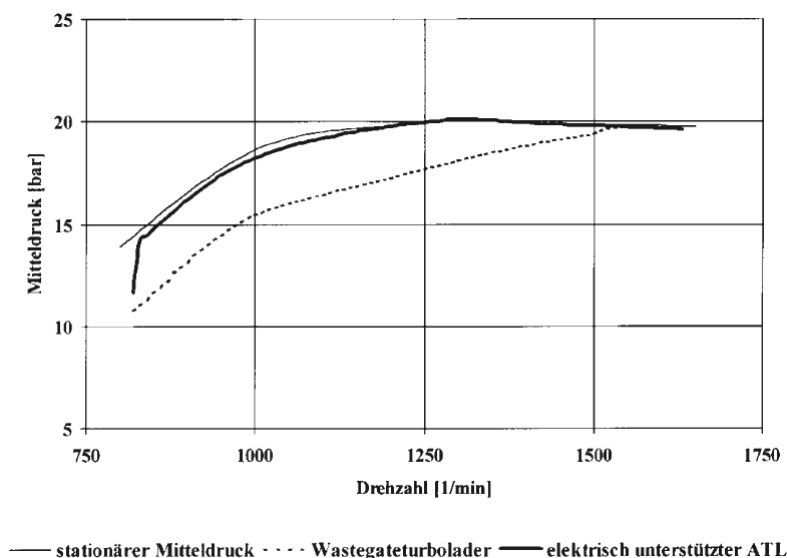


Figure 3.9: Break mean effective pressure vs. engine speed diesel engine TC with waste gate / electrically powered TC, from (Zellbeck et al., 1999)

Yasuaki (2006) concluded, based on a simulation study, that the steady state torque output can be increased for the low speed range by up to 250%, as shown in Figure 3.10. No information is given about the compressor surge phenomena.

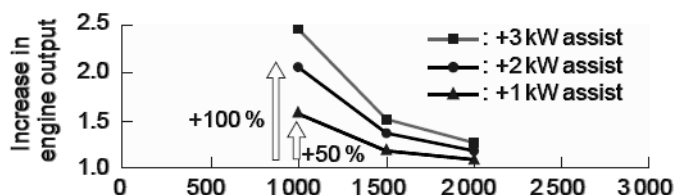


Figure 3.10: Improvement of low-speed engine torque output by assisting turbocharger, adapted from Yasuaki (2006)

Within Delft University of Technology, a Master thesis has been conducted by Rusman (2018), in which an enlarged operating envelope was found for steady state operation when the turbocharger is assisted with an electric motor. Rusman (2018) has done a simulation based research into the effects of a hybrid electric turbocharger on the operating envelope of a marine sequentially turbocharged diesel engine. One of two turbochargers was assisted by means of adding torque to the turbocharger shaft resulting in an enlarged operating envelope for the mid-speed range. The available engine power rises from about 2500 to 3000 kW with assisting the turbocharger with the electric motor. The area of the whole operating envelope is increased by 4.6% when turbocharger assistance is enabled. However the compressor model did not incorporate a measure to notice unrealistic compressor output results when it would be operated in the unstable surge region.

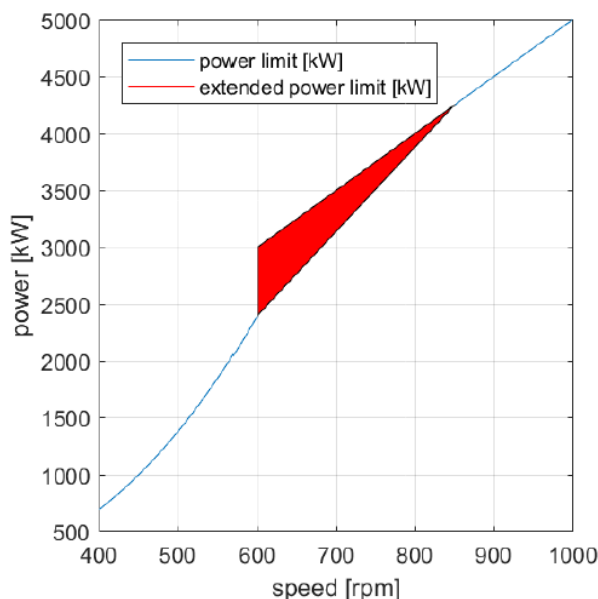


Figure 3.11: Operating envelope enlargement with enabling a hybrid electric turbocharger on the W26 marine diesel engine, from (Rusman, 2018)

### 3.6. Conclusions

Integrating an electric machine into the turbocharger setup gives two additional modes: 1. turbocompounding to increase the system efficiency, and 2. increase angular acceleration of turbocharger to improve load acceptance engine. The results from literature given above, highlights the lack of detailed results with regard to:

- The effect of turbocompounding on the system efficiency. There is a lack of detailed information about the system efficiency gain with a hybrid electric turbocharger for various engine speeds, loads and engine settings. Moreover the effect of turbocompounding on engine operating parameters such as the thermal loading, air excess ratio, pressure levels in inlet and outlet are virtually not shown or discussed;

- The effect of turbocharger assistance on the operating envelope, especially with regard to the compressor surge are hardly not discussed. Results shown in literature with regard to steady-state torque output for the low-speed range are not consistent. Several researchers did not include compressor surge behaviour in their hybrid electric turbocharger model. Research results with included compressor surge phenomena shows a very limited potential to increase the low speed engine torque output, while results without sophisticated compressor model concludes an enormous potential to boost the output torque, even up three times the baseline torque output for low engine speeds.
- Literature shows an increased load acceptance when the turbocharger is assisted. However, very limited results are shown without an extensive explanation about the control strategy and engine parameters used to determine the maximum load step capability of the engine. Moreover, virtually no other types of engine loading are investigated.

Questions that arises in this literature study are:

- Up to which extent can the engine efficiency be enhanced by extracting energy from the turbine?
- Is it possible to enhance the engine efficiency at low load and speed by supporting the turbocharger with the electric machine?
- Can the operating envelope for low to mid speed range be enlarged by assisting the turbocharger?

# 4

## Model Approach

### 4.1. Introduction

The application of a hybrid electric turbocharger for assisting the dual fuel engine, discussed in this thesis, is a typical case in which multiple disciplines are involved in one system. A simulation model should be composed to virtual prototype the system under investigation. Virtual prototyping is a widely acknowledged method for analysis and development of systems without the necessity of building them in reality. Simulation models make it possible to analyse the system's behaviour before a prototype is built, which reduces costs and possible risks, and enables the investigation of system conditions that are even hard to represent in real life testing. Multiple simulations with varying system parameters can be performed within a relative short period of time which means a considerable reduction of the time consumption. Even the real life system performance could be negatively influenced when no sufficient effort is spent on, for example, the control strategy. Virtual prototyping enables the investigation of several control strategies in an early design stage.

The given benefits of virtually prototyping rises the need for a simulation model. However, one must be available or must be developed, which can be a time consuming task. Within the department of Marine Engineering of Delft University of Technology, several engine models are available, each with a specific purpose and application area. This chapter contains the framework that is used, from model selection, matching, verification to validation.

The research question that will be answered in this chapter is:

*Is it possible to model a hybrid electric turbocharger with one of the available mean value first principle diesel engine models and validate this model with available measurement data?*

This chapter starts with a model overview to illustrate the components of the system under investigation. Secondly the modelling approach and terminology will be discussed, which is used in this chapter. A classification of available diesel engine models will be given continued with the global build-up of this model. The matching procedure will be discussed together with the matching results after which the engine model is validated. The integration of the hybrid electric turbocharger and its control strategy are discussed as well.

### 4.2. Model overview

The system under investigation in this thesis comprises two distinct parts: the dual fuel engine model and the hybrid electric turbocharger model. The integration of a hybrid electric turbocharger requires additional measures such as the electric machine controller (EAT/ETC controller) and energy storage next to the dual fuel engine. The system components are connected together via energy and sensor data flows, as can be seen in Figure 4.1.

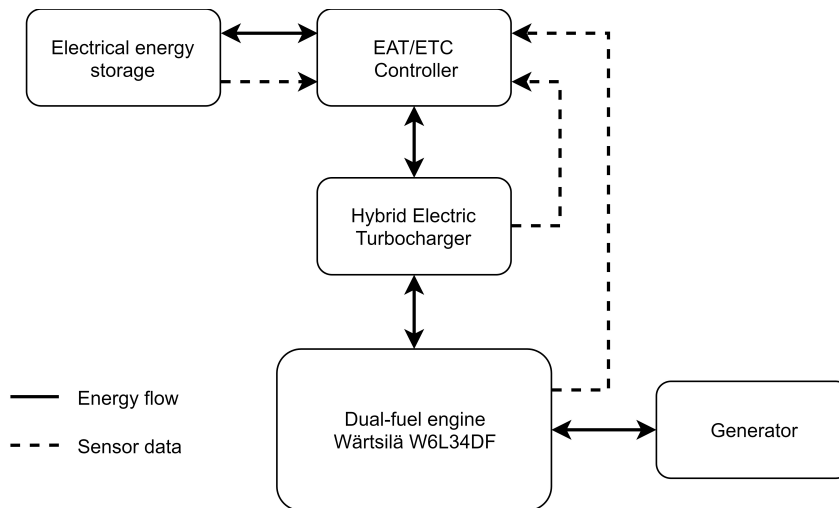


Figure 4.1: System lay-out

### 4.3. Modelling terminology

The purpose of the simulation model is to support the research activities. Therefore the model to be chosen has to represent reality up to a sufficient accurate level within the area of operation, in this case the operational envelope of the dual fuel engine. Selecting a certain simulation model, matching, verification and validation of this model can be a tough job if no systematic approach is applied. Why is a certain model selected, which parameters determine the performance of the model, how to qualify and quantify the area of application of the model? More of these questions can arise afterwards when no solid systematic approach is chosen.

Refsgaard and Henriksen (2004) have established a methodology for bridging the gap between scientific philosophy and pragmatic modelling, which is shown in Figure 4.2. The methodology is build up of four main elements: reality, conceptual model, the model code and, last, the model itself. The inner arrows describe the processes that relate those four elements and the outer circle refers to the procedures to evaluate the credibility of those processes. Refsgaard and Henriksen (2004) used this methodology for developing a framework for creating models that describe water flows, water quality and ecology. However their theoretical approach can be used for engine modelling as well.

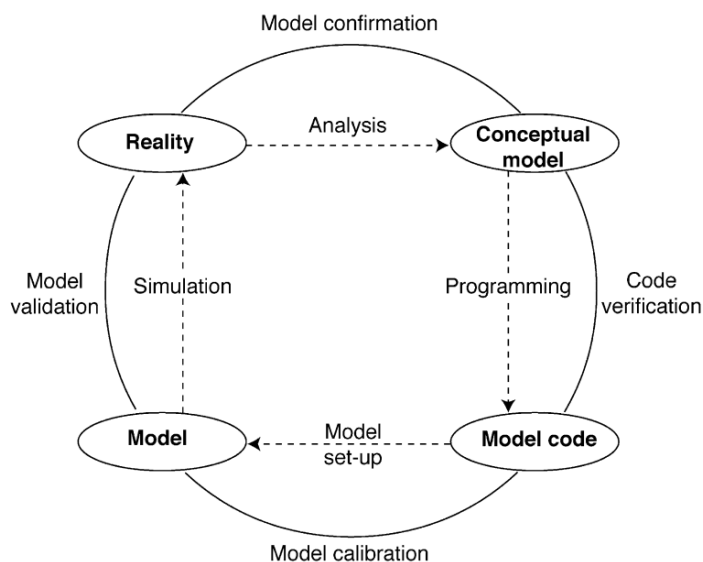


Figure 4.2: Elements of a modelling terminology, from Refsgaard and Henriksen (2004)

Reality comprises the study area, in this case the dual-fuel engine. The conceptual model contains equations, governing relationships or natural laws that are used to describe reality. The conceptual model is composed based upon measurements and observations of operating engines. The model code comprises the computer

program which governs the aspects given in the conceptual model. The input variables and parameters of the conceptual model must be implemented in the model code in such a way, that different study areas can make use of this model code. In this case, the model code is the generic dual fuel engine model. Code verification is necessary to check if the model code output is a true representation as intended with the conceptual model. In this case, code verification comprises, for example, the check if the fuel consumption lowers when the engine efficiency parameter is raised while keeping the engine power output the same. The model set-up process is used to convert the generic model into a mean-value model for a certain engine type, in this case the Wärtsilä 6L34DF dual fuel engine. Engine related researchers mostly call this process matching instead of calibration. Matching is used to check if the engine predicts the operational behaviour within a certain accuracy range. After matching, the last step is to validate the model. Independent operational measurements has to be available to compare the model's prediction with reality.

The presented methodology, proposed by Refsgaard and Henriksen (2004), will be further elaborated in this chapter from the selection of a certain conceptual model up to the validation procedure.

## 4.4. Engine model classification

In literature various models are mentioned which all fit for a particular research objective. These engine models can be divided into analytical and empirical models.

### 4.4.1. Difference between analytical and empirical engine models

The empirical models consist of lookup tables and/or best-fit polynomials which are based on measured data. The benefit of empirical models is the low computational time required and accuracy depending on the availability of measured data. The main drawback of empirical relationships is that they are not generic, so the relationship is only meant for a specific engine type. The empirical model generates the same output as measured in reality, therefore it can only be used to represent the engine with the same operating conditions as during the measurements. When the input parameters for the empirical models change, due to the selection of other operational conditions, the predictions of the empirical model should be carefully interpreted to prevent invalid predictions. The same holds for changing the engine size, or even more using another engine type, without validating the empirical model with measurements from the changed engine. The second drawback is that it is not possible to generate other engine output conditions than measured because the only relationship available is the measured engine input and output used for setting-up the empirical relationship (Schulten, 2005).

The analytical models have in common that they consist of a set of algebraic and differential equations which are derived from physical processes. Physically based models are developed using established scientific principles, such as the laws of physics and chemistry to describe, for instance, the processes such as heat and flow dynamics in the engine core. This way of modelling processes give much more insight into the phenomena of certain processes compared with the black box approach of an empirical relation. Loonstijn (2016) states the difference between analytical and empirical models: "physical models are able to **predict** outcomes based on **proven theory**, whereas empirical models can **replicate** outcomes based on **experimental data**".

Loonstijn (2016) mentions an intermediate class of models that can be referred to as semi-empirical models. These models incorporate physical properties which are grouped together into groups of dimensionless numbers. The advantage of dimensionless numbers is that they reduce the amount of measurements needed to determine the system's performance (Eriksson, 2007). Another benefit of dimensionless numbers is that they can be used for scaling purposes such as the sizing of different components (Loonstijn, 2016). Schulten (2005) states that there is not a clear distinction between analytical and empirical models found in practice. Every analytic model at some level incorporates empirical parts.

### 4.4.2. Available analytical engine models

Schulten (2005) gives a list of analytical engine models in order of complexity that can be found in literature:

- CFD models,
- Phenomenological multi zone models,
- Filling and emptying / crank angle models,
- Mean value models,
- Transfer function models.

The CFD-based and phenomenological multi zone models provide detailed information about the gas dynamics in the cylinder process. However this type of model does not cover the overall engine operating conditions. The filling and emptying model comprises the inlet receiver, cylinder and outlet receiver. The model's analytical expressions are solved for every crank angle, therefore these models are classified as crank angle models. This way of modelling the engine processes is a very time consuming way of calculating the in-cylinder processes. This is of particular interest when the main research is related to the in-cylinder combustion processes. A crank angle engine model is available within Delft University of Technology, called the Diesel C model. If no in depth in-cylinder processes needs to be modelled, the time step of one crank angle can be replaced by a mean value model which levels out these processes over a whole cycle/revolution. Overall engine parameters such as maximum in-cylinder pressure and temperature, air excess ratio, turbocharger speed, inlet receiver and outlet manifold conditions can be modelled with a mean value model (Schulten, 2005). Two mean value models are available, the Diesel A and Diesel B model which will be further discussed in Section 4.4.3. The simulation purpose of this thesis requires no outputs from gas dynamics, or crank angle based processes. Therefore the mean-value model is selected, because it suits the research objective. The available diesel engine models within the department of Marine Engineering of Delft University of Technology are shown in Table 4.1.

Table 4.1: Available engine models

Engine model	Type of model	Dual-fuel model	Turbocharger model
Diesel A	Mean-value	Yes	Power balance (Buchi)
Diesel B	Mean-value	Yes	Model to represent compressor and turbine characteristics
Diesel C	Crank angle	Yes	Not implemented

#### 4.4.3. Selection of appropriate mean-value engine model

The Diesel B model is selected to be used in this research as conceptual model because it enables the research of turbocharger power take in/out on system efficiency, gas exchange as well as thermal loading. The mean value models are of particular interest in this research due to the predictive capabilities of the overall engine parameters. Two mean value models have been developed at Netherlands Defence Academy (NLDA) and Delft University of Technology (TU Delft), a simplified mean value model (Diesel A model) for engine arrangement research, and a more comprehensive mean value model (Diesel B model) for more detailed research into the engine dynamics. Geertsma et al. (2017) have chosen the "Diesel A model" to simulate the diesel engine with as particular interest the thermal loading of the engine. The "Diesel A model" comprises the turbine inlet temperature ( $T_{or}$ ), air excess ratio ( $\lambda$ ) and exhaust valve temperature ( $T_{exh, valve}$ ) to quantify the thermal loading of the engine. However, a very simple first order method is used to predict the turbocharger dynamics. A power balance and a time constant for the time related dynamics is used to predict extracted turbine power and boost air conditions after the compressor. However, it does not include compressor limiting factors such as surge, maximum speed and choked flow because no compressor and turbine characteristics are used. Next to the turbocharger limits of the "Diesel A model", the five-point Seiliger cycle was incorporated in the cylinder model, while the six-point Seiliger cycle was already included in the "Diesel B model". Later on, Geertsma et al. (2017) improved the "Diesel A model" with the six-point Seiliger cycle, but the absence of a sophisticated turbocharger model resulted in the selection of the Diesel B model.

Table 4.2: An indication of the complexity difference between the Diesel A and B models. Loonstijn (2016)

	Diesel A model	Diesel B model
Input parameters	22	148
Continuous integrators	2	17
Memory blocks	0	14
Subsystems	22	291

The Diesel B model is the model code used in this research because of the gas exchange model, the analytical turbine-compressor model and the possibility to model thermal overload as well as engine operating conditions due to back pressure.

The development of this model is done by Dijkstra (2004); Grimmelijs et al. (2007); Schulten (2005) An extensive explanation of the Diesel B model can be found in Dijkstra (2003, 2004); Stapersma (2010a,b,c,d, 2013) Grimmelijs et al. (2007) Dijkstra (2004) Stapersma (2010a) and Schulten (2005) and is available at Delft University of Technology within the department of Maritime and Transport Technology. The model code is pro-

grammed in Matlab & Simulink, which includes facilities for analysis as well as modelling and simulation of amongst others continuous systems.

The Diesel B model is a complex model compared with the Diesel A model, because it requires many parameters from the reality, which are partly not available. Table 4.2 shows the number of elements and parameters which indicates the complexity difference between the A and B model.

Sapra et al. (2017) have chosen the "Diesel B" mean value model because of the gas exchange model, the analytical compressor-turbine model for researching the effects of different engine valve overlaps and turbocharger configurations against back pressure. Loonstijn (2016) has chosen the "Diesel B model" for conducting simulations for different turbocharger configurations because of the simple first order turbocharger model in the A model. Rusman (2018) merged the analytical turbocharger model from the Diesel B model with the improved Diesel A model from Geertsma et al. (2017). This approach to build a "in between model" is not the approach chosen in this thesis because it adds a new model to the library of the department without improving the modelling capabilities other than available in the A or B model.

## 4.5. Model build-up

In this section, the background of the dual-fuel mean value Diesel B model will be given. First, the two basic elements that are used to compose the model will be discussed, thereafter the differences between the well-known Diesel B model and the dual fuel combustion model of Georgescu et al. (2016b) must be addressed. The last part of this section will deal the turbocharger fundamentals that are important to understand for the hybrid electric turbocharger operation including compressor limitations.

The dual fuel model composed by the writer is built up of the newest Diesel B model, version B5\_44\_434\_2016-12-13. All the gas parts included by Georgescu et al. (2016b) in the older Diesel B model, version B5\_44\_434\_2013\_07\_30 DF, are merged into the latest version of the Diesel B model.

### 4.5.1. Dual fuel engine

The chosen engine model is the mean value "TU Delft Diesel B" model, version B5\_44\_434\_2016-12-13. Research, development and modelling of gas injection and dual fuel combustion was done by Georgescu et al. (2016a) during her Master thesis internship. Georgescu et al. (2016a) included the dual fuel Diesel combustion into the Diesel B model, version B5\_44\_434\_2013\_07\_30, and these additions will be further elaborated in Section 4.5.3. Dijkstra (2004); Schulten (2005); Stapersma (2010a,b,c,d) describe the background and build-up of the general Diesel B model in detail. Therefore only the headlines of this model with respect to the application of a hybrid electric turbocharger for the dual-fuel engine will be discussed.

### 4.5.2. Basic elements of B model

The Diesel B model is built up of several sub-models, as can be seen in Figure 4.3. Two distinct sub-models are used in this model, the volume element for the upper and the resistance element in the lower horizontally placed elements. The primary inputs of this model are the desired engine speed ( $n_{eng,des}$ ) and propeller/generator load ( $P_{load}$ ). The fuel rack controller uses as input the error between actual engine speed ( $n_{eng}$ ) and the desired engine speed ( $n_{eng,des}$ ) and has as output the fuel mass flow ( $\dot{m}_{fuel}$ ) going into the cylinder. The primary output of the engine is engine torque  $M_{eng}$ . Secondary inputs of the model are the ambient pressure ( $p_{amb}$ ) and temperature ( $T_{amb}$ ) and the cooling water temperature ( $T_{cw}$ ) Dijkstra (2004). The difference in delivered engine torque  $M_{eng}$  and engine load  $M_{gen}$  is integrated to calculate the engine speed  $n_{eng}$ , however this later part is not shown in Figure 4.3.

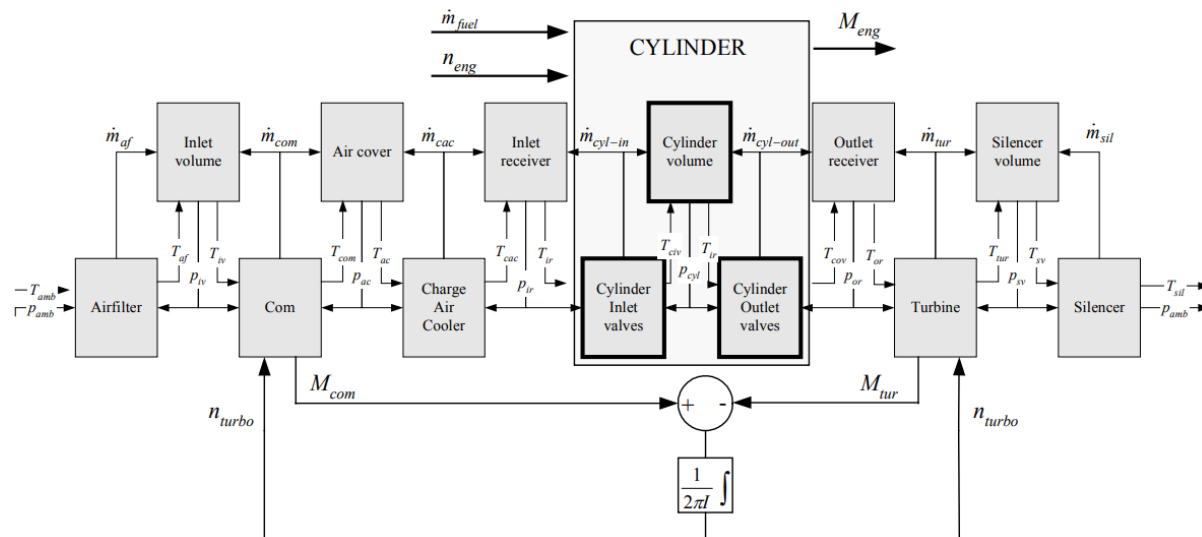


Figure 4.3: Diesel engine model concept, from Dijkstra (2004)

The control volumes (inlet volume, air cover, inlet, outlet receiver and silencer volume) make use of the conservation of mass and energy to calculate its outlet pressure and temperature based upon the net mass flow through this type element. The element’s internal mass is instantaneously calculated by integrating the net mass flow. The temperature of the volume element’s internal mass results from the energy flow balance. The temperature and mass flow from the previous resistance element is the ingoing energy. The outgoing mass flow together with the volume’s internal temperature is the outgoing energy flow. Resistance elements are used to connect the control volumes together. The resistance element incorporates an orifice for which the momentum equation is used to calculate a mass flow based upon the resistance inlet and outlet conditions. An extensive explanation of the incorporated formulas for these volume and resistance elements can be found in (Schulten, 2005) and in (Loonstijn, 2016) Appendix E.

**4.5.3. Characterization of cylinder process**

The cylinder sub model contains an open and closed thermodynamic system. The open system is used for the gas exchange, fresh air induction into the cylinder and expulsion of the combustion products into the exhaust manifold, as shown in Figure 4.4. The open and closed cylinder processes take place within every two crankshaft rotations.

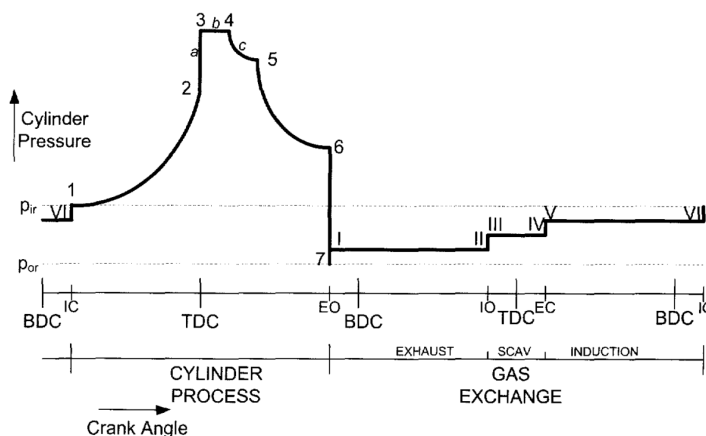


Figure 4.4: Diesel process divided in discrete processes, from Schulten (2005)

The closed cylinder process contain the six point Seiliger cycle for both the diesel as the dual-fuel cylinder process. The six parts of this closed cylinder process for dual-fuel combustion are equal to the diesel combustion. Therefore only a brief explanation will follow.

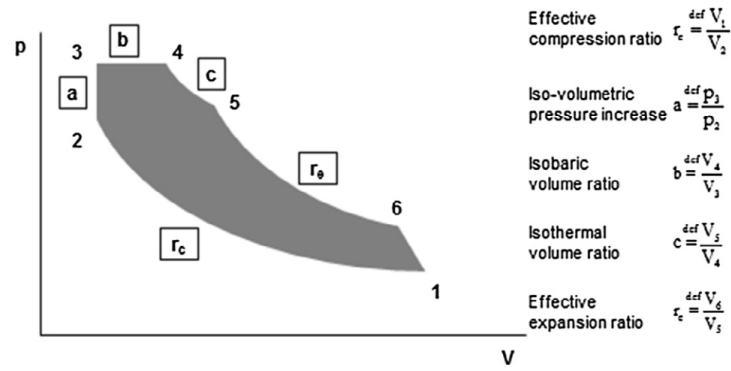


Figure 4.5: Typical six point Seiliger or dual cycle in pressure ( $p$ ) – volume ( $V$ ) plot, consisting of compression (1–2), isochoric combustion (2–3), isobaric combustion (3–4), isothermal combustion (4–5) and expansion (5–6), from Stapersma (2010a)

The six parts of the closed cylinder process are shown in Figure 4.4, polytropic compression (1-2), isochoric combustion (2-3), isobaric combustion (3-4), isothermal combustion (4-5) and polytropic expansion (5-6). The equations used for the six-point Seiliger process are given in Table 4.3.

Table 4.3: Seiliger cycle equations, from Stapersma (2010a)

Seiliger stage	Volume $V$	Pressure $p$	Temperature $T$	Specific work $w$	Specific heat $q$
Compression 1-2	$\frac{V_1}{V_2} = r_c$	$\frac{p_2}{p_1} = r_c^{k_a}$	$\frac{T_2}{T_1} = r_c^{(k_a-1)}$	$w_{12} = \frac{R_a(T_2-T_1)}{k_a-1}$	-
Isochoric combustion 2-3	$\frac{V_3}{V_2} = 1$	$\frac{p_3}{p_2} = a$	$\frac{T_3}{T_2} = a$	-	$q_{23} = c_{v,a}(T_3 - T_2)$
Isobaric combustion 3-4	$\frac{V_4}{V_3} = b$	$\frac{p_4}{p_3} = 1$	$\frac{T_4}{T_3} = b$	$w_{34} = R_a(T_4 - T_3)$	$q_{34} = c_{p,a}(T_4 - T_3)$
Isothermal combustion 4-5	$\frac{V_5}{V_4} = c$	$\frac{p_4}{p_5} = c$	$\frac{T_5}{T_4} = 1$	$w_{45} = R_a T_4 \ln(c)$	$q_{45} = R_a T_4 \ln(c)$
Expansion 5-6	$\frac{V_6}{V_5} = \frac{r_{e0} r_c}{bc}$	$\frac{p_5}{p_6} = \left(\frac{r_{e0} r_c}{bc}\right)^{n_{exp}}$	$\frac{T_5}{T_6} = \left(\frac{r_{e0} r_c}{bc}\right)^{n_{exp}-1}$	$w_{45} = \frac{R_a(T_6-T_5)}{(n_{exp}-1)}$	-

Schulten (2005) has developed a model for calculating the Seiliger shape parameters based on measurements on a marine diesel engine. These equations (left column Table 4.4) are engine speed and fuel flow dependent. Georgescu et al. (2016b) has done a simulation-based research to find these shape parameters for the combustion of natural gas in a diesel engine. Georgescu et al. (2016b) used the Diesel C crank angle based model for simulating the dual-fuel combustion. This C model uses the Vibe parameters to represent the heat release rate of natural gas combustion with diesel as pilot ignition. Empirical formulas were composed based upon the air excess ratio ( $\lambda$ ), total heat input ( $q_{in}$ ), and temperature after compression ( $T_2$ ) or temperature after isochoric combustion ( $T_3$ ) and specific heat constant volume ( $c_v$ ) and pressure ( $c_p$ ). The empirical model for natural gas combustion is built into the Diesel b model. However, this empirical model for heat release rates are done with the geometrical dimensions of the SWD12V280 diesel engine which is a Stork Werkspoor diesel engine which is rated at 3660 kW at 1000 rpm with a bore x stroke of 280 x 300 mm. The major drawback of empirical models is that they are not generic, as explained in Section 4.4. Empirical models generate the same output for certain conditions as simulated in the crank angle based C model. Other operating conditions, in this case changing the engine type, cannot be done with these empirical models.

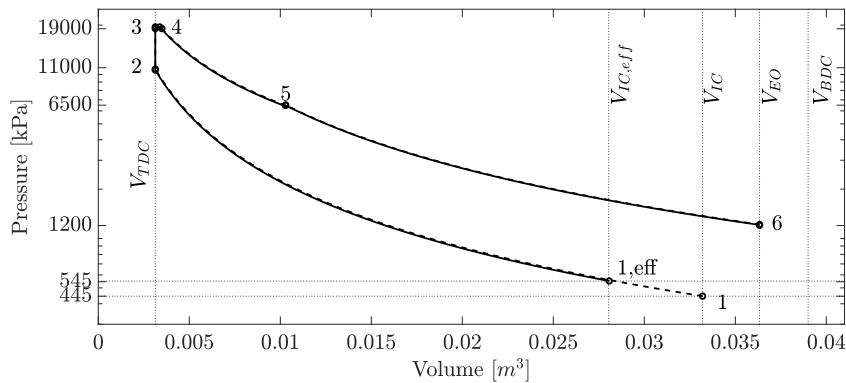
Table 4.4: Comparison Seiliger shape parameters for Diesel and Dual-fuel combustion

Diesel mode	Dual-fuel mode
$a = 1 + \frac{(X_N + X_c) \cdot \tau_{id} \cdot q_{cb}}{c_v \cdot T_2}$	$a = 1 + q_{in} \cdot \frac{c_1 \cdot e^{-c_2 \cdot \lambda^{c_3}} \cdot \lambda^{c_4}}{c_p \cdot T_2}$
$bb = b \cdot a = 1 + \frac{X_b \cdot q_{cb}}{c_p \cdot T_2}$	$b = 1 + q_{in} \cdot \frac{c_5 \cdot e^{-c_6 \cdot \lambda^{c_7}}}{c_p \cdot T_3}$
$c = e^{\frac{q_{45}}{R_{45} \cdot T_4}}$	$c = e^{\frac{q_{45}}{R_{45} \cdot T_4}}$

#### 4.5.4. Advanced Miller timing

In the gas exchange sub model of the Diesel B model, the pressure in the cylinder just after inlet valve closure is assumed to be equal to the pressure in the inlet receiver, so  $p_1 = p_{ir}$ . This can be assumed for inlet valve closure up to a certain degree before BDC without considerably influences on the cylinder process. However, the W6L34DF has advanced Miller timing where the inlet valve closes  $\approx 55^\circ$  before BDC, therefore this assumption is found to be not valid for advanced Miller timed engines. Zammit et al. (2015) states that the early closure of the inlet valve leads to less maximum valve lift. The acceleration of the valve train is limited, therefore the inlet valve lift is reduced when a shorter opening duration is used. Lowering the maximum valve lift has an additional restrictive effect on the inlet mass flow, which increased the pressure drop over the inlet valves. In the Diesel B gas exchange submodel, only geometric parameters are used to calculate the compression ratio ( $CR_g$ ). Zammit et al. (2015) shows that other parameters of the gas exchange, such as the valve lift, are not incorporated when only geometric parameters are used. The introduction of an effective compression ratio ( $CR_{eff}$ ) enables to include other parameters by replacing the volume at which the inlet valve closes, to the volume at which the in-cylinder pressure first reaches the inlet receiver pressure. Figure 4.6 shows the in-cylinder Seiliger diagram for both the initial in-cylinder matching without and with an effective compression ratio.

The rejection of the assumption ( $p_1 = p_{ir}$ ) was found to be necessary due to the prediction of a too high exhaust mass flow ( $\dot{m}_{exh}$ ) without an effective compression ratio ( $CR_{eff}$ ). Using  $p_{ir} = 4.5$  bar gave satisfying results for nominal power and speed, however matching failed for  $p_{ir} = 5.5$  bar because a far too high induction cylinder mass flow was predicted ( $\dot{m}_{ind}$ ). Moreover, according to R. Teir, product manager of the Wartsila 34DF engine group, the inlet receiver pressure ( $p_{ir}$ ) is about 5.2 - 5.4 bar. This rises the question why the Diesel B model output is far above the desired mass flow. A solution was found in the effective compression ratio theory explained above. Figure 4.6 shows the implementation of this theory, where the effective compression ratio ( $CR_{eff}$ ) leads to the same maximum cylinder pressure ( $p_3$ ) prediction as the initial approach. Introducing another  $\approx 20^\circ$  up to the given VIC of  $\approx 55^\circ$ , gave an appropriate engine exhaust mass flow ( $\dot{m}_{exh}$ ).

Figure 4.6: Seiliger cycle for W6L34 diesel mode with  $V_{IR,eff}$  approach

#### 4.5.5. Turbocharger fundamentals

The characteristics of the turbo machine have large influence on the part load behaviour and transient performance of the engine. A sophisticated turbo machine model is required to describe the inlet receiver conditions for various loads and engine speeds. In 1997, Stapersma (1997) started to develop an analytical model which requires a number of parameters to fit the single stage characteristics of a turbomachine. Both the compressor

and turbine model calculates its mass flow and efficiency based on the turbocharger speed and the pressure levels over the compressor and turbine. Stapersma (1997) introduced four shape parameters to fit this analytical model better to actual turbomachines: the loading of the stage, the sensitivity to incidence losses, mismatch between stator and rotor and margin to choking were introduced. Dijkstra (2003) improved the turbocharger model and introduced three additional shape parameters to improve the matching of the model with measurements. An overview of the equations used in the turbomachine models can be found in Appendix B. In 2013, Stapersma (2013) published an updated version of the turbocharger model which is used in the latest Diesel B model. A detailed derivation of all the equations and reasoning behind this model can be found in: "A general model for off-design performance of a single stage turbomachine Stapersma (2013)". The turbomachine equations, given in Appendix B, are used to visualise the compressor model, as shown in Figure 4.7. The input parameters (pressure ratio and compressor speed) leads to a certain compressor mass flow ( $\dot{m}_{com}$ ) and compressor efficiency ( $\eta_{com}$ ). This compressor map is used to assess the compressor model's behaviour during simulations. The surge line is an important boundary in this compressor map which should not be crossed into the surge region.

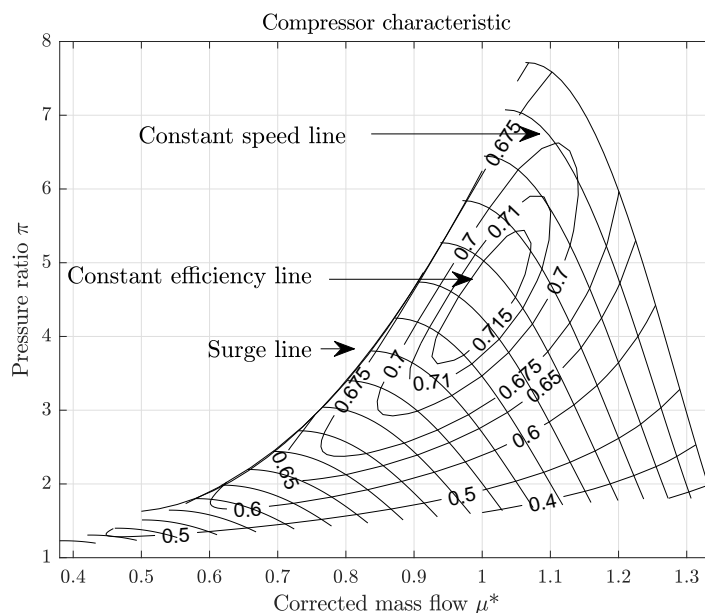


Figure 4.7: Visualisation of compressor equations

## 4.6. Dual-fuel model verification

Verification is the first check after building a model if the outcomes comply with the theoretical knowledge used while building the model. The focus of the verification process is to check if the model simulates trends and processes correctly. For more than a decade, the Diesel B model is under investigation within the marine engineering department of Delft University of Technology. Therefore it is assumed that this Diesel B model is verified due to the extensive usage of this model in various Master assignments and PhD researches. No verification is done for both the latest Diesel B and dual-fuel Diesel B from Georgescu et al. (2016b). After merging the dual fuel combustion into the latest Diesel B model, the new composed dual fuel engine model, used in this thesis, is verified by comparing 244 signals of this model with both the latest conventional Diesel B model as well as the dual fuel model from Georgescu et al. (2016b).

Comparing the outputs of both dual-fuel models manually took too much time because implementation errors are hard to find in the Diesel B model. Therefore a comparison tool was developed to compare 244 variables of both models in order to verify the composed dual-fuel model with the dual-fuel model from Georgescu et al. (2016b). This manner of comparing models resulted in the elimination of several implementation errors which sneaked into the model when adding the dual fuel parts in the latest Diesel B model. As an example, Figure 4.8 and 4.9 show the similar behaviour of Georgescu et al. (2016b)'s dual-fuel model with the new composed dual-fuel model. The new composed model is verified for dual-fuel combustion, assuming that the older dual-fuel model, developed by Georgescu et al. (2016b), was verified during her Master thesis work. Georgescu et al. (2016a) have written a paper about the dual-fuel theory, which rises the quality of the older dual-fuel model.

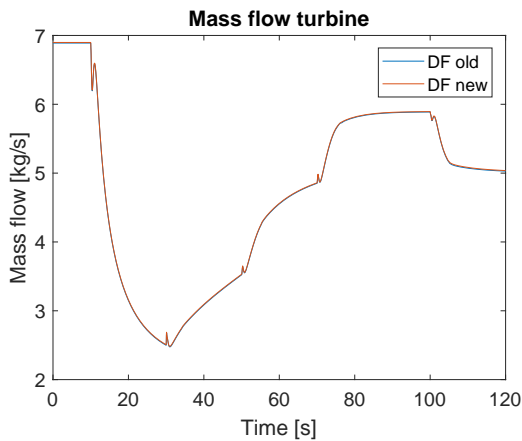


Figure 4.8: Comparison: Exhaust mass flow

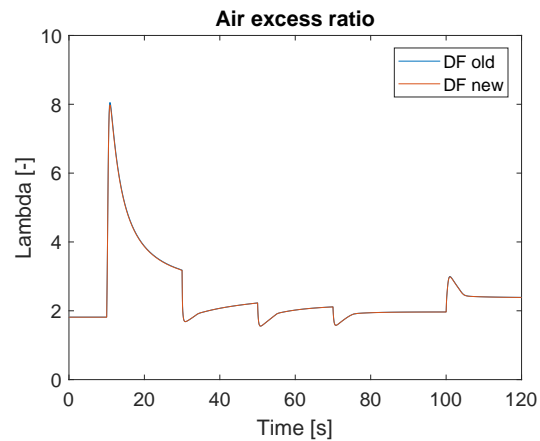


Figure 4.9: Comparison: Air excess ratio

## 4.7. Matching of the engine model

At this point in the modelling approach, the latest Diesel B model is extended with dual-fuel combustion and is verified with an earlier version. This means that there is a generic engine model available for simulating the Wärtsilä 6L34DF dual fuel engine. Next step is the matching procedure to convert the generic dual fuel B model into a simulation model that predicts the operational behaviour of a specific engine. The Wärtsilä 6L34DF is selected to be used in this research, because the engine is used in one or more Royal IHC's dredging vessels and, therefore, engine data is available. Detailed engine parameters can be found in Appendix A.

### 4.7.1. Matching parameter groups

The chosen Diesel B model is a complex simulation model that requires a large number of input parameters, as mentioned earlier in Section 4.4.3. These parameters can be divided into two groups: physical and model parameters. The physical parameters exist in reality, which are for example engine dimensions, material properties or other parameters that can be found in reality. The model parameters do not exist in reality but are required for the model. Certain compressor shape parameters do not exist in reality, but are required to represent compressor behaviour which can be measured in reality.

Schulten (2005) divides the parameters in three groups: the known, the arbitrary and the unknown parameters. The first category, the known parameters, can be found in product data, classification documents or can be found in literature. These are, for example, the cylinder dimensions, number of valves, crank angle timing of valves, fuel and fresh air mass flows, temperatures and pressures at certain (but not for all) locations. The second category, the arbitrary parameters, are unknown but these parameters lie in most cases within a certain range based on matching expertise. The last category contains the unknown parameters which are used to adjust the model's predictions to the measurement data. An example is the charge air cooler dimensions which can be used to adjust the air temperature in the inlet receiver, or the friction related parameters to match the engine output torque up to the value which can be found in engine related documents.

### 4.7.2. Matching assumptions

The data used for matching is gathered from the engine manufacturer Wärtsilä. The data contains measurements for four engine loading points at nominal speed for the Wärtsilä 9L34DF, which is the parent engine of the 6L34DF. The quality of the matching data can be assumed to be higher than the engine data provided in the general product guide. Although the measurement data is given for the 9-cylinder 34DF engine, these values are scaled down to the six-cylinder engine by using the following assumptions:

- Charge air, fuel and exhaust mass flows are linearly scaled down as function of number of cylinders
- Temperature and pressure level for inlet, outlet and cylinder are not a function of number of cylinders
- Turbocharger delivers a linearly scaled down mass flow at constant turbocharger speed, compressor inlet and outlet pressure and temperature levels

### 4.7.3. Matching approach

The arbitrary and unknown parameters must be varied one by one in order to understand its influence on the model's output. However, varying one parameter could affect the output of multiple outputs. Therefore

matching expertise is needed to find the relationship between certain model parameters and their influence on the processes occurring in the Diesel B model. To reduce the time needed for getting matching expertise, Loonstijn (2016) has applied a Design of Experiments (DOE) method in his Master thesis for matching the Diesel B model with available data. A systematic method was constructed to determine the relationship between parameters affecting a process and the output of that process. In general, this method replaces the manually, large time demanding model matching task, with an automated systematic approach. The output of this DOE methodology is a set of parameters which gives the best fit for the point of interest between simulation output and available data of the engine. However, developing this DOE method did not fit within the scope of this thesis assignment, therefore matching the Diesel B model to the available data is done manually. There is no clear step-wise approach for conducting this matching process in a proper way. Dijkstra (2003) proposes a high-level matching procedure.

The required maximum deviation between simulation predictions and measurements is up to the modeller, he/she decides if the model is well matched, depending on the availability of data and time. The head lines of this manual fitting task will be discussed in the next subsections and are based on the matching procedure given in Dijkstra (2003).

#### 4.7.4. In-cylinder process matching

The cylinder model with the diesel engine model was reduced to the block diagram as shown in Figure 4.10. The valve timing, as shown in Figure 4.11, is used to define the in-cylinder volumes corresponding to the opening and closing of the valves. The induction mass flow ( $\dot{m}_{ind}$ ) is determined by the displacement of the piston and the valve timings while the scavenge mass flow ( $\dot{m}_{sc}$ ) depends on the resistance of the inlet and outlet valves. Unfortunately, the outlet receiver was connected to the cylinder as a volume element, due to the lack of available outlet receiver data which does not benefit the matching procedure of the cylinder sub-model. Instead of putting a constant known outlet receiver pressure ( $p_{or}$ ) and temperature ( $T_{or}$ ) on the cylinder model, a constant exhaust mass flow ( $\dot{m}_{exh}$ ) was used from outlet receiver to the turbine.

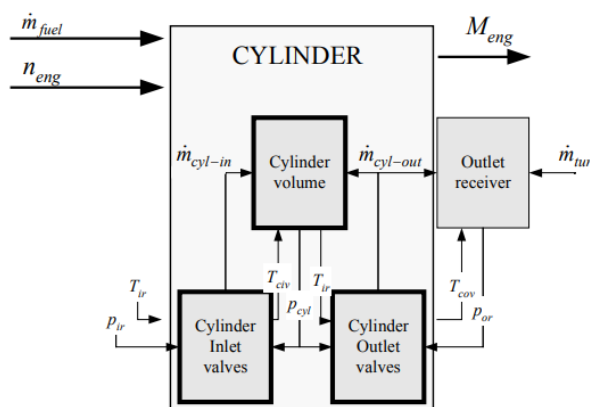


Figure 4.10: Matching cylinder with inlet pressure and temperature and exhaust manifold mass flow, rebuild from Schulten (2005)

The input of the cylinder process is the engine speed ( $n_{eng}$ ), the fuel mass flow ( $\dot{m}_f$ ) and mass of fuel per cycle ( $m_{f,cycle}$ ), the inlet receiver pressure ( $p_{ir}$ ), temperature ( $T_{ir}$ ) and composition ( $x_{ir}$ ). The parameter of the cylinder sub-model that influences the scavenge air mass flow ( $\dot{m}_{sc}$ ) from inlet to outlet receiver, is the resistance of the valves. Next to the resistance parameter of the valves, the isochoric combustion parameters ( $X_{a,c}$  and  $X_{a,n}$ ) and combustion ratio parameters ( $X_{b,c}$  and  $X_{b,n}$ ) can be varied until the cylinder power output sufficiently match the available engine data for four engine loadings at nominal speed. The cylinder output, used to determine the quality of matching, are for example the peak cylinder pressure ( $p_3$ ), fuel consumption ( $sfc$ ) and engine torque ( $M_{eng}$ ).

TDC	Top Dead Center
BDC	Bottom Dead Center
IVO	Inlet Valve Opens
IVC	Inlet Valve Closes
EVO	Exhaust Valve Opens
EVC	Exhaust Valve Closes
FI	Fuel Injection starts

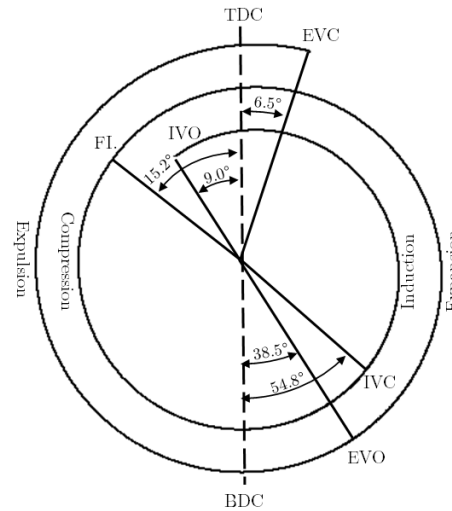


Figure 4.11: Valve timing diagram for W6L34DF

#### 4.7.5. Turbocharger matching

The compressor and turbine sub-models should be disconnected from the engine model. The compressor outlet conditions ( $p_{com}$ ,  $T_{com}$  and  $\dot{m}_{com}$ ) should be at least known, but preferably the inlet conditions ( $p_{inlet}$ ,  $T_{inlet}$ ) are also given in the available engine data. When the compressor and/or turbine map are available, this data can be used to match the scaling parameters of the compressor/turbine sub-model. However, for the W6L34DF both the compressor as well as the turbine map are not available.

Based on the pressure ratio of the compressor ( $\pi_{com}$ ) and fresh air mass flow ( $\dot{m}_{com}$ ), the matching procedure of the compressor and turbine is done. No compressor outlet temperature ( $T_{com}$ ) is available, which does not benefit the quality of matching. The point of best compressor efficiency usually lies somewhat lower than the nominal operating point of the engine (Dijkstra, 2003). For the W6L34DF it is assumed that the compressor point of best efficiency (BEP) lies in the nominal operating point (NOP) of the engine because this dual fuel engine type is mostly used for generator sets to produce electrical power at nominal power and speed.

#### 4.7.6. Inlet/outlet piping matching

The inlet and outlet piping can be matched when pressure drops over these components is available. The resistive effect of the resistance models (orifice equation) can be adjusted with the effective area of these components. The pressure drop together with the component's mass flow have to be available from product data. The next step is to reconnect the compressor to the inlet piping, and the turbine to the outlet piping as shown in Figure 4.14. Both the inlet and outlet conditions must be checked because small deviations in component conditions leads to new equilibrium for the reconnected system.

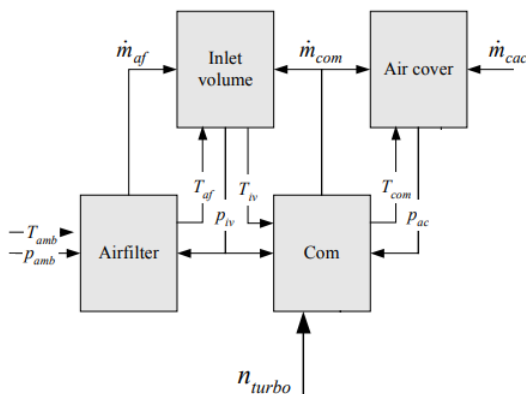


Figure 4.12: Block diagram used for matching inlet parameters

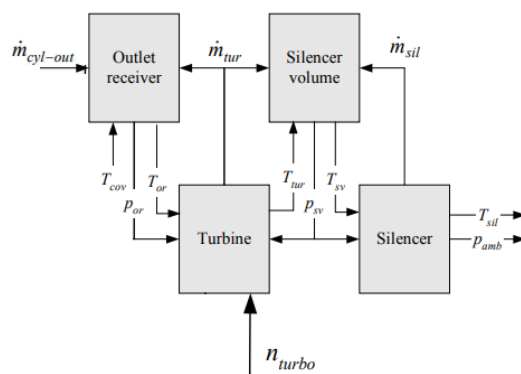


Figure 4.13: Block diagram used for matching outlet parameters

Figure 4.14: Matching inlet and outlet piping, modified from Schulten (2005)

#### 4.7.7. Matching of other parts

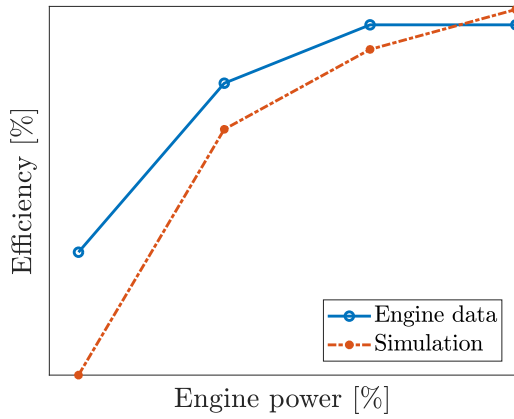
In the generic mean-value engine model, the pump speed of the charge air cooler is coupled to the engine speed. In practice, the pump is mostly driven via a geared transmission from the crankshaft, therefore the mass flow of the cooling water through the charge air cooler is proportional to the engine speed. However, a recirculation valve is added in the Wärtsilä 9L34DF cooling water piping after the charge air cooler. This valve recirculates already hot water to the inlet of the cooler in order to regulate the cooled down charge air temperature. This is achieved in the mean-value model by disconnecting the pump speed from the crankshaft and controlling the speed via a feedback loop with as set point the desired inlet receiver boost air temperature ( $T_{ir}$ ).

#### 4.7.8. Matching results dual fuel engine model

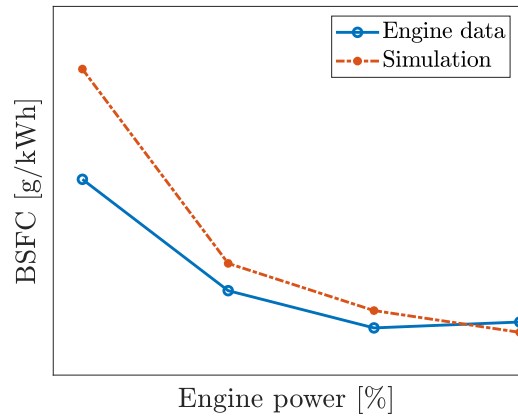
The matching procedure, as discussed before, is applied for the W6L34DF engine in the mean value dual fuel model. Due to uncertainties with respect to the Advanced Miller Timing (Section 4.5.4), a lower inlet receiver pressure ( $p_{ir} = 445 \text{ kPa}$ ) was used to lower the engine fresh air mass flow. Using a lower inlet receiver pressure does not affect the in-cylinder conditions compared with using a higher pressure level and introducing additional losses due to early inlet valve closure (IVC). However, lowering the inlet receiver pressure ( $p_{ir}$ ) affects the operating conditions of the compressor and turbine. Therefore it is possible that there is a mismatch between the matched turbocharger in the mean value model compared with the operating conditions in practice.

The goal of the previous matching process is that the model's output predictions match with specific operating points as accurate as possible. The level of accuracy is up to the modeller, a certain deviation will always be there because a simulation model never covers all the relevant processes occurring in reality. With respect to the thesis objective, it was inevitably to accept the matching results obtained so far. More research must be done in the Advanced Miller Timing of this W6L34DF to improve the mean value model predictions. The matching results shown in Figure 4.15 are sufficient to continue with the W6L34DF as engine type for researching the effect of a hybrid electric turbocharger.

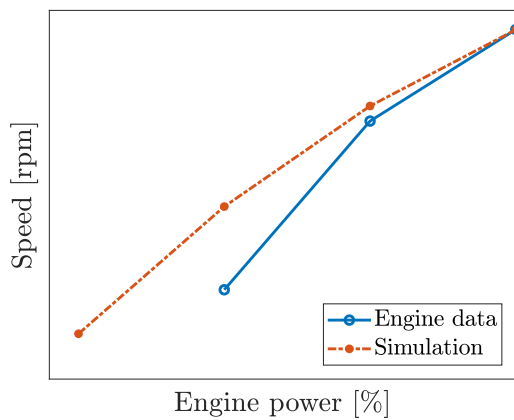
*Figures on the next page*



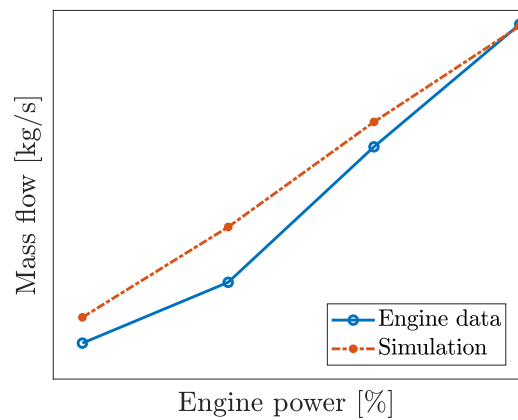
(a) Comparison: engine net efficiency



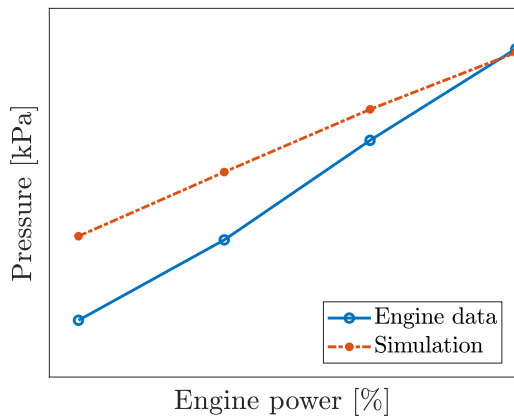
(b) Comparison: brake specific fuel consumption



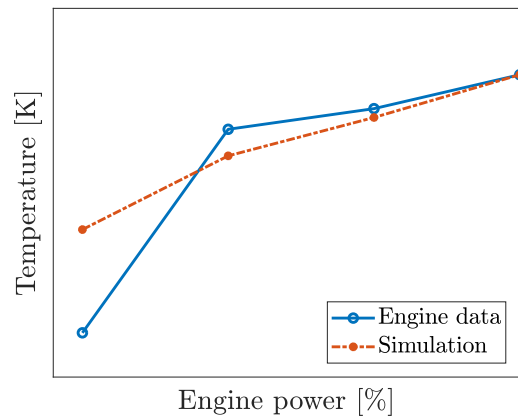
(c) Comparison: turbocharger speed



(d) Comparison: exhaust gas mass flow



(e) Comparison: pressure inlet receiver



(f) Comparison: temperature outlet receiver

Figure 4.15: Comparison of available engine data with simulation predictions

*AXIS NUMBERS HAVE BEEN REMOVED BECAUSE OF CONFIDENTIAL INFORMATION*

### 4.8. Model validation

After matching, the model’s capability to make predictions must be evaluated against independent data which is retrieved from measurement data provided by Mestemaker (2014). The test bench data was gathered in 2016 after which the development of the Wärtsilä 34DF continued. The engineers of Wärtsilä have been improving the engine compared with the engine of which data is used in this research. During the test bench session, a maximum cylinder pressure ( $p_3$ ) of about 150 bar was found, as can be seen in Figure 4.16b, however it is already increased up to about 210 bar according to R. Teir, product manager of the Wärtsilä 34DF engine group. This mismatch in cylinder pressure deteriorates the quality of independent data, however due to the lack of other higher quality data it was inevitably to use this test bench data for validating the engine model. The load applied to the test bench engine is used as generator load in the mean value model, as shown in Figure 4.16a. Initially the turbocharger speed (Figure 4.16c) matches with test bench speed, the different valleys for test bench data was observed due to, probably, varying inlet valve closure settings, which were not included in the mean value model for validation purpose. The turbocharger test bench data was used to vary the model’s turbocharger shaft inertia until corresponding acceleration/deceleration was observed between simulation and test bench results. The deviation between maximum in-cylinder pressure ( $p_3$ ) is due to the upgraded W6L34DF as already explained above. The largest deviation obtained from the validation procedure was the exhaust gas temperature in the outlet after the turbine expansion stage. The temperature deviation starts with 50K difference between test bench and simulation results. However the temperature trend goes down for the test bench results where the simulation show an increasing trend. The mismatch in compressor pressure ratio ( $\pi_{com} = 4.45$  instead of  $\pi_{com} = 5.45$ ) can be the reason why there is a mismatch in exhaust gas temperature between test bench data and model predictions.

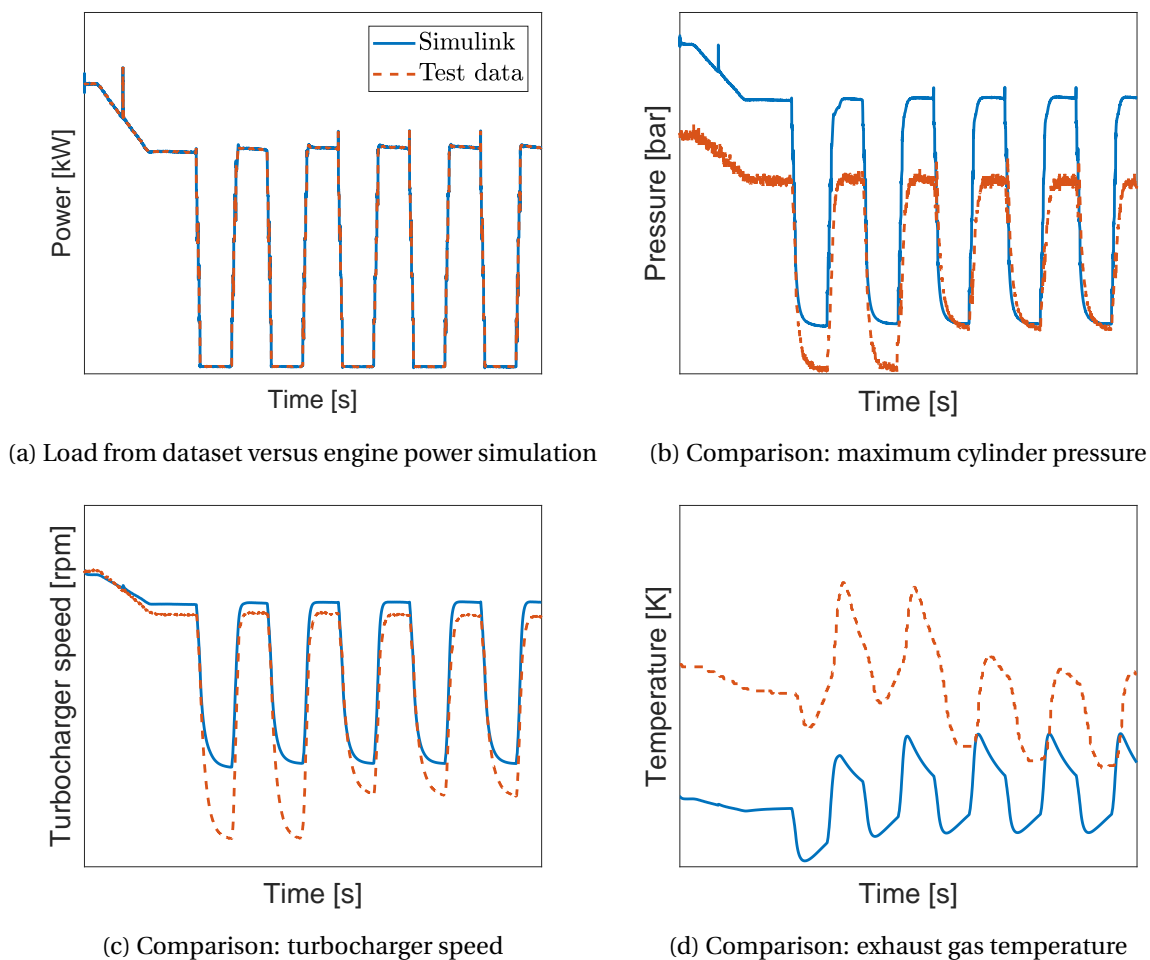


Figure 4.16: Validation of independent test bench data with simulation predictions

AXIS NUMBERS HAVE BEEN REMOVED BECAUSE OF CONFIDENTIAL INFORMATION

## 4.9. Control strategy electric machine

The model parameter used as set point for the main controller is an estimated air excess ratio ( $\lambda_{estimate}$ ). The dual fuel engine has for natural gas combustion a limited operating range, as shown in Figure 2.11. For gas mode, the set point must be varied in order to operate between the knock and misfire limits. However the gas mode is rejected for the W6L34DF due to semi-empirical heat ratio relationships, as explained in Section 4.5. For liquid fuel combustion, in this case marine diesel fuel (MDF), a constant air excess ratio set point was assumed for the whole operating envelope of the engine. As set point  $\lambda = 2.0$  is used, because normal air excess ratio values lay between 1.8 to 2.2 (Stapersma, 2010a).

The objective of the main controller is to keep the air excess ratio ( $\lambda$ ) close to the defined set point value. The torque of the electrical machine is controlled depending on the error when  $\lambda_{desired}$  is compared with  $\lambda_{estimate}$ . The main controller's objective is to keep the air excess ratio as close as possible to a desired value. Torque is either supplied or extracted without taking into account the physical limitations of the system. Boundary controllers limits the output of the main controller in order to comply with these physical limitations.

Eight boundary controllers are included to operate within physical boundaries:

- Crossing the surge line
- Thermal overloading: Temperature outlet receiver
- Smoke limit: Air excess ratio
- Overspeeding turbocharger: Maximum turbocharger speed
- Stalling turbocharger: Minimum turbocharger speed
- Exceeding the maximum allowed engine torque
- Exceeding the maximum in-cylinder pressure
- State of Charge of energy storage

### 4.9.1. Main controller: air excess ratio

The purpose of the EAT controller is twofold, it must control the amount of energy provided/extracted to/from the electrical machine depending on the air excess ratio ( $\lambda$ ). Energy needs to be supplied when the air excess ratio ( $\lambda$ ) drops below a certain defined value resulting in an increased turbocharger shaft rotational speed ( $n_{TC}$ ). This in turn affects the outgoing mass flow of fresh air from the compressor to the cylinder. The air excess ratio ( $\lambda$ ) can decrease such that it passes the smoke limit below which visible smoke is emitted due to incomplete combustion. On the other hand, a high air excess ratio can lead to a lower combustion temperature which will cause incomplete combustion due to quenching with the corresponding higher emission of hydrocarbons.

### 4.9.2. Boundary controllers to operate within boundaries

The eight boundary controllers are implemented with the following reasoning:

- The surge boundary controller is included to prevent unrealistic compressor output and to prevent compressor damage. Compressor surge should be avoided due to the large pressure fluctuations which cause mechanical wear and even breakdown of the the compressor, therefore the compressor should not operate in this unstable region.
- Another limitation must be added to prevent thermal overloading of the engine. As discussed in Section 2.2.1, the temperature of the exhaust valve is an indicator for thermal overloading of the engine. However the temperature of the exhaust valve is parameter which can be hard to retrieve. Sapra et al. (2017) proposes to use the exhaust gas temperature in the outlet receiver ( $T_{or}$ ) because both the exhaust valve temperature ( $T_{exh, valve}$ ) as well as the outlet receiver temperature ( $T_{or}$ ) have the same trend. Limiting the turbocompounding power is done with only an upper limit: the maximum outlet receiver temperature ( $T_{or, max}$ ).
- The smoke limit ( $\lambda_{SL}$ ) is included to prevent incomplete combustion which causes, next to visible smoke, an increase of emissions. Implementing a smoke limit (SL) while the main controller already controls the air excess ratio ( $\lambda$ ) is done because the smoke controller PI gains have a relative high value compared with the main controller PI gains. This smoke limit boundary controller can be seen as a main controller with two sets of gains where one set is used close to the smoke limit and the other one for no smoke conditions.

- The provided energy from the energy storage to the electrical machine can result in higher turbocharger speeds than allowed. Overspeeding must be prevented due to mechanical wear, or even worse, in mechanical damage. The maximum turbocharger speed is limited by  $(n_{TC,max})$ .
- The opposite, a higher power extracted in generating mode than available on the turbocharger shaft leads to a standstill of the turbocharger shaft. In this case, the turbocharger has no added value for the engine operation besides being a resistance that obstructs both the fresh air as well as the exhaust mass flow. Therefore a lower turbocharger speed limit  $(n_{TC,min})$  is required.
- The maximum engine output torque  $(M_{eng})$  is limited for the turbocharger assisting mode. The engine is prone to overboosting with a hybrid electric turbocharger due to a raised inlet receiver pressure  $(p_{ir})$ , therefore the maximum output torque  $(M_{eng})$  is limited.
- The maximum in-cylinder pressure  $(p_3)$  should be limited as well to prevent overloading of the cylinder structure and in-cylinder moving parts.
- The last boundary controller limits the assisting power to the turbocharger which uses the state of charge of the energy storage.

### 4.9.3. Implementation of an anti-windup

An anti-windup feedback loop is used in controllers that have to deal with non-linear effects. The system output behaves not linearly to its input parameter due to the non-linearities of the actuators within the system. Every physical actuator is subjected to saturation owing to its maximum or minimum limits. The remaining tracking error between the desired and obtained system output leads to integrator wind-up. The controller keeps integrating the tracking error, even if the input of the system is saturating. An example when no anti-windup action is used, is the mismatch between the desired (low) and actual (high) air excess ratios. The controller mathematical actions increase the power generated by the electrical machine. However, if the physical boundary of the actuator, in this case the maximum power that can be generated is reached, the torque extracted from the shaft cannot be increased. Hence the air excess ratios mismatch (tracking error) is unchanged. The integrating action of the controller adds every loop this tracking error resulting in windup of the controller.

Tracking back calculation, as explained in Choi and Lee (2009), is used as anti-windup scheme for both the main as well as the boundary controllers. This anti-windup scheme, as shown in Figure 4.17, compares the unsaturated and saturated control signals. The saturation captures the physical limitations of the actuator such as the maximum turbocharger shaft torque that can be withdrawn or supplied with the electric machine. Once the controller output exceeds the physical limitations, a feedback signal is generated which lowers the input of the integrator where  $K_{awu}$  is a tuning parameter in the feedback loop.

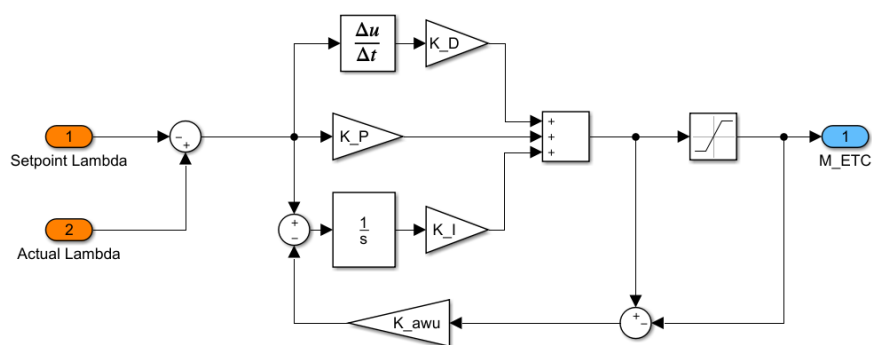


Figure 4.17: PI controller structure with anti-windup feedback loop, from mean-value Diesel B model

### 4.9.4. Overview control strategy

An overview of the control strategy is shown in Figure 4.18 on the next page. On the left, the main controller is located in the left upper corner with the desired set point  $(\lambda_{setpoint})$  and the feedback signal, the estimated air excess ratio  $(\lambda_{estimate})$ . The "min" block saturates the control signal to implement an upper limit for turbo-compounding (extraction of turbocharger shaft torque) for the given boundary controllers. The "max" limits the assisting mode for the given boundary controllers. The control strategy of the electrically assisted turbocharger for either generating or assisting mode is shown in Section 4.9.

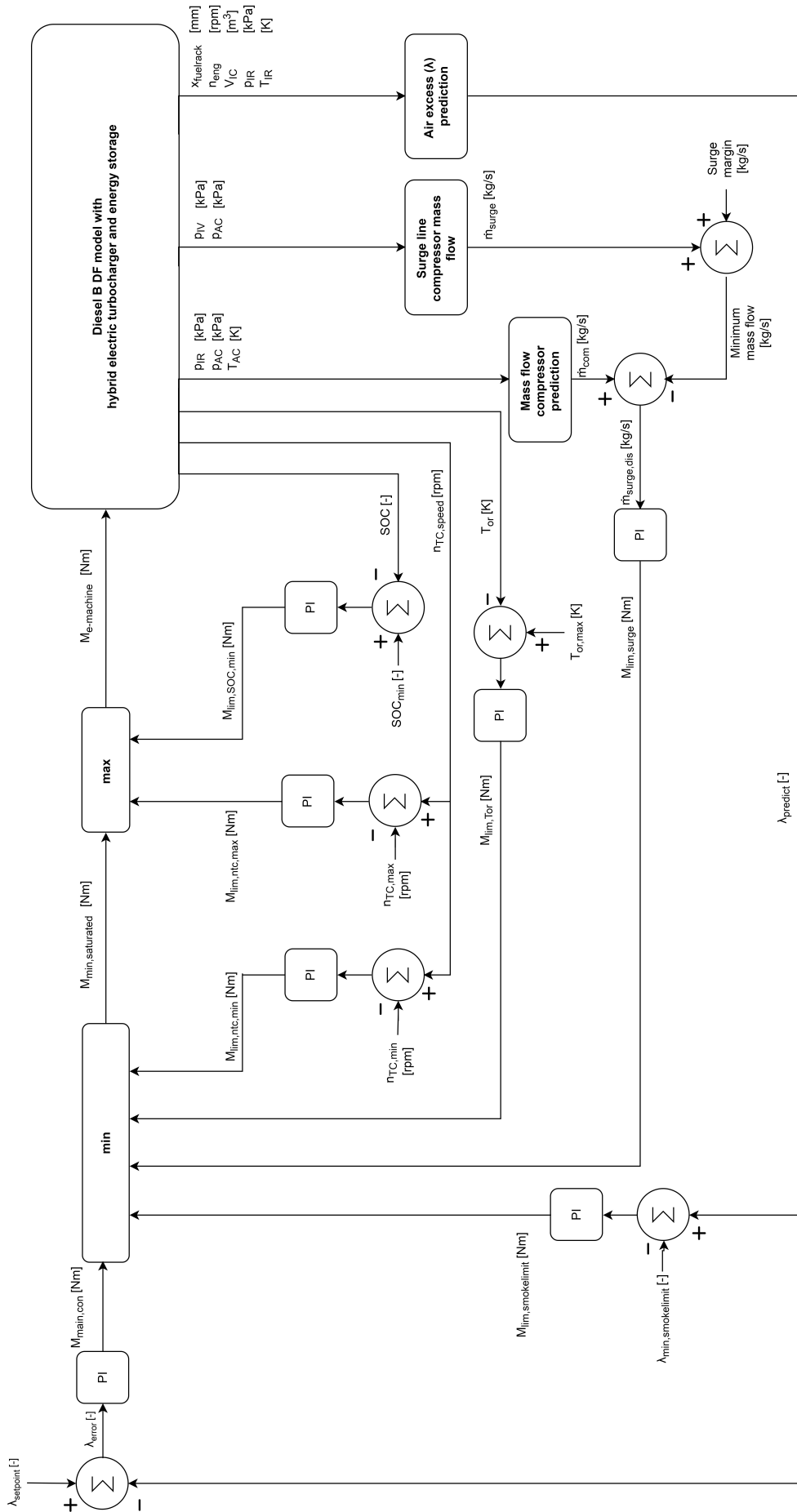


Figure 4.18: Control strategy electric machine with main and boundary controllers

#### 4.9.5. Air excess ratio estimation

The control strategy has as feedback signal the actual air excess ratio ( $\lambda$ ). In order to use the air excess ratio as control objective, it should be estimated. The estimation is based on theory used in the Diesel B model (Stapersma, 2010a,b,e). In the Diesel B model, an sophisticated gas exchange model is build which include the partition of mass flows as shown in Figure C.2. The gas exchange sub model determines the partition of air available for the combustion process and retained combustion flue gasses extensively. However for the air excess ratio estimation, a simplified model is derived which is explained in Appendix C with as final result Equation (4.5) given below.

A turbocharged diesel engine with positive pressure difference over inlet and outlet valves ( $\delta p_{ir-or}$ ): almost complete fresh air, therefore an ideal scavenging process is assumed which leads to no fouling due to retained flue gasses. Therefore the trapped mass ( $m_{tr}$ ) is equal to the fresh mass ( $m_{fresh}$ ):

$$m_1 = m_{fresh} = m_{ca} \quad (4.1)$$

In this case the pseudo air excess ratio ( $\lambda^*$ ) is equal to the air excess ratio ( $\lambda$ ):

$$\lambda^* = \lambda \quad (4.2)$$

The air excess ratio can be found with the pseudo air excess ratio as follows:

$$\lambda = \lambda^* = \frac{\dot{m}_{fresh}}{\dot{m}_{fuel}} \quad (4.3)$$

$$\dot{m}_{fresh} = ((V_{IC} - V_{EC}) + (\eta_{ret} \cdot V_{EC})) \cdot \left( \frac{p_{IR}}{R_{IR} \cdot T_{IR}} \cdot \frac{N \cdot i}{k} \right) \quad (4.4)$$

Combining these equations results in the following equation:

$$\lambda_{estimate} = \frac{((V_{IC} - V_{EC}) + (\eta_{ret} \cdot V_{EC})) \cdot \left( \frac{p_{IR}}{R_{IR} \cdot T_{IR}} \cdot \frac{N \cdot i}{k} \right)}{x \cdot \dot{m}_{nom, fuel}} \quad (4.5)$$

wherein the parameters can be obtained from product data, or can be retrieved from real-time measurements such as the pressures and temperatures. The retained efficiency ( $\eta_{ret}$ ) can be used as tuning parameter to fit the estimated air excess ratio ( $\lambda_{estimate}$ ) with the nominal ( $\lambda_{nom}$ ) obtained from high quality measurements such as during the development stage of the engine.

#### 4.9.6. Compressor mass flow estimation

The resistive effect of the charge air cooler on the compressor mass flow is used in combination with an artificial orifice equation to determine the compressor mass flow. The compressor mass flow estimation is shifted to a charge air cooler mass flow estimation. This restrictive element of the charge air cooler can be mimicked with an artificial orifice plate (Figure 4.19). Pressure sensors are already available at the compressor exit and inlet receiver with as intermediate part the charge air cooler. An extensive explanation about the mass flow estimation can be found in Appendix C.

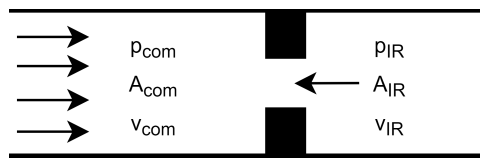


Figure 4.19: Overview of used parameters in artificial orifice

Equation (4.6) is the obtained equation which is used in the simulation model to estimate the compressor mass flow based on pressure measurements and a "resistive constant"  $R_{CAC}$ . This resistive parameter can be found with the nominal fresh air mass flow and pressure levels from available product data.

$$\dot{m} = R_{CAC} \cdot \sqrt{2 \cdot \rho (p_{com} - p_{IR})} \quad (4.6)$$

## 4.10. Conclusions

- The diesel B model is chosen because of the available compressor and turbine characteristics. Thereafter, an available dual fuel diesel B model from 2013 is merged with the latest Diesel B model (2016). The dual fuel model is verified, matched and validated. The matching results show that for maximum power and speed, the model's predictions are close to the engine data. However for lower loads, the predictions start to break off.
- An effective compression ratio should be implemented to include additional pressure loss over the inlet valve due to Advanced Miller Timing. The theory found and verified, shows the possibility to include this pressure loss with an effective compression ratio.
- A control strategy is composed of a main air excess ratio feedback controller and eight boundary controllers to control the electric machine of the hybrid electric turbocharger. The boundary controllers limit the main controller's actions to avoid situations that should not be reached in reality such as higher in-cylinder peak pressure levels.
- The actual air excess ratio is estimated based on a simplified gas exchange model. This air excess estimation is used as feedback signal for the main controller of the control strategy.
- The location of the surge line in the compressor map is quantified based on theory which was already available, but which was not implemented in the diesel B model. The location of the surge line is an input of the control strategy.
- The compressor mass flow is estimated with an artificial orifice equation which uses the pressure drop over the charge air cooler. This mass flow is used to find the location of the actual operating conditions in the compressor map.

# 5

## Static Analysis

### 5.1. Introduction

The effects of a hybrid electric turbocharger integrated into the Diesel B mean-value model on steady-state engine operation are discussed in this chapter for both turbocompounding as well as electrically assisted turbocharging. This chapter is divided in two parts. The first part will cover the steady-state turbocompounding potential with regard to the engine efficiency and the second part is related to electrical assisted turbocharging.

The two research questions that will be answered in this chapter are:

1. *Analyse the effect of recovering energy from the exhaust gasses on the total power plant efficiency*
2. *Analyse the engine's static behaviour improvement possibility to shape the operating envelope*

The first part shows the effects of using a hybrid electric turbocharger to increase the overall system efficiency, which includes both the engine power output together and the electrical power recovered by the hybrid electric turbocharger. The operating envelope used in this chapter is retrieved from the engine manufacturer's product data. The impact of withdrawing power from the turbocharger shaft on the engine's gas exchange process is discussed. Thereafter the effect of turbocompounding on thermal loading of the engine parts will be dealt. A sensitivity analysis is performed in order to investigate the effect of varying engine parameters, moreover some component sizing parameter sweeps are shown.

The second part of this chapter is related to electrically assisted turbocharging, further named for steady state research: operating envelope shaping. The effect on the operating envelope of assisting the turbocharger by adding torque to its shaft is investigated. Combining the hybrid electric turbocharger with additionally external gas exchange valves (BPV and BOV) are discussed in order to get an almost constant engine torque output.

An overview of above mentioned cases is visualised below:

<b>Section</b>	<b>Turbocompounding</b>
5.2	Baseline W6L34DF without turbocompounding
5.3	Effect on system efficiency
5.4	Effect of turbocompounding on gas exchange
5.5	Effect of turbocompounding on thermal loading engine
5.6	Comparison of three engine cases
5.7	Sensitivity Analysis
5.8	<b>Operating envelope shaping</b>
5.9	Assistance
5.10	Assistance and BOV/BPV

## 5.2. Operating envelope baseline Wärtsilä 6L34DF

Figure 5.1 shows the operating envelope of the simulated baseline W6L34DF without turbocompounding. The operating envelope published in product data of the Wärtsilä 6L34DF is used to determine the power range for each engine speed. The peak efficiency lays, as matched, at nominal power and speed: 3000 kW at 750 rpm, see Figure 5.1c. The effect of delayed inlet valve closure below 25% load (750 kW) can be recognised in Figures 5.1g and 5.1h. The air excess ratio ( $\lambda$ ) at nominal power and speed (Figure 5.1g) gives an indication that turbocompounding could be feasible due to the relative high air excess ratio ( $\lambda > 2.5$ ) only when the control strategy make use of a lower set point value such as ( $\lambda_{setpoint} = 2.0$ ).

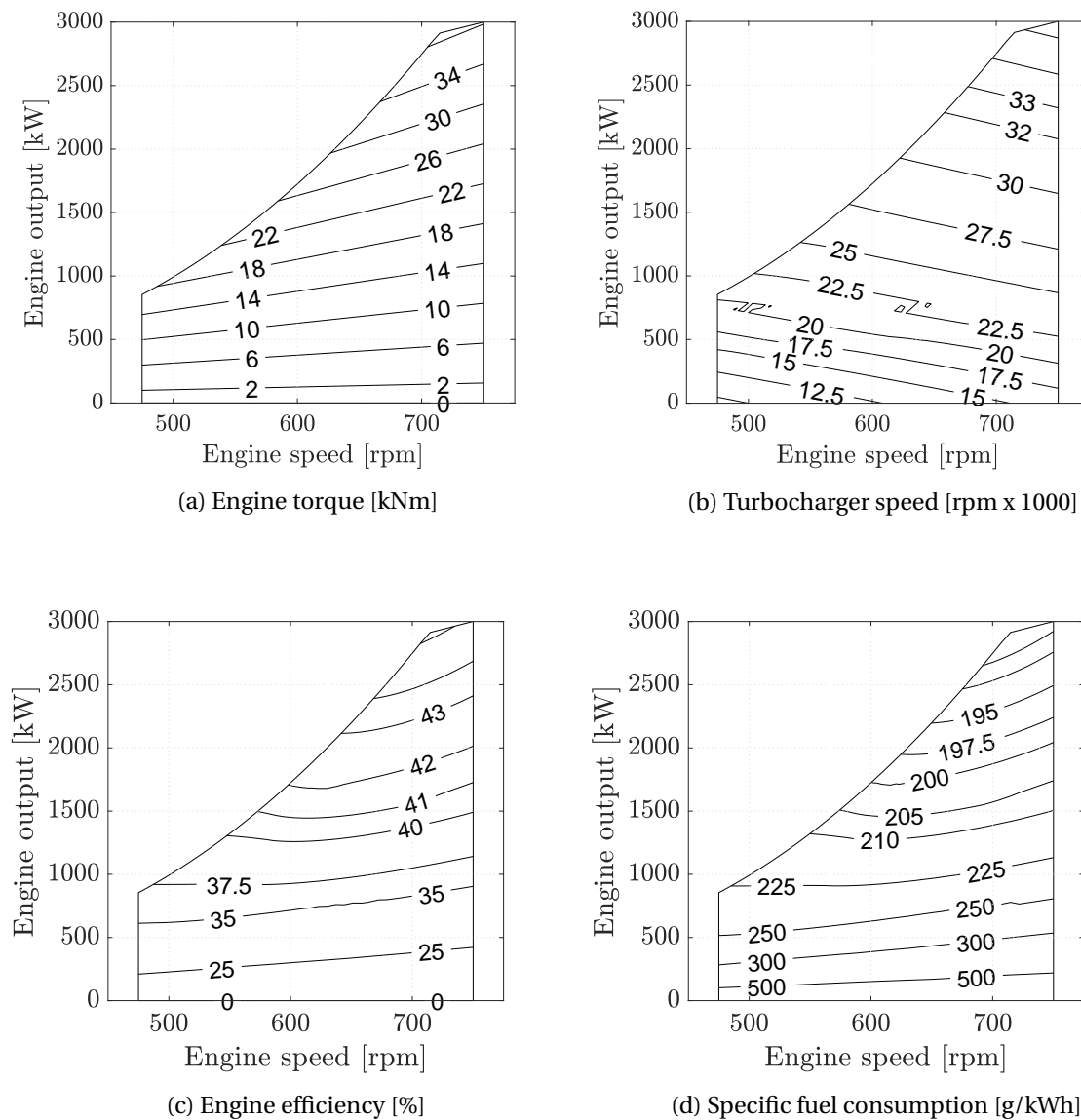
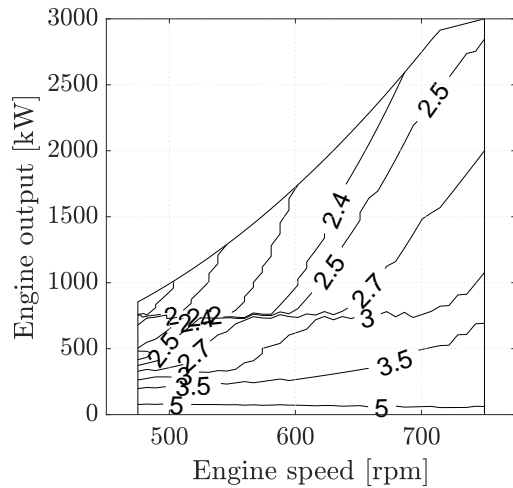
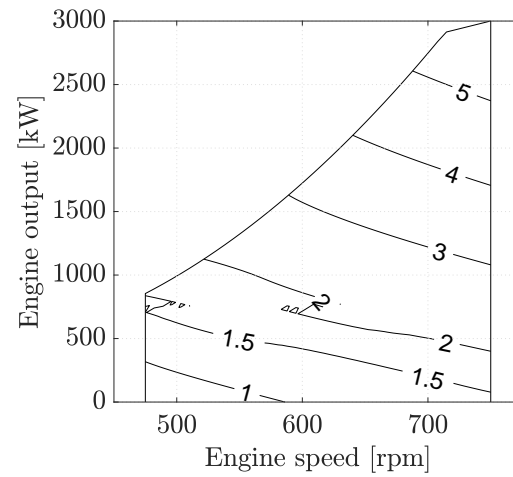
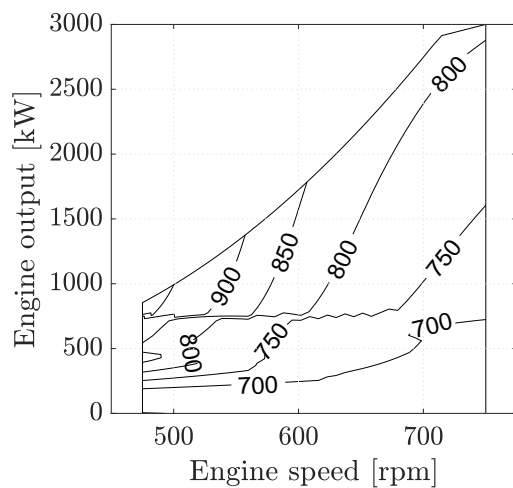


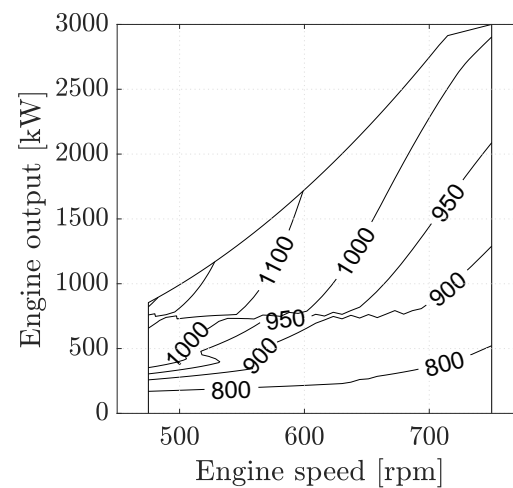
Figure continuous on next page

(e) Air excess ratio  $\lambda$  [-]

(f) Exhaust mass flow [kg/s]



(g) Temperature exhaust gas in outlet receiver [K]



(h) Temperature outlet valve [K]

Figure 5.1: Power speed characteristics of baseline W6L34DF model

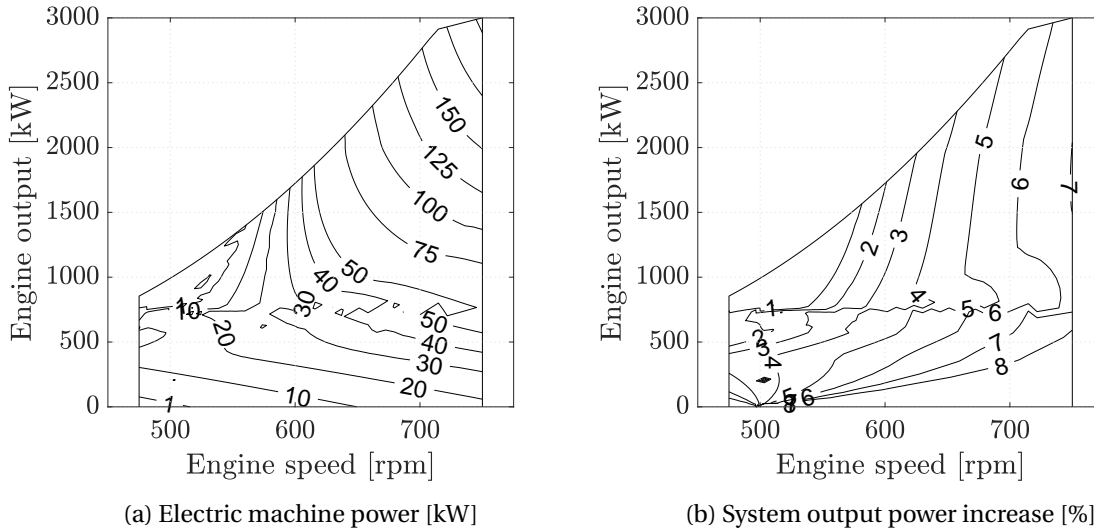
### 5.3. Effect of turbocompounding on system

This section will show the effect of turbocompounding on the following specific engine conditions with the air excess ratio based control strategy, discussed in Section 4.9.1, and an air excess ratio set point ( $\lambda_{setpoint} = 2.0$ ).

- System power output
- Gas exchange
- System efficiency
- Fuel consumption
- Thermal loading

### 5.3.1. Turbocompounding: System power output

The maximum recovered power with the hybrid electric turbocharger goes up to 200 kW at nominal load and speed (3000 kW at 750 rpm). The total system power output at this nominal point is increased from 3000 kW for the baseline engine to 3200 kW, which accounts for a system power output percentage increase of 6.6% (Figure 5.2b). Turbocompounding is a manner to have a more power dense system due to the increased system power output while keeping its dimensions almost equal, however the latter depends on the need for additional power electronics.



### 5.3.2. Turbocompounding: Gas exchange

Taking power from the turbocharger shaft with the electric motor has a negative impact on the gas exchange of the in-cylinder process for both the inlet as well as the outlet receiver gas flows. The developed turbine power is consumed by the compressor to pressurize the intake charge air mass flow. When power is drawn from the turbocharger with the electric machine, less power is available for the compressor which affects in the end the charge air pressure and mass flow. Turbocompounding affects the power distribution of the turbocharger even worse, the power produced by the turbine drops as well, as can be seen in Figure 5.3b. The combination of decreased available turbine power and taking power off with the electric machine harms the power provision to the compressor. Therefore the power available for the compressor drops by almost one third compared to the baseline provided compressor power, as shown in Figure 5.3a.

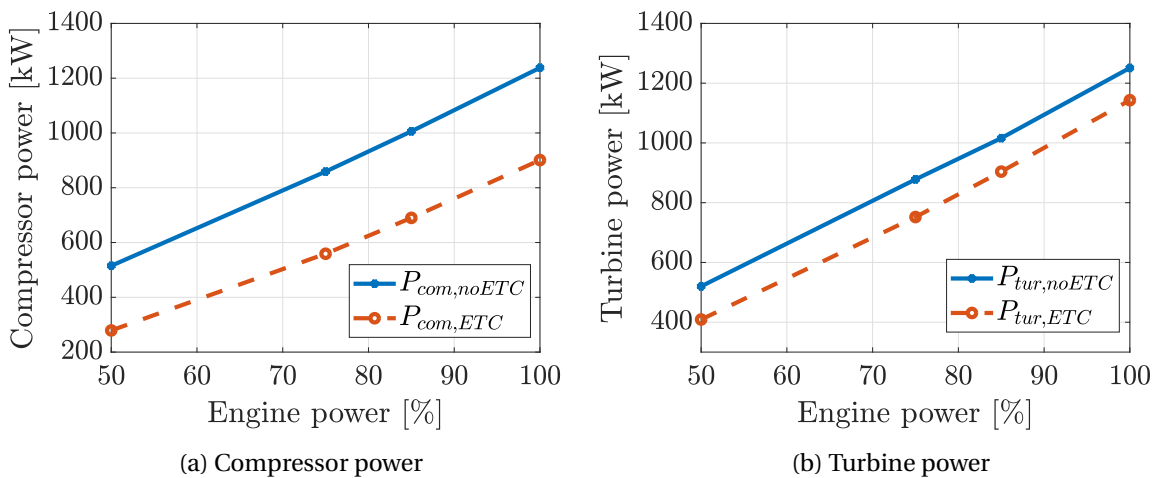
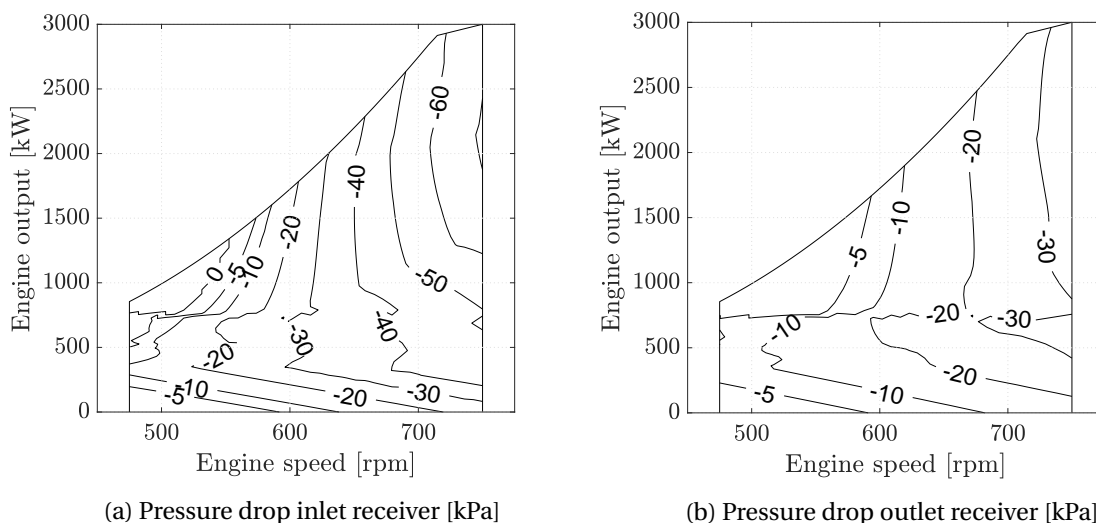


Figure 5.3: Compressor (a) and turbine (b) power for different engine loads at nominal speed

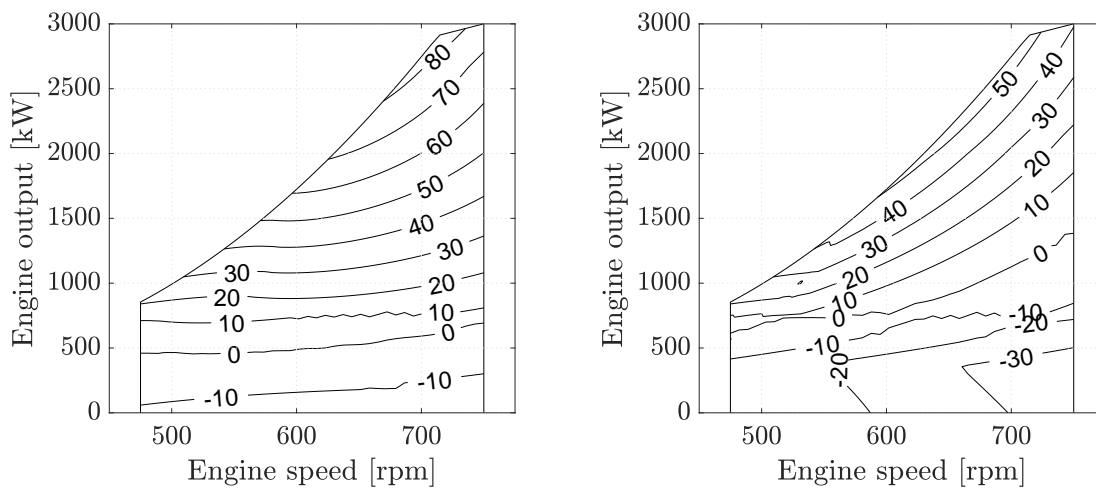
Figure 5.4 shows the drop of inlet and outlet receiver pressure level ( $\Delta p_{ir}$  &  $\Delta p_{or}$ ) for the turbocompounding case compared to the baseline engine. A lower compressor power results in a maximum charge air pressure drop ( $\Delta p_{ir}$ ) of about 65 kPa at nominal conditions, as depicted in Figure 5.4a. The outlet receiver pressure ( $p_{or}$ ) lowers with about 35 kPa for nominal load and speed (Figure 5.4b).



(a) Pressure drop inlet receiver [kPa] (b) Pressure drop outlet receiver [kPa]

Figure 5.4: Pressure difference inlet and outlet receiver between turbocompounding and baseline case

Scavenging is deteriorated when turbocompounding is applied. The pressure difference over the cylinder ( $\Delta p_{ir-or}$ ) drops from 80 kPa (Figure 5.5a) to 50 kPa for the turbocompounding case (Figure 5.5b). The back flow limit lays almost constant around 500 kW for the baseline engine over the whole engine speed range, below which exhaust gasses flows back into the cylinder due to a negative pressure difference over the cylinder. When turbocompounding is enabled, the operating condition for which back flow starts, increases up to 1500 kW at nominal speed.



(a) Pressure over cylinder baseline engine [kPa] (b) Pressure over cylinder turbocompounding [kPa]

Figure 5.5: Pressure difference over cylinder baseline engine (a) and with turbocompounding (b)

### 5.3.3. Turbocompounding: System efficiency

The system efficiency can be improved with turbocompounding up to 1.32% with the selected engine and control strategy for nominal load and speed, as shown in Figure 5.7b. The engine efficiency, with as input the fuel's energy and as output the crankshaft power without the power recovered with turbocompounding, drops when power is taken from the turbocharger shaft, as shown in Figure 5.7a.

The engine efficiency drops due to the decreased charge air pressure ( $p_{ir} = p_1$ ). The compression ratio remains constant, leading to a lower peak in-cylinder pressure ( $p_3$ ). However, no engine dimensions are changed, therefore the mechanical and heat input losses does not considerably change, except a decrease due to the reduced peak pressure ( $p_3$ ) (Stapersma, 2010a). The thermodynamic efficiency of the Seiliger cycle increases with a decreased charging pressure ( $p_{ir}$ ), explained in the causality diagram depicted in Figure 5.6. The mechanical and heat input efficiency lowers with decreasing charge air pressure and counterbalance the increase of the thermodynamic cycle efficiency ( $\eta_{th}$ ). Combining these two effects, leads to a drop of engine efficiency (Stapersma, 2010a).

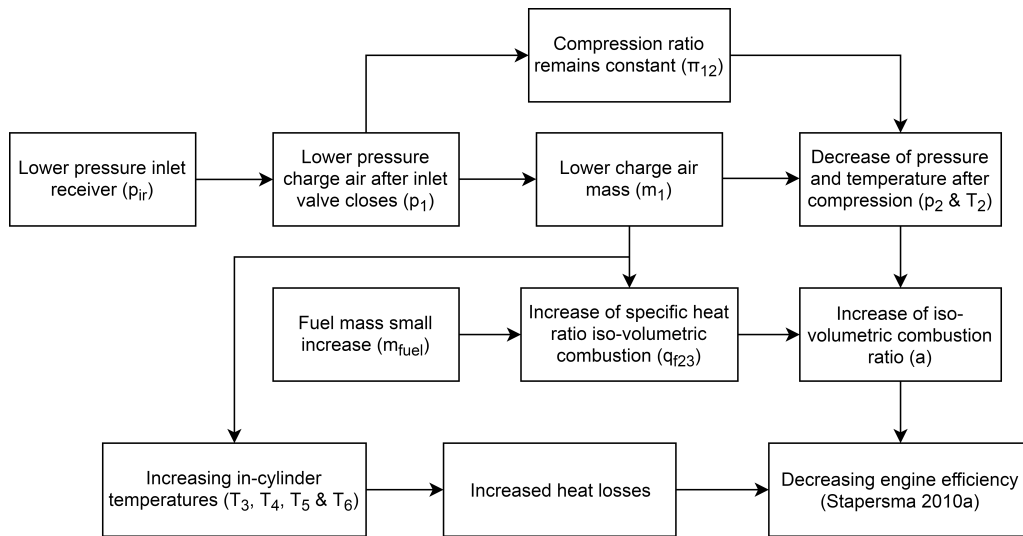
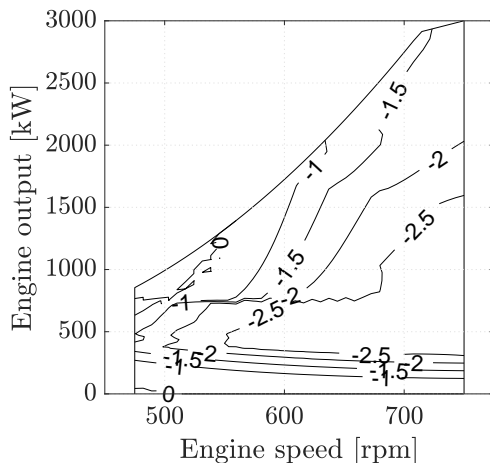
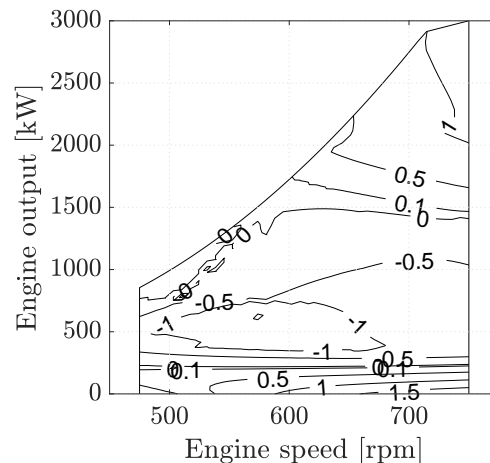


Figure 5.6: Causality diagram decreasing engine efficiency

Although the engine efficiency ( $\eta_{eng}$ ) decreases, the amount of recovered electric power compensates this loss up to such an extent, that for certain regions in the operating envelope the system efficiency increases above the baseline case. A system efficiency increase is only found for the operating region close to the nominal operating point. For lower loads, the system efficiency is deteriorated compared with the baseline case. The amount of recovered energy by the electric machine is not sufficient to compensate the drop of engine efficiency, therefore the system efficiency decreases. The air excess control strategy, proposed in Section 4.9, lacks of an overall system efficiency limiter to prevent turbocompounding for lower loads and speeds.



(a) Engine efficiency decrease [%]



(b) System efficiency increase [%]

### 5.3.4. Turbocompounding: Fuel consumption

Turbocompounding to increase the system power output requires a higher quantity of fuel ( $\dot{m}_{fuel}$ ) to be injected compared to the baseline case, however the specific fuel consumption (g/kWh) is found to be decreased for nominal load and speed. As shown in Figure 5.7a, a lower engine efficiency ( $\eta_{eng}$ ) is obtained with turbocompounding. More fuel has to be injected to obtain a power output of 3000 kW at the crankshaft without taking into account the power output from turbocompounding. At nominal load and speed, a fuel mass flow increase of about 4% is required, as depicted in Figure 5.7c. The Wärtsilä 6L34DF is designed to deliver a maximum power output of 110% for only short periods of time to increase the engine response to loads Wärtsilä Engines (2012). The fuel delivery system has to inject the quantity of fuel that is needed to develop 110% engine power. Therefore the increased fuel mass flow for nominal load and power (Figure 5.7c) with turbocompounding is probably no limitation, otherwise changes to the fuel delivery system are required. Although the fuel mass flow ( $\dot{m}_{fuel}$ ) is increased, the specific fuel consumption for the system power output (engine + turbocompounding power) is reduced by up to 5%, as depicted in Figure 5.7d, for nominal load and speed compared with the baseline engine case.

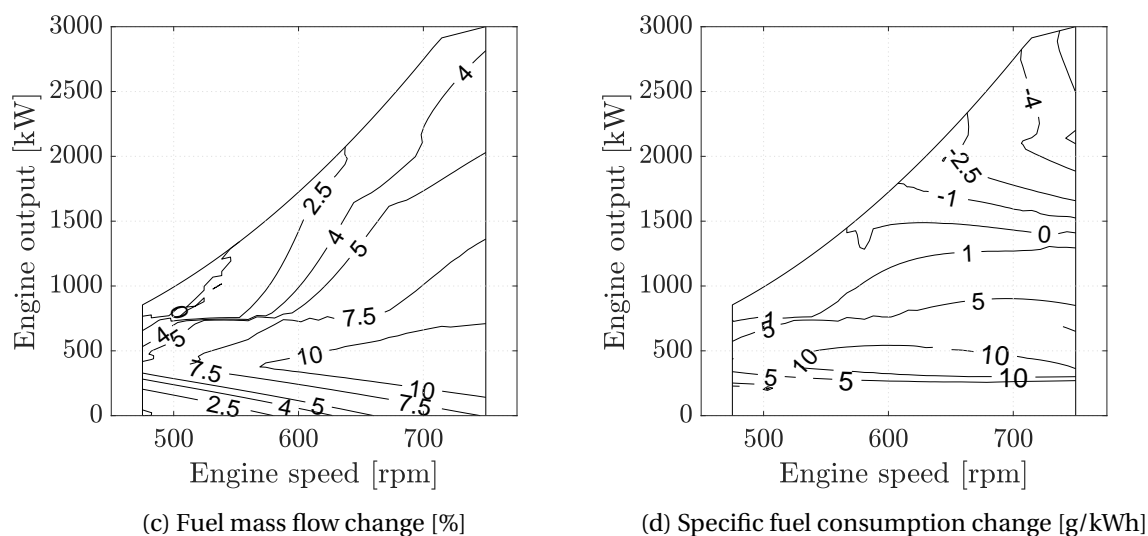
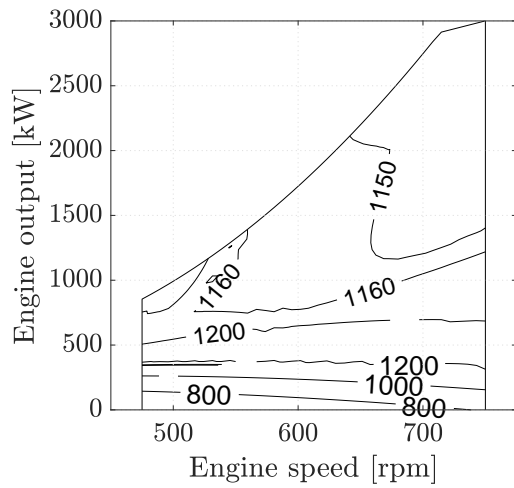


Figure 5.7: Increase in fuel mass flow [%] (a) and change of specific fuel consumption [g/kWh] (b)

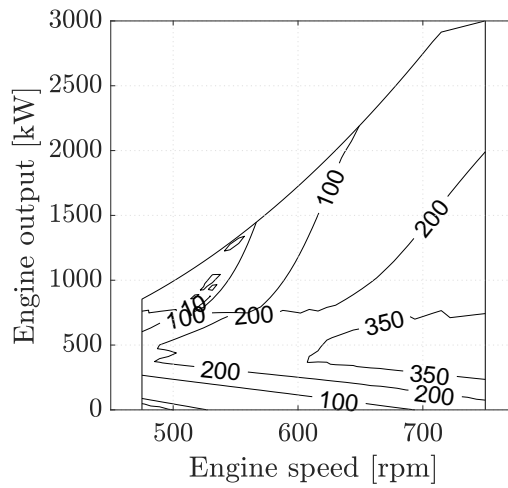
### 5.3.5. Turbocompounding: Thermal loading engine

Turbocompounding increases the engine's thermal loading due to the reduced fresh air mass induced and retained in the cylinder. Lowering the inlet receiver pressure, due to turbocompounding as shown in Section 5.3.2, affects the amount of fresh air induced into the cylinder while the supplied fuel even increases, as depicted in Figure 5.7c. Next to the in-cylinder conditions, the scavenge process is deteriorated as discussed in Section 5.3.2. These two gas exchange processes leads to an increased temperature of several engine components such as the piston, cylinder liner, cylinder head and, in particular, the exhaust valves. Next to the exhaust valve, the outlet receiver is an indicator for thermal overloading.

The temperature of the exhaust valve ( $T_{exh, valve}$ ) increases of about 150K at nominal power and speed, while an increase up to 200 - 300 K is found for mid power and speed range.

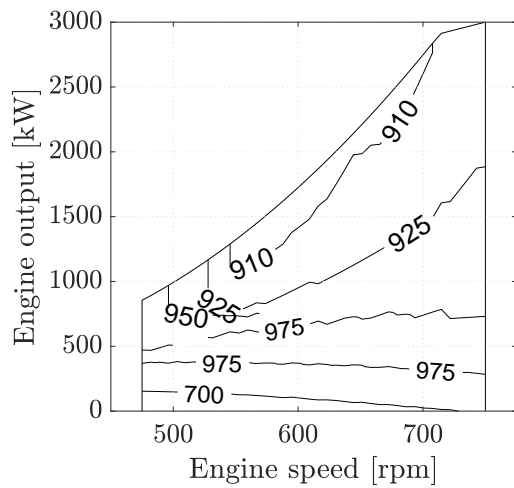


(a) Temperature exhaust valve with turbocompounding [K]

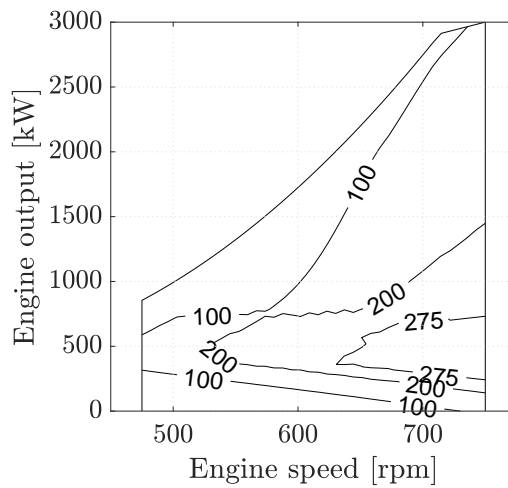


(b) Temperature increase exhaust valve with turbocompounding [K]

but also the outlet receiver temperature ( $T_{or}$ ) level gives an indication of the thermal loading of the engine.



(a) Temperature outlet receiver with turbocompounding [K]



(b) Temperature increase outlet receiver with turbocompounding [K]

Figure 5.9: Thermal loading indicators exhaust valve (a), exhaust valve temperature increase (b), temperature outlet receiver (c) and temperature increase outlet receiver (d)

### 5.3.6. Effect of set point on system power output and efficiency

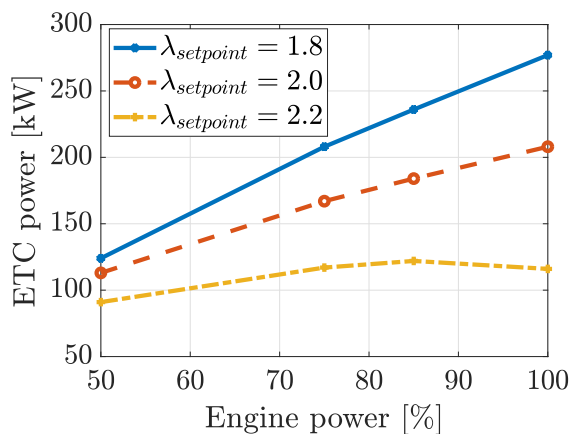
Lowering the control strategy's set point from  $\lambda_{setpoint} = 2.2$  to 1.8 results in an increased total system power output. The lower the set point, the higher the total system power output which is obtained up to 3277 kW for  $\lambda_{setpoint} = 1.8$  at nominal power and speed. Maximum electric power (277 kW) can be obtained at nominal power and speed for the lowest set point ( $\lambda_{setpoint} = 1.8$ ), however for 50% engine load, the electric power drops almost to the same power level as the other two cases ( $\lambda_{setpoint} = 2.0$  and 2.2). What stands out is the rather flat electric power curve for ( $\lambda_{setpoint} = 2.2$ ), as shown in Figure 5.10a.

As already shown in Section 5.3, the engine efficiency ( $\eta_{eng}$ ) decreases when turbocompounding is used. The energy recovered with turbocompounding should exceed the drop in engine efficiency in order to have a system efficiency gain. Figure 5.10c shows that a low set point leads to a maximum system efficiency gain at nominal power and load, however at 50% load turbocompounding does not compensate the drop in engine efficiency, resulting in a lower total system efficiency compared with the baseline engine without turbocompounding.

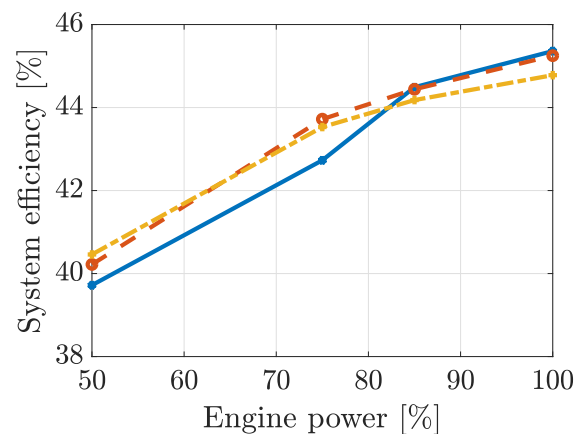
The change of system efficiency with turbocompounding compared to the baseline engine is shown in Figure 5.10c. The lowest set point gives a system efficiency increase at nominal load and speed, while for 50% load a lower system efficiency is obtained when energy is taken from the turbocharger shaft. Selecting a higher set point value resulted for the four load cases in a positive system efficiency change.

Table 5.1: System efficiency comparison of three set point cases:  $\lambda_{setpoint} = 1.8, 2.0$  and 2.2

$\lambda_{setpoint}$			Engine power output			
			50%	75%	85%	100%
1.8	$P_{ETC}$	[kW]	124	208	236	277
	$\eta_{sys}$	[%]	39.7	43.7	44.5	45.4
	$\Delta\eta_{sys}$	[%]	-0.28	1.09	1.22	1.43
2.0	$P_{ETC}$	[kW]	113	167	184	208
	$\eta_{sys}$	[%]	40.2	43.7	44.4	45.3
	$\Delta\eta_{sys}$	[%]	0.22	1.08	1.17	1.32
2.2	$P_{ETC}$	[kW]	91	117	122	116
	$\eta_{sys}$	[%]	40.5	43.5	44.2	44.8
	$\Delta\eta_{sys}$	[%]	0.46	0.89	0.91	0.85

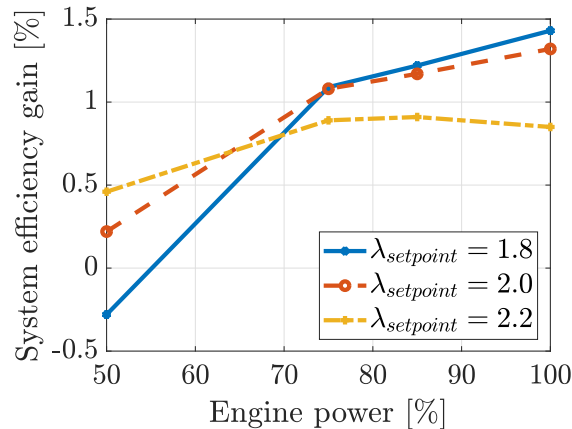


(a) Electric machine power [kW]



(b) System efficiency [%]

Figure continuous on next page



(c) System efficiency change [%]

Figure 5.10: Effect of lower air excess ratio  $\lambda$  set point on electric machine power output (a) on total system efficiency (b) and comparison with system efficiency with/without turbocompounding (c)

#### 5.4. Turbocompounding for three turbocharger matching conditions

The operating point for which the turbocharger is matched with the engine has determines if and up to which extent turbocompounding is possible or not with the control strategy used in this research. In Section 5.3, the depicted system efficiency increase suggests that it is possible to harness energy from the exhaust gasses due to a rather high air excess ratio at nominal operating point. To find the effect of the matching point of the turbocharger, a waste gated turbocharger is compared with a non waste gated turbocharger. The engine under investigation in this thesis has one stage turbocharging without a waste gate. In order to analyse the effect of a waste gated turbocharger, the W6L34Df is not used, but the STA12V280 and STA12V280WG are compared. These engines are already available in the Diesel B model and represent the SWD12V280, a Stork Werkspoot engine without a waste gate and with a waste gate. These models are composed by Stapersma (2010a) and are assumed to be matched, verified and validated. The engine parameters are the same, merely the turbocharger for the STA12V280WG is matched at a lower power output, for higher power outputs the waste gate is opened to prevent turbocharger overspeeding.

The results are shown in Appendix D, some relevant results are discussed below.

The baseline STA12V280 is matched with an air excess ratio (Figure D.1b) of about  $\lambda = 2.0$  for nominal load and speed. This condition leads to a very negligible increase in obtainable system efficiency (Figure D.3) at nominal operating conditions due to the corresponding air excess ratio ( $\lambda$ ) at nominal load and speed and the set point of the electric machine controller. On the contrary, the waste-gate in the STA12V280WG bypasses a part of the exhaust gas around the turbine, therefore the air excess ratio ( $\lambda$ ) drops for higher engine loads and speeds compared to the matching conditions, as can be seen in Figure D.4a. Replacing the function of the waste gate with the hybrid electric turbocharger results in a maximum system efficiency gain of about 2.3%, as shown in Figure D.2b.

#### Quantification of turbocompounding potential

The highest turbocompounding potential can be obtained with an air excess ratio control strategy when a waste-gated turbocharger is replaced with a hybrid electric turbocharger. The system efficiency increase for the three cases discussed above: W6L34DE, STA12V280 and STA12V280WG, is quantified as the area within the operating envelope for which the gain exceeds a certain threshold compared to the total area of the operating envelope. As an example, Figure 5.11 shows the area of the operating envelope where no system efficiency increase is possible for low loads, and about one third of the operating envelope for which the system efficiency gain  $> 0.1\%$  in the higher load region. Table 5.2 shows the result of this approach for the three engine cases.

Table 5.2: Comparison of area with a certain system efficiency gain compared to total operating envelope

Engine type	Percentage area with efficiency gain higher than:								
	> 0.05%	> 0.1%	> 0.5%	> 1.0%	> 1.25%	> 1.50%	> 1.75%	> 2.0%	> 2.25%
W6L34DF	26%	24 %	18 %	9 %	0 %	0 %	0 %	0 %	0 %
STA12V280	33 %	30 %	4 %	0 %	0 %	0 %	0 %	0 %	0 %
STA12V280WG	29 %	27 %	18 %	10 %	8 %	7 %	5 %	4 %	3 %

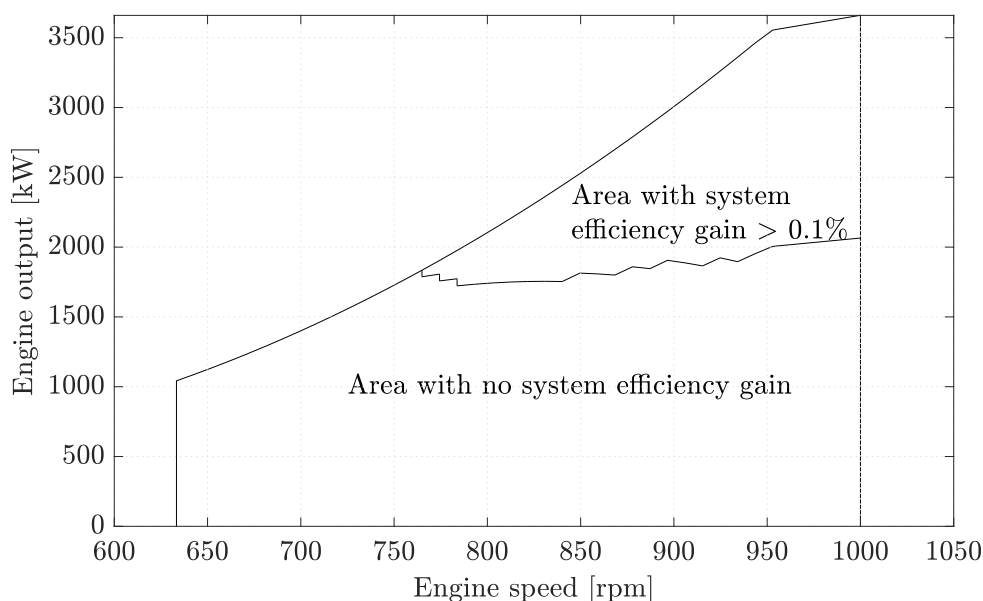


Figure 5.11: Example of area in operating envelope in which an system efficiency gain of > 0.1% can be reached

The STA12V280WG has almost the same area in the operating envelope wherein turbocompounding has a positive effect on the system efficiency compared to the non waste-gated STA12V280. A difference arises when the system efficiency gain threshold is increased. The system efficiency for the waste-gated STA12V280WG rises faster in the direction of the peak system efficiency compared to the other engine cases, as depicted in Figure 5.12. The almost negligible system efficiency increase for the STA12V280 was already noticed in Figure D.2b.

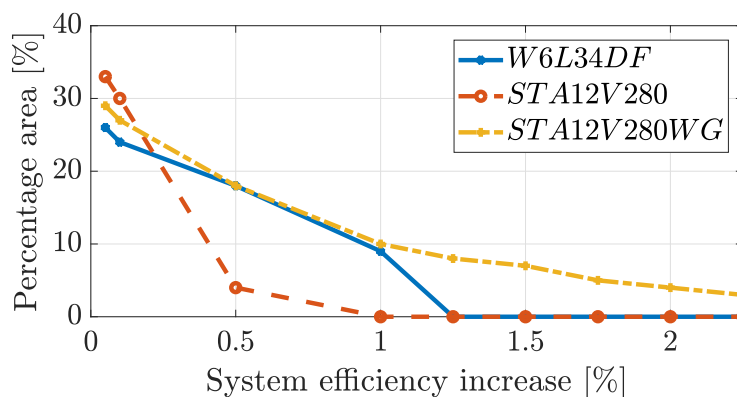


Figure 5.12: Percentage area of specific system efficiency increase with turbocompounding, based on data shown in Table 5.2

## 5.5. Sensitivity analysis

In this section, a sensitivity analysis (SA) is performed to find how different values of an independent variable influences a specific dependent output variable. To do this the "one factor at a time" (OAT) approach is used, all the parameters are kept constant and their value is set equal to the values retrieved from the matching procedure, except the parameter under study. The Variable Of Interest (VOI) is introduced as dependent output parameter under investigation, for instance the system efficiency increase. The independent parameter, for instance the set point  $\lambda$  is varied around its nominal value for plus minus five cases, denoted in variable  $s$ . This independent input parameter is called below ( $CV_{var}$ ), where "var" means the independent variable used in that comparison.

$$s = 1 \pm [0.01, 0.05, 0.1, 0.15, 0.2]$$

$$CV_{var} = CV_{var,nom} \cdot s$$

$$VOI_{change} = 100\% \cdot \frac{VOI_{CV,var}}{VOI_{CV,nom}}$$

This sensitivity analysis is done for 28 independent parameters, which are shown in Table 5.3. A script is written which determines the influence of the changing independent input variables to the dependent output variables for four load cases: 50, 75, 85 and 100%. Because of the high number of independent simulations, again Matlab Simulink in combination with the Parallel Computing Toolbox was used to increase the computational speed.

Table 5.3: Parameters used in sensitivity analysis

Components	Parameters	Description	Units
Controller	$\lambda_{setpoint}$	Set point main controller: air excess ratio	[-]
Cylinder	$\alpha_{IC}$	Crank angle at which inlet valve closes	[deg]
	$\alpha_{IO}$	Crank angle at which inlet valve opens	[deg]
	$\alpha_{EC}$	Crank angle at which exhaust valve closes	[deg]
	$\alpha_{EO}$	Crank angle at which exhaust valve opens	[deg]
	$\alpha_{IT}$	Crank angle at which fuel is injected	[deg]
Compressor	$\dot{m}_0$	Nominal mass flow	[kg/s]
	$\eta_0$	Nominal compressor efficiency	[-]
	$\phi_{0,r}$	Nominal flow coefficient NOP relative to BEP	[-]
	$v_{0,r}$	Nominal rotor speed NOP relative to BEP	[-]
	$\pi_0$	Nominal pressure ratio	[-]
	$\Psi_0$	Nominal enthalpy coefficient	[-]
	$x$	Sensitivity to entrance losses	[-]
	$y$	Loss dependency on rotational speed	[-]
	$Ma_0$	Nominal Mach number	[-]
	$e$	Spread of constant speed curves	[-]
	$s$	Spread of constant speed curves	[-]
Turbine	$\eta_0$	Nominal compressor efficiency	[-]
	$\dot{m}_0$	Nominal mass flow	[kg/s]
	$\phi_{0,r}$	Nominal flow coefficient NOP relative to BEP	[-]
	$v_{0,r}$	Nominal rotor speed NOP relative to BEP	[-]
	$\pi_0$	Nominal pressure ratio	[-]
	$\Psi_0$	Nominal enthalpy coefficient	[-]
	$x$	Sensitivity to entrance losses	[-]
	$y$	Loss dependency on rotational speed	[-]
	$Ma_0$	Nominal Mach number	[-]
	$e$	Spread of constant speed curves	[-]
	$s$	Spread of constant speed curves	[-]

NOP = Nominal Operating Point; BOP: Best Efficiency Point

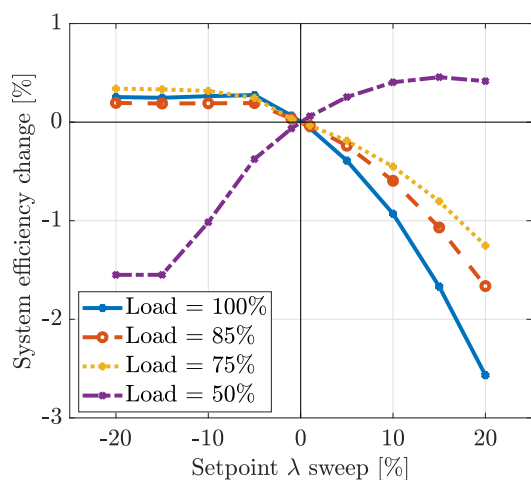
In the next subsections, some remarkable results are shown obtained from this sensitivity analysis.

### 5.5.1. Sensitivity to controller parameter sweep

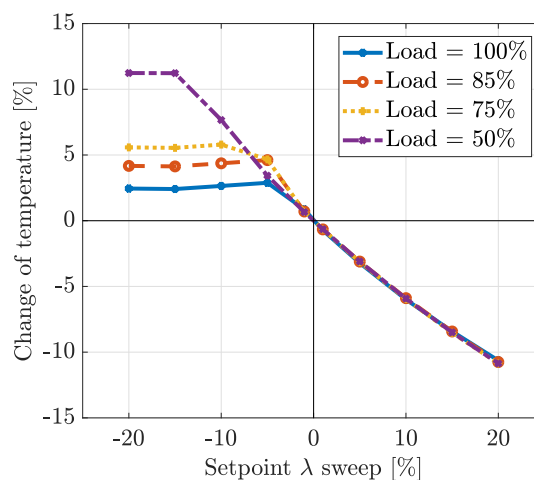
Selecting a lower air excess ratio ( $\lambda$ ) leads to a marginal system efficiency increase (Figure 5.13a). A rather flat system efficiency gain is found and there is no large deviation between the parameter sweeps for 75 - 100% load. However, the trend for the 50% case is opposite to the other load cases. Using a low set point does not lead to a system efficiency benefit. Increasing the set point results in a system efficiency drop where the 100% load case decrease faster than the lower load cases. These results are in accordance with the results already shown in Figure 5.10c.

The outlet receiver temperature (Figure 5.13b) shows an increased thermal loading for low set point values and low engine load. For higher set point values, the thermal loading decrease is the same for all load cases.

Parameter of Interest	Nominal value	Units
$\lambda_{setpoint}$	2.0	[-]



(a) System efficiency



(b) Temperature outlet receiver

Figure 5.13: Sensitivity of air excess ratio  $\lambda$  on system efficiency gain (a), and outlet receiver temperature (b)

### 5.5.2. Sensitivity to cylinder parameters

The timing of inlet valve closure and exhaust valve opening are varied with SA approach as described above. Each parameter is varied above/below its nominal value (Section 5.5.2).

Parameter of Interest	Nominal value	Units
$\alpha_{IC}$	54.8	[deg] bBDC
$\alpha_{EO}$	38.5	[deg] bBDC

#### Inlet valve closure timing

Early inlet valve closure does not benefit the system efficiency in contrast to a convention engine where Advanced Miller timing is used to increase its efficiency. Figure 5.14a shows that increasing the moment of inlet valve closure bBDC results indeed in an increased engine efficiency as commonly known. The compression ratio is lower than the expansion ratio, the work needed for the compression stroke is reduced while the expansion stroke is unchanged. The hybrid electric turbocharger changes the behaviour of the system efficiency when the moment of inlet valve closure is varied. The opposite trend is found (Figure 5.14b) for the system efficiency, delaying the inlet valve closure leads to an increased system efficiency gain.

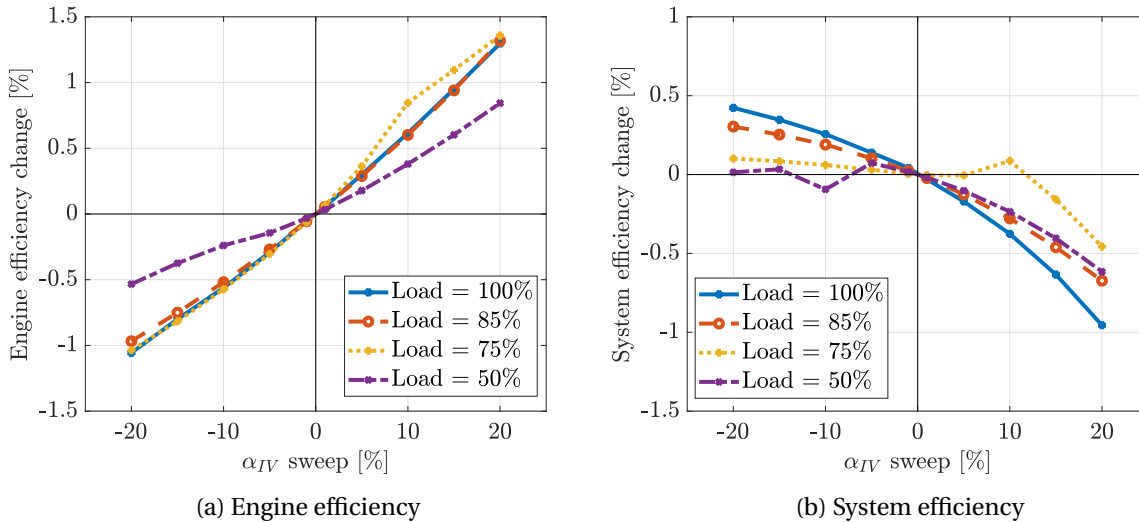
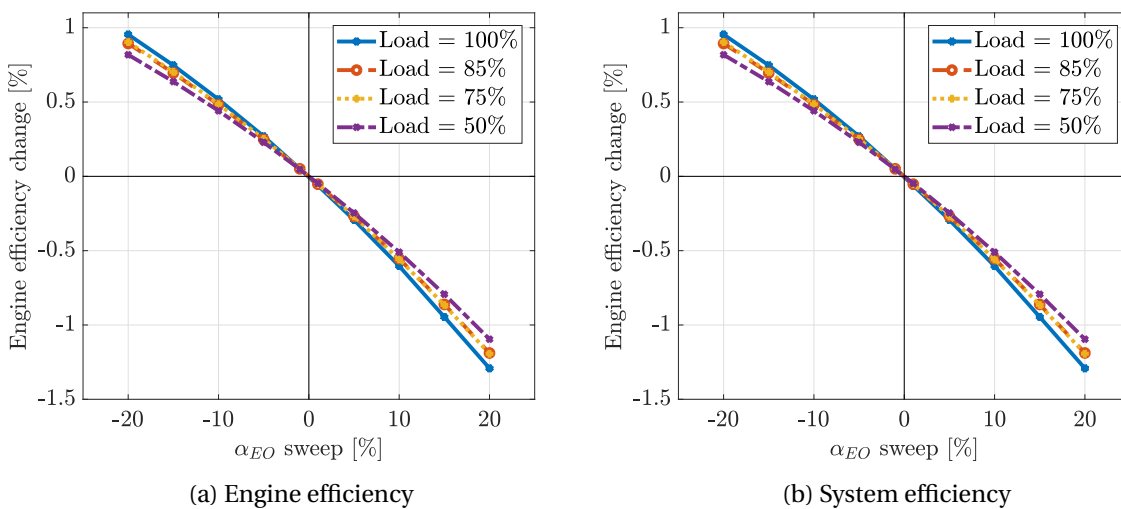


Figure 5.14: Sensitivity of timing inlet valve closing on engine efficiency gain (a), and system efficiency (b)

### Exhaust valve opening timing

Advancing the opening of the exhaust valve reduces the engine as well as the system efficiency while the generated electric energy increases. The timing of the exhaust valve determines when the in-cylinder expansion process ends wherein work at the crankshaft is obtained and from which moment the blow down starts into the outlet receiver. Lowering the expansion ratio reduces the engine efficiency (Figure 5.15a) as expected. The blow down of the exhaust gasses in the outlet receiver and the internal conditions of the outlet receiver together forms the turbine gas inflow. An advanced ending of the expansion stroke leads to a higher energy content of the turbine ingoing flue gas flow, indicated by the outlet receiver temperature Figure 5.15d. The increased energy available at the turbine inlet results in an increased generated power, as shown in Figure 5.15c. However the generated electrical power by the hybrid electric turbocharger does not close the drop of engine efficiency gap. Therefore for advancing the exhaust valve opening, the system efficiency decreases (Figure 5.15b).

The other way around applies to extending the exhaust valve opening timing to have an increased expansion ratio. The engine efficiency increases, the temperature of the exhaust gasses going into the turbine lowers, the generated electrical power reduces. In terms of efficiency, the cylinder is more sensitive to varying exhaust valve timing than the hybrid electric turbocharger.



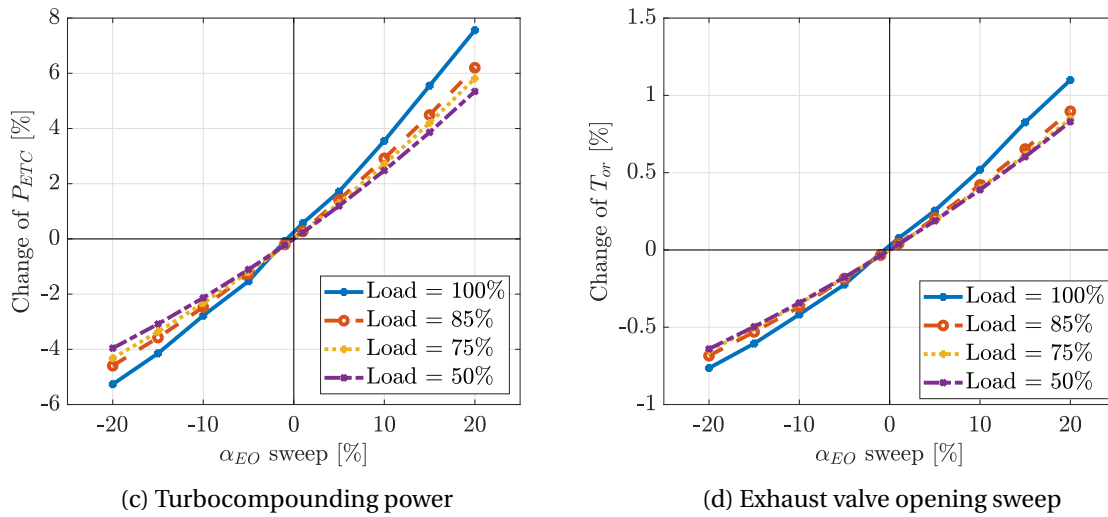


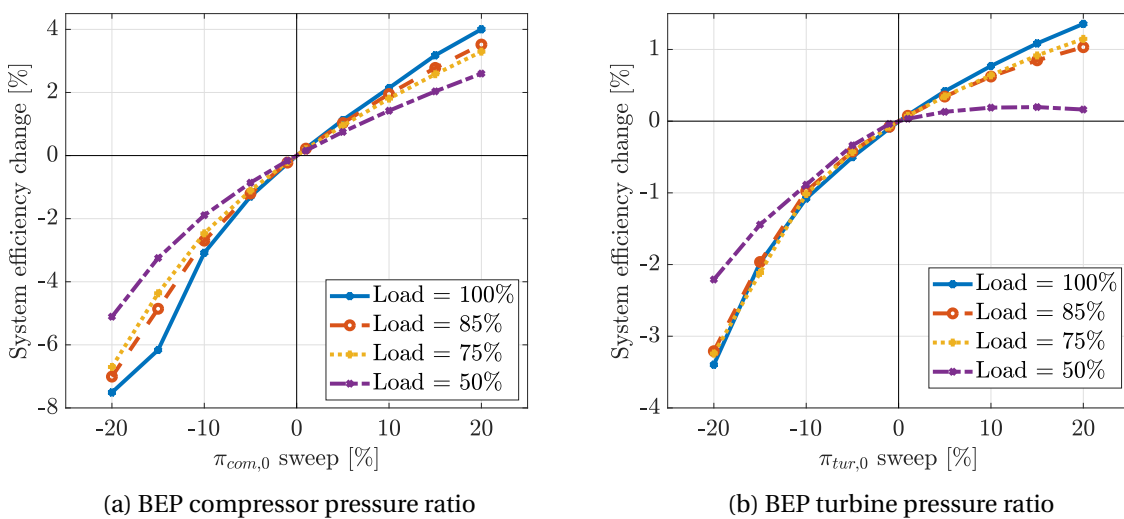
Figure 5.15: Sensitivity of timing exhaust valve opening on engine efficiency gain (a), system efficiency (b), turbocompounding power (c) and outlet receiver temperature (d)

### 5.5.3. Sensitivity of compressor and turbine parameters

Three turbocharger parameters are varied, the pressure ratio of the compressor and turbine where the Best Efficiency Point (BEP) is located, and the nominal compressor mass flow. Each parameter is varied above/below its nominal value (Section 5.5.3).

Parameter of Interest	Nominal value	Units
$\pi_{com,0}$	4.48	[-]
$\pi_{tur,0}$	0.274	[-]
$\dot{m}_{com,nom}$	5.69	[kg/s]

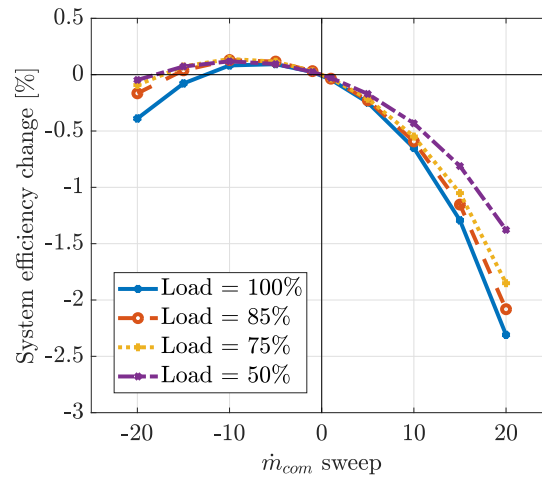
Increasing the pressure ratio of the compressor's BEP (Figure 5.16a), means it moves in the direction of the nominal operating point. The efficiency of the compressor increases leading to a lower power consumption by the compressor. The hybrid electric turbocharger in turbocompounding mode can take more power from the turbocharger shaft which results in an increased system efficiency. The same holds for the pressure ratio of the turbine's BEP to the system efficiency. Moving the BEP away from the nominal operating point lowers the system efficiency.



(a) BEP compressor pressure ratio

(b) BEP turbine pressure ratio

Figure 5.16c shows that the system efficiency can be increased if the compressor's nominal mass flow is decreased. The turbocharger is matched for the baseline engine without turbocompounding. With turbocompounding, the inlet receiver pressure ( $p_{ir}$ ) and charge air mass flow ( $\dot{m}_{ca}$ ) are decreased, as discussed in Section 5.3.2. Therefore, the fresh air mass flow ( $\dot{m}_{fresh}$ ) is reduced with turbocompounding compared to the baseline engine. The compressor operating condition moves away from the nominal operating point with the corresponding lower compressor efficiency. The compressor is not rematched for this reduced fresh air mass flow, which gives room for improvement when a smaller compressor is implemented.



(c) Compressor mass flow sweep

## 5.6. Approach of Operating Curve Shaping

This section shows the effect of electrically assisting the turbocharger (EAT) by means of the electric machine in order to enlarge the operating envelope. The calibrated engine in the mean value model does not match well with the product data, as shown in Section 4.7.8. Therefore also the operating envelope published in product data, does not match as can be seen in Figure 5.17. However, the operating envelope obtained from the simulation model will further be used in order to investigate the effect of turbocharger assistance.

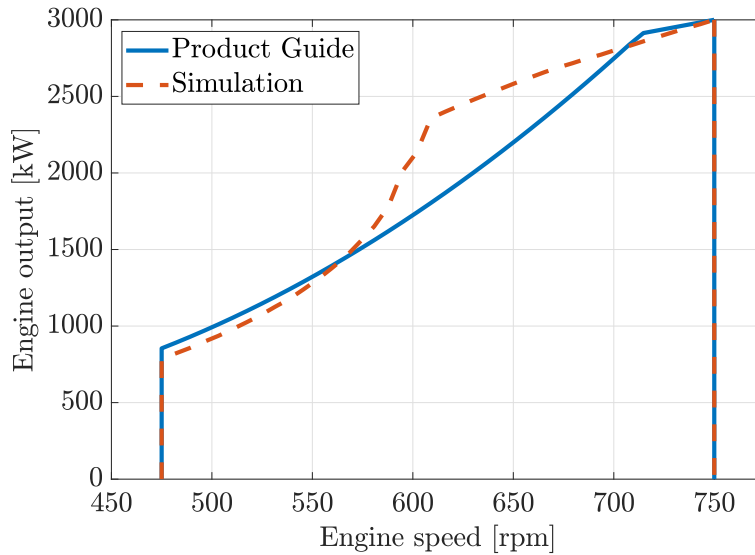


Figure 5.17: Operating envelope obtained from product guide vs obtained from simulation model

Next to the boundary controllers described in Section 4.9, two other constraints are considered for operating envelope curve shaping. The maximum in-cylinder pressure ( $p_3$ ) and the maximum engine torque ( $M_{ETC}$ ) are included. The turbine and electric machine power together to an increased availability of power for the compressor resulting in a raised inlet receiver pressure level. For nominal load and speed, the maximum in-cylinder pressure is exceeded due to the raised inlet condition and the unchanged in-cylinder compression ratio. A second constraint that is introduced, is the maximum allowable engine torque which should not be exceeded.

No limitations are found which lower the maximum power at 600 rpm from 2200 kW to 1700 kW as given in the product guide. The case "2200 kW at 600 rpm" lies on the simulation-based operating envelope boundary. The engine limits are quantified for the simulation-based operating envelope in Table 5.4. The peak in-cylinder pressure is no limitation for this case because  $p_3 = 170 < 191 \text{ bar}$  compared to the nominal operating point. The exhaust valve temperature is no limit too, because  $T_{exh, valve} = 1124 < 1265 \text{ K}$  for the low speed case (900 kW at 475 rpm). The same holds for the turbocharger speed ( $n_{TC}$ ), the air excess ratio ( $\lambda$ ) and temperature of the outlet receiver ( $T_{or}$ ). The mismatch between both operating envelopes is, probably, the result of the lacking matching results.

Table 5.4: Quantified engine operating limits

$P_{eng}$	kW	900	1700	2200	3000
$n_{eng}$	rpm	475	600	600	750
$\lambda$	-	1.78	2.2	2.0	2.42
$p_3$	bar	94	144	170	191
$T_{or}$	K	971	851	870	805
$T_{exh, valve}$	K	1265	1092	1124	1006
$n_{TC}$	rpm	21051	28632	31117	35517

### 5.7. Compressor surge limit reduces operating envelope

Assisting the turbocharger reduces the maximum power output because compressor surge limits further increase of power. Two assisting torque levels were used for the whole operating envelop, firstly with 25Nm additional torque and secondly with 50Nm torque. The drop of power in the surge region is clearly shown in Figure 5.18. From literature, discussed in Section 3.5, an enlarged operating envelope was expected, although the influence of compressor surge in most cases was not mentioned.

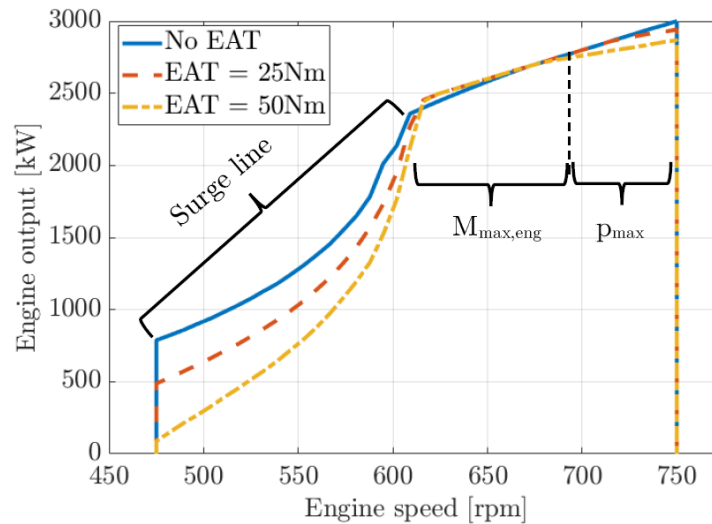


Figure 5.18: Operating envelope engine with without EAT, EAT = 25Nm and EAT = 50 Nm

The operating path in the compressor map is visualised in Figure 5.19 for the no turbocharger assistance and for the second assisting case: EAT = 50 Nm. The engine load is very slowly increased from 5% to the maximum power corresponding to the operating envelope of the non assisted engine. Indeed when no assistance is used, the operating point of the compressor just hits the surge line in contrast to the assisted case, where the operating point moves into the unstable surge region.

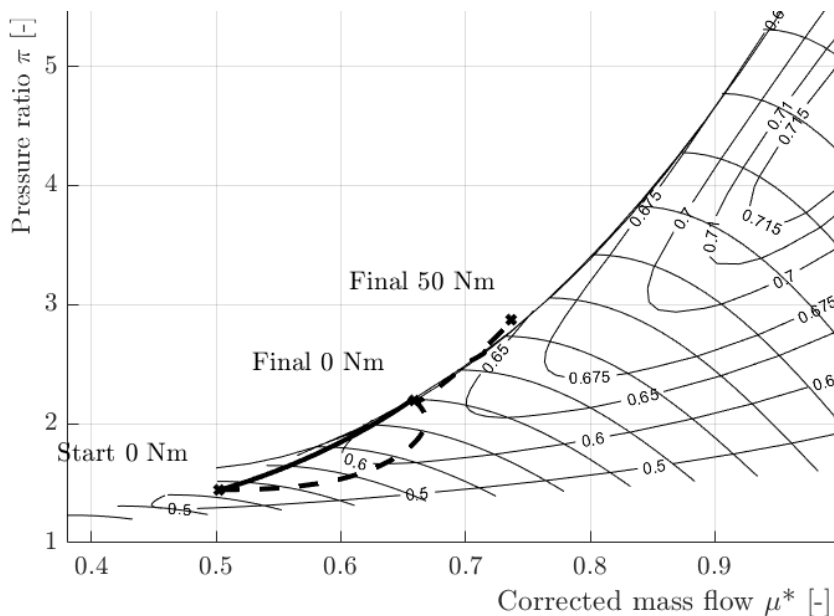


Figure 5.19: Operating paths in compressor map for No EAT and EAT = 50 Nm without BOV/BPV valves

Increasing the steady state power output above the unassisted power limit by assisting the turbocharger is impossible. Compressor surge does limit the increase of power for the unassisted engine, moreover it even lowers the maximum allowed engine power corresponding to a specific engine speed.

### 5.8. Operating curve shaping with EAT and Blow-off Valve

The operating envelope can be enlarged when the Blow-Off Valve is used to increase the compressor mass flow in order to avoid limitations from compressor surge. Compressor surge does not limit the power output for lower engine speed range because the operating point in the compressor map is moved to the right away from the surge line (Figure 5.21). The operating path is shown for a very slow load increase from 500 to 2000 kW at 525 RPM. Assisting the turbocharger with 50 Nm and a closed BOV is impossible due to compressor surge. When the BOV is used to increase the compressor mass flow, compressor surge is avoided. The operating envelope can be significantly increased up to almost the maximum engine torque constraint.

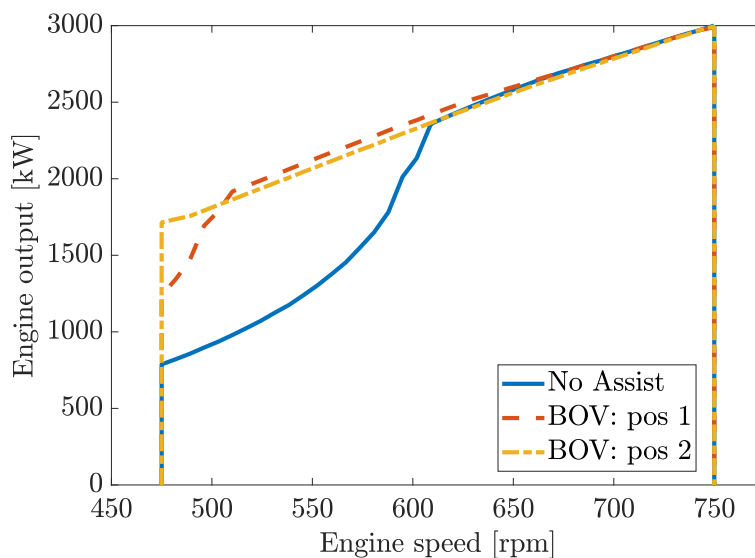


Figure 5.20: Operating envelope for baseline compared to EAT & two BOV positions

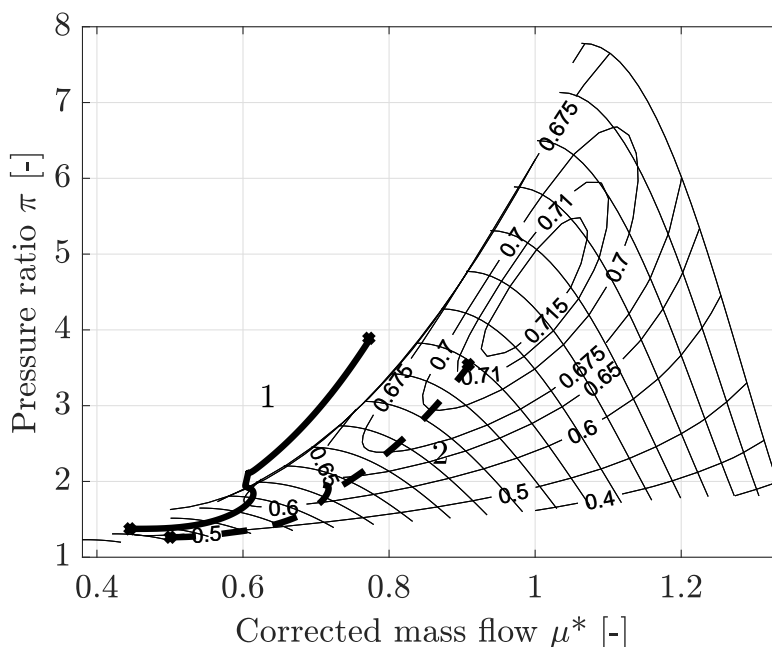


Figure 5.21: Operating paths in compressor map for  $M_{ETC} = 50 Nm$  &  $BOV = 0$  and  $BOV = 1$

As shown in Figure 5.20, the operating envelope gives the indication that the engine almost operate with a constant torque over the entire speed range. Figure 5.22 shows a flat torque line for the two assisted cases when the BOV is used. As can be seen, the torque output at low speed drops for the BOV pos 1 case, indicating that the bypassed mass flow should be increased in order to prevent compressor surge, which is done for the BOV pos 2 case.

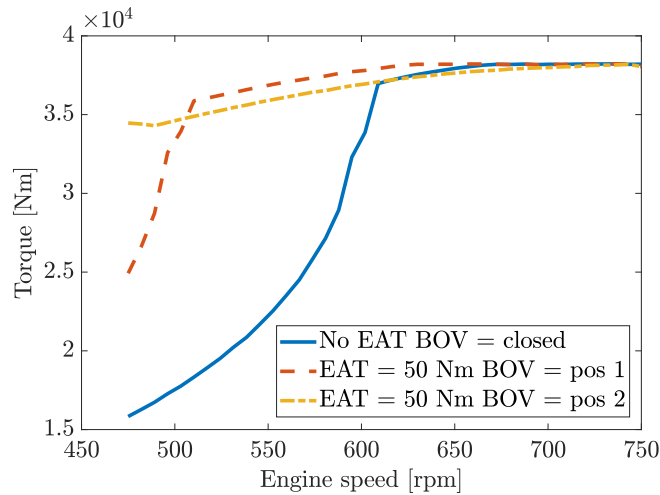


Figure 5.22: Engine torque for baseline compared to EAT & two BOV positions

For these simulations, a constant assisting torque is applied over the whole speed range, however from 600 - 750 rpm, no benefit is found for the operating envelope, therefore turbocharger assistance only benefits for the lower speed range. Assisting the turbocharger takes energy from the system, that is the reason why the major part of the system efficiency, for the two assisted cases, lies below the unassisted efficiency line. However, for the low speed region, the system efficiency even increases above the efficiency of the unassisted engine.

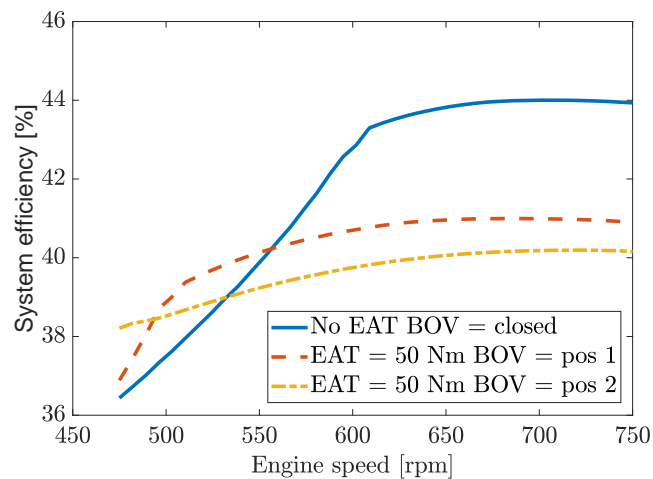


Figure 5.23: System efficiency for baseline compared to EAT & two BOV positions

The thermal loading of the exhaust valve is reduced for the low to mid engine speed range with turbocharger assistance and opening of the blow off valve. At nominal speed, the case with turbocharger assistance and the large BOV opening leads to an increased the thermal loading due to a lowered inlet receiver pressure. The bypassed air mass flow through the BOV is too large, resulting in a deteriorated gas exchange.

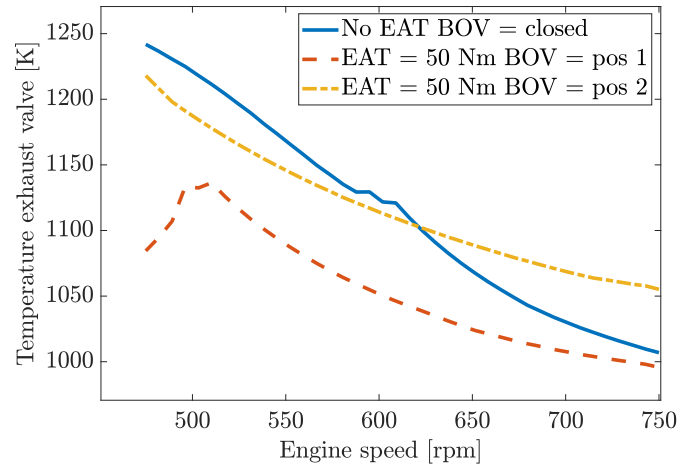


Figure 5.24: Temperature exhaust valve for baseline compared to EAT & two BOV positions

### 5.9. Operating curve shaping with EAT and Bypass Valve

Using the bypass valve (BPV) instead of the BOV has the same result with respect to the power increase at lower engine speeds. The power development of the engine for the low to mid speed range is significantly increased, as shown in Figure 5.25.

The overall system efficiency trend with the BPV enabled compared to the BOV, is that the drop in engine efficiency is lower. However, for BPV pos 1, the low engine speed efficiency drops below the engine efficiency, where the "BOV= pos 2" case remains above the baseline engine efficiency.

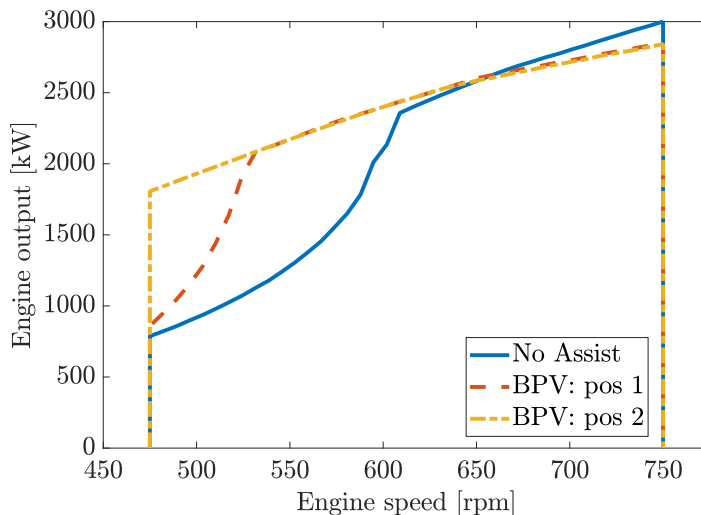


Figure 5.25: Operating envelope for baseline compared to EAT & two BPV positions

The BPV valve is necessary to prevent compressor surge (Figure 5.26) to increase the compressor's mass flow. The operating point in the compressor map moves from the surge region into the stable region.

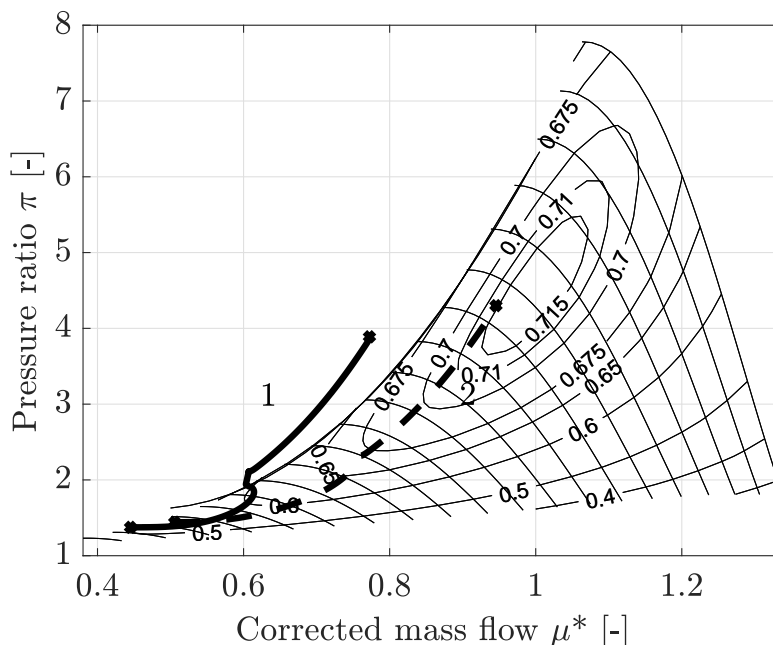


Figure 5.26: Operating paths in compressor map for  $M_{ETC} = 50 Nm$  & BPV = 0 and BPV = 1

The engine torque output for the low to mid engine speed range is increased when turbocharger assistance is combined with the bypass valve. For the low BPV opening, still compressor surge limits the low speed torque development. Increasing the bypassed air mass flow, increases the compressor's mass flow such that no compressor surge limits further increase of the engine torque development. However, for the higher engine speed range, a lower maximum power output is obtained compared to the BOV case. This is, probably, due to the increased outlet receiver pressure because charge air is partly directed from the inlet to the outlet receiver where the BOV case directs part of the charge air direct into environment. The increased inlet receiver pressure for nominal power and speed leads to high in-cylinder pressure level. Therefore the maximum power obtainable at nominal speed is reduced to prevent overboosting. However, in the higher engine speed range, there is no benefit of assisting the turbocharger because the maximum engine torque is already obtained without turbocharger assistance.

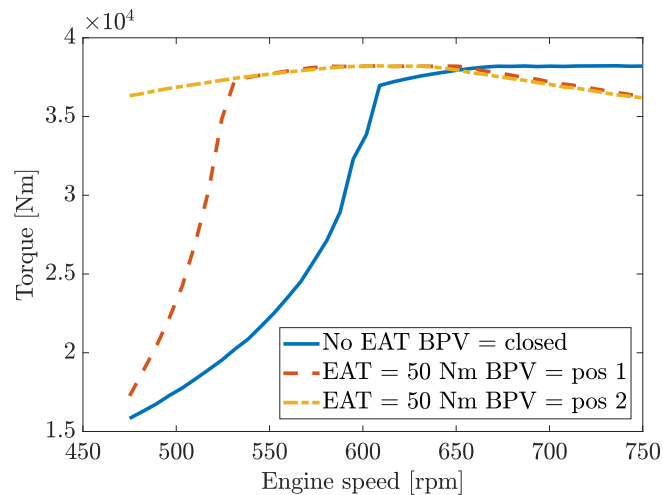


Figure 5.27: Engine torque for baseline compared to EAT & two BPV positions

The system efficiency can be improved for the low engine speed range, as already shown for the turbocharger assistance and blow off valve. A relative flat efficiency curve can be obtained by assisting the turbocharger for the low engine speed range while bypassing a part of the compressor's mass flow from the inlet to the outlet receiver.

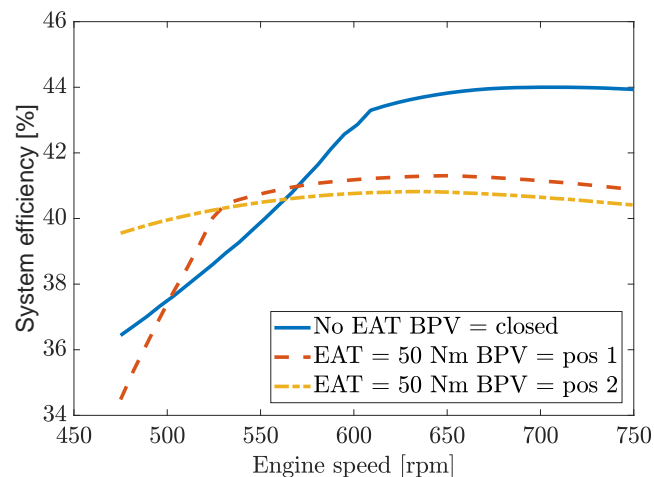


Figure 5.28: System efficiency for baseline compared to EAT & two BPV positions

Thermal loading is no limitation for turbocharger assistance combined with the BPV as depicted in Figure 5.29. The temperature of the exhaust valve is decreased for the whole engine speed range compared to the baseline engine.

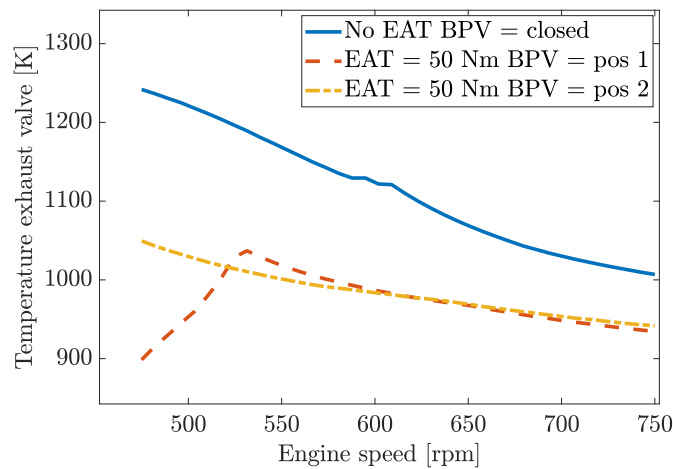


Figure 5.29: Temperature exhaust valve for baseline compared to EAT & two BPV positions

## 5.10. Conclusions

Turbocompounding to increase the system efficiency results in:

- a small efficiency increase which can only be obtained for nominal load and speed. For lower loads and speed, the system efficiency is deteriorated, turbocompounding should be turned off.
- a higher obtainable system efficiency when a waste gate is replaced for the hybrid electric turbocharger. The quantity of recoverable energy, as well as the area of the operating envelope in which turbocompounding is possible, increases.
- a reduced power available for the compressor. The inlet receiver pressure drops, leading to a lower charge air mass, scavenging gets worse due to the reduced pressure difference over the inlet and outlet valves.
- an increased thermal loading of the engine as result of the deteriorated gas exchange.
- a reduced system efficiency gain with Advanced Miller Timing. Early closure of the inlet valve has the opposite effect to the turbocompounded engine compared with the baseline engine for which Advanced Miller Timing is a measure to increase the engine efficiency.

Assisting the turbocharger results in:

- a smaller operating envelope due to compressor surge. The surge limit in the operational envelope moves down compared with the non-assisted engine.
- an increased operating envelope when assistance is combined with bypass valves. Both the bypass valve (BPV) as well as the blow off valve (BOV) increases the compressor's mass flow resulting in no surge line limitation.
- an almost constant engine torque output when turbocharger assistance is used with bypass valves for the low engine speed range.
- an improved engine efficiency for low engine speed compared to the baseline engine, but reduces for higher engine speeds.

Turbocharger assistance lowers maximum power output at lower speed range due to compressor surge  
BOV and BPV enables increase of power output due to increased compressor mass flow

*FURTHER EXPLANATION CONCLUSION TO BE CONTINUED*

# 6

## Dynamic Analysis

### 6.1. Introduction

The effects of a hybrid electric turbocharger integrated into the Diesel B mean-value model on dynamic engine operation are discussed in this chapter for increasing the loading capability of the engine.

The research question to be answered in this chapter:

- *Analyse the engine's dynamic behaviour for multiple loading functions at varying engine load points*

Four engine loading functions are discussed: 1. three consecutive load steps, 2. instant load step, 3. load ramp and, last, 4. sinusoidal load.

- First the effect of assisting the turbocharger for three consecutive load steps from 0 - 33 - 66 - 100% are investigated. Regulations are drawn up to which extent a generator set should be able to take the consecutive load steps, as discussed in Section 2.3 from literature.
- The second loading function is the instant load step. Manufacturers show the instant load step capability of their engine in the product guide. Up to which extent does turbocharger assistance increase the allowable instant load step.
- The load ramp is the third loading function investigated in this chapter. Does turbocharger assistance lead to a shorter time needed to take a load ramp from zero to full engine power will be discussed.
- The last case is the sinusoidal load function, what benefit can be obtained with turbocharger assistance for the engine loaded with a sinusoidal load.

An overview of above mentioned cases is visualised below:

<b>Section</b>	<b>Loading function</b>
6.2	IACS's three consecutive load steps
6.3	Instant load step
6.4	Load ramp
6.5	Sinusoidal load

## 6.2. Loading capability: Three consecutive load steps

The diesel engine response to three consecutive load steps from 0 to 100% load shows that enabling EAT during the load step, lowers the recovery time needed after a load step depending on the additional inertia of the turbocharger shaft. At  $t = 5$  s, the first load step (0 - 33%) is suddenly applied to the engine. According to Section 2.3, the following engine output states are used to determine when the next load step could be applied to the engine:

1. Engine power output response within error band
2. Air excess ratio output response within error band
3. Turbocharger speed output response within error band

The engine speed is not considered as a fourth output state because no reasonable speed drop was found due to immediately governor action when a small engine speed deviation was found. Moreover, due to high PI control parameter values, the speed drop is very limited. The governor controller was not changed to limited the fuel injection for low air excess ratios ( $\lambda < 1.7$ ). In reality, the engine has a fuel limiter when the engine speed drops due to a considerable engine loading, however it is not implemented due to the scope of this project to investigate multiple loading functions.

First, the load step results are shown to visualise the engine's response thereafter the shown results are quantified in Table 6.1.

### 6.2.1. Engine load

Figure 6.1 shows the three load steps for four cases: with and without EAT, for conventional turbocharger shaft inertia ( $J_{TC} = 100\%$ ) and doubled inertia ( $J_{TC} = 200\%$ ). Less time is needed for the engine to take the three consecutive load steps when the turbocharger is assisted. Doubling the turbocharger's inertia negatively affect the time needed for the three load steps compared to the non-assisted case.

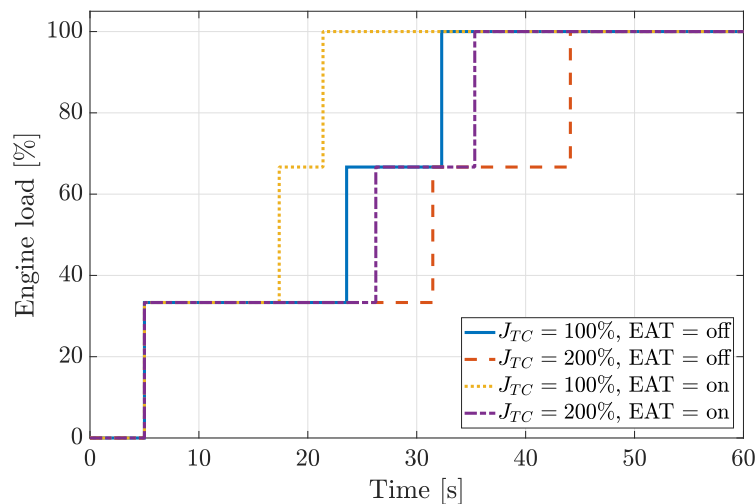


Figure 6.1: Load step capability 0 - 33 - 66 - 100% as function of time

### 6.2.2. Air excess ratio

Figure 6.2 shows the air excess ratio ( $\lambda$ ) for the baseline TC shaft inertia with and without turbocharger assistance (EAT). The doubled TC shaft inertia is not shown to keep a readable figure. One important aspect shown in Figure 6.2, is the low air excess ratio ( $\lambda = 1.0 - 1.1$ ) after the first load step as a result of no governor limitation to avoid operating with a low air excess ratio. No confirmation can be found in literature if this low air excess ratio is momentarily reached in practice during a load step, but according to Stapersma (2010a) it is far below normal operating conditions. Further research has to be done to investigate the effect of a governor limiter on the engine's capability to take three consecutive load steps.

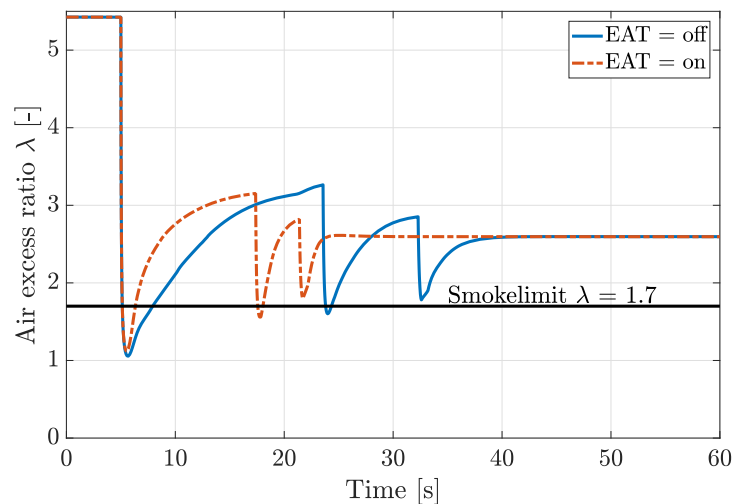


Figure 6.2: Air excess ratio as result of load steps

### 6.2.3. Turbocharger speed

The turbocharger spools up faster when it is assisted leading to an improved turbocharger response, as shown in Figure 6.3. There is a small speed overshoot with assistance, as can be seen in Figure 6.3. The reduced increase for  $J_{TC} = 100\%$  &  $EAT = on$  case, is a result of hitting the maximum electric machine torque (Figure 6.5), for which 150 Nm is chosen as peak torque.

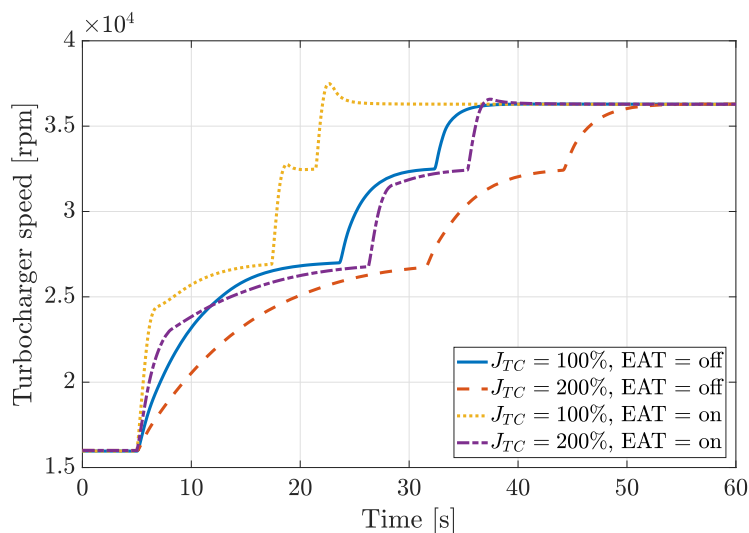


Figure 6.3: Turbocharger speed response as result of load steps

### 6.2.4. Fuel mass flow

The fuel mass flow response after a load step is equal for all the four cases, as depicted in Figure 6.4. The moment of time and duration is different, but the shape of the response is equal as result of the governor controller which only make use of the engine speed to control the fuel to be injected.

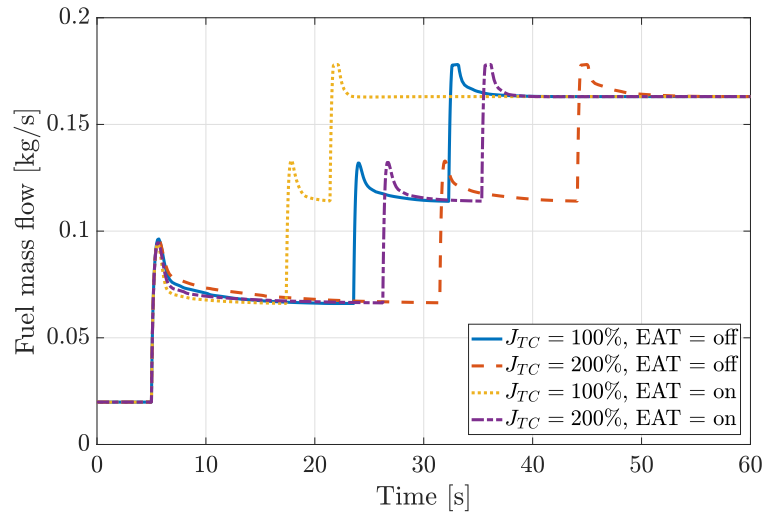


Figure 6.4: Injected fuel mass flow response as result of load steps

### 6.2.5. Electric machine torque

After a load step is applied to the turbocharger, more fuel is injected leading to a drop in air excess ratio. The control strategy starts to assist the turbocharger via the electric machine to increase the air excess ratio up to the desired set point value. The turbocharger starts to spool up much faster than the baseline engine, however the electric machine reaches its maximum torque output after which the turbocharger response rise less fast and, finally, reaches steady state before a next load step is applied.

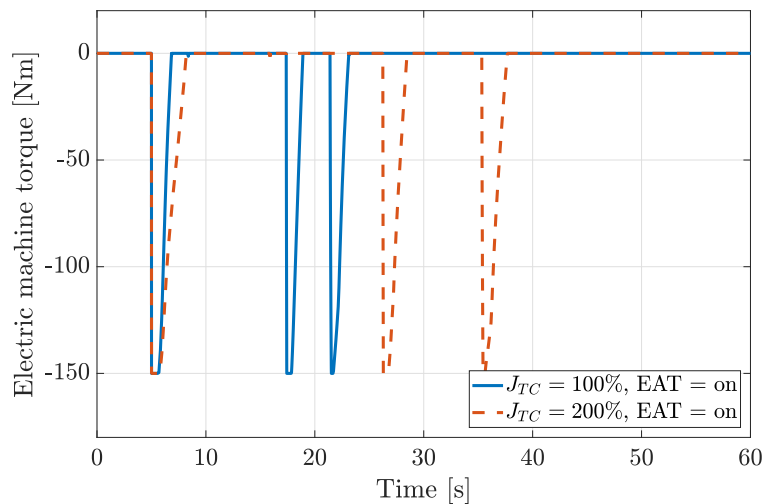


Figure 6.5: Electric machine torque response as result of load steps

### 6.2.6. Inlet receiver pressure

Assisting the turbocharger improves inlet receiver pressure response (Figure 6.6), the faster the inlet receiver pressure reaches a higher pressure level, the earlier the engine develops power to withstand the load increase. The doubled inertia deteriorates this boost pressure build up as expected from the results depicted in Figure 6.3.

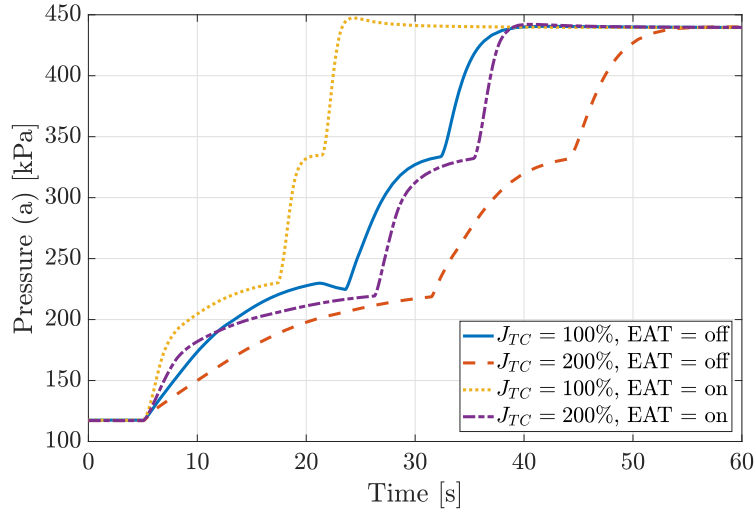


Figure 6.6: Inlet receiver pressure as result of load steps

### 6.2.7. Quantification of consecutive load steps

Assisting the turbocharger reduces the recovery time needed before the next load step can be applied on the engine. Table 6.1 shows the quantification of previously presented figures. The low turbocharger shaft inertia and turbocharger assistance enabled, leads to the fastest recovery after every load step. This case has by far the highest turbocharger shaft acceleration of about  $780 \text{ rad/s}^2$  which is almost 2.5 times higher than the unassisted case. This increased shaft acceleration results in a obvious lower settling time after which the following load step can be applied. A higher turbocharger inertia leads to a longer time span needed to take the three load steps but also increases the duration for which the engine is operating below the smoke limit. The smoke limit used is  $\lambda = 1.7$ . The low turbocharger inertia combined with turbocharger assistance results in the shortest duration in which black smoke and increased unwanted emissions are emitted in atmosphere.

Table 6.1: Quantification of four cases with turbocharger assistance on/off and two turbocharger shaft inertias (100% and 200%)

W6L34DF case	Load step settling time [s]			Maximum TC angular acceleration [ $\text{rad/s}^2$ ]			Operating time below smoke limit [s]
	0 - 33%	33 - 66%	66 - 100%	0 - 33%	33 - 66%	66 - 100%	
$J_{TC} = 100\%$ , EAT off	15.2	8.6	8.1	264	302	333	4.7
$J_{TC} = 200\%$ , EAT off	24.6	12.9	7	132	157	182	7.2
$J_{TC} = 100\%$ , EAT on	8.6	4.7	6	779	767	785	2.5
$J_{TC} = 200\%$ , EAT on	17	8.1	8	396	408	427	3.3

### 6.3. Loading capability: Instant load step

This section shows the results for the loading type: instant load steps. The maximum instant load step is determined as function of the initial engine power level. A minimum allowable air excess ratio ( $\lambda = 1.7$ ) is used to determine the maximum instant load step. However, in reality the dual fuel engine's loading capability is not only limited by the minimum air excess ratio, but even more by the maximum speed droop as result of the limited governor response. Due to high PI control parameters in the simulation model, there was almost no speed droop. Further research has to be done to determine the maximum load step capability limited by the engine speed droop.

#### 6.3.1. Load step capability as function of acceptable air excess ratio

Three minimum air excess ratios ( $\lambda$ ) are selected in order to find the maximum instant load step capability without turbocharger assistance (EAT). As expected, the lower the acceptable minimum constraint, the higher the allowable instant load step (Figure 6.7).

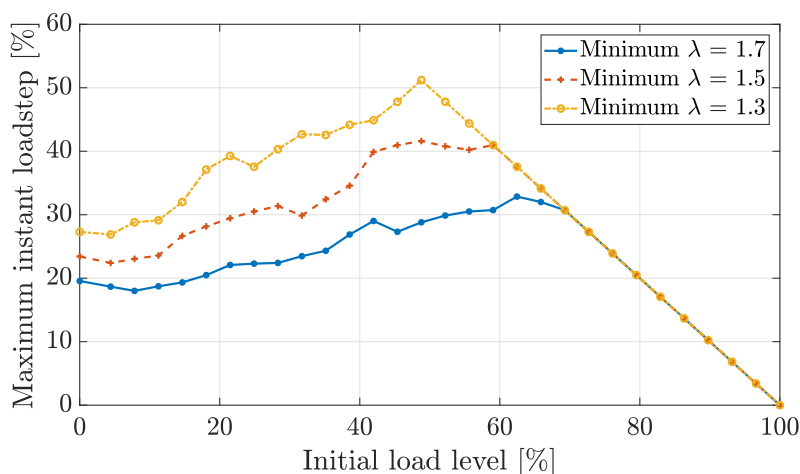


Figure 6.7: Instant load step capability for three minimum air excess ratios ( $\lambda$ )

#### 6.3.2. Load step capability with variable inlet valve closure

Reducing the advanced Miller timing (early inlet valve closure) results in the ability to take a higher instant load step compared with an engine that uses advanced Miller timing (Figure 6.8). Advanced inlet valve closing leads to less fresh air induced into the cylinder, and therefore in a lower air excess ratio. When the initial air excess ratio has a higher value, there is more room to decrease due to the load step compared with a lower initial air excess ratio.

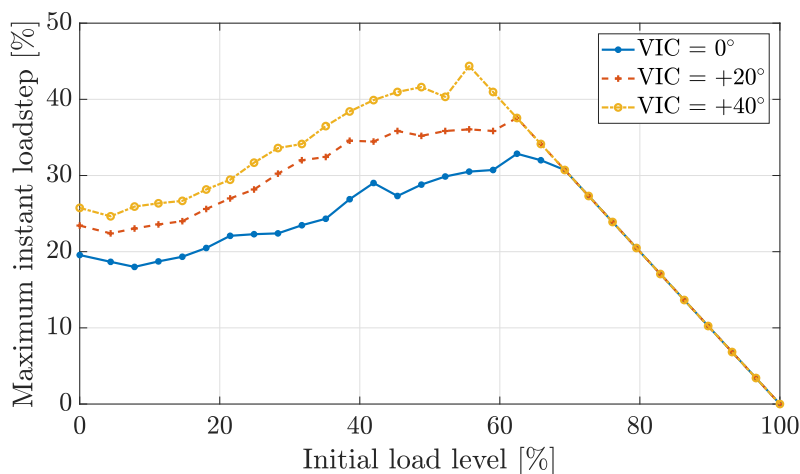


Figure 6.8: Instant load step capability for three inlet valve closure settings

### 6.3.3. Load step capability with and without ETC

When an instant load step is applied to the engine, EAT has no significant benefit with respect to the minimum air excess ratio ( $\lambda$ ) that is reached. The instant load step capability is almost equal to the unassisted engine case, as shown in Figure 6.9. Another case is wherein the hybrid electric turbocharger is used to increase the system efficiency by turbocompounding. When initially the system is in turbocompounding mode, and an instant load is applied, the turbocharger has to build up boost pressure up to the level of the baseline engine. The gap between turbocompounding and the baseline turbocharger conditions has to be closed, thereafter assistance starts to assist the turbocharger. Recovery from turbocompounding mode up to turbocharger assistance mode takes time, therefore the instant load step capability is low, as shown in Figure 6.9.

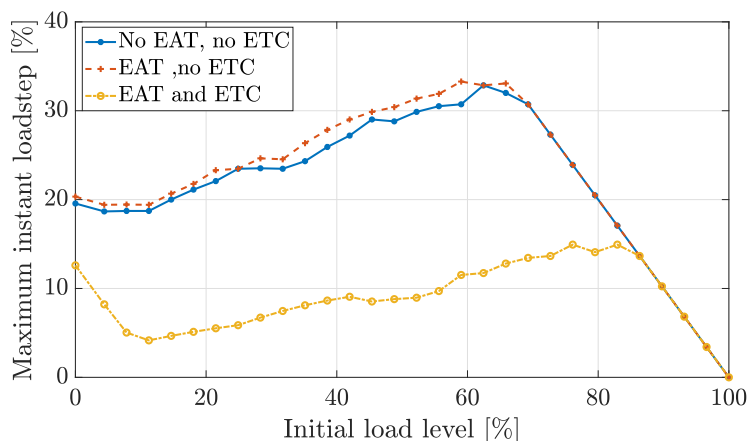


Figure 6.9: Instant load step capability for EAT and ETC on/off settings

### 6.3.4. Load step capability with preboost

In Section 6.3.3, it is shown that the instant loading capability does not increase by starting to assist the turbocharger at the same time as the load step is applied to the engine. However, if the electric machine already starts to assist the turbocharger a couple of seconds before the load step is applied to the engine, the load step capability can be increased. This case, further called preboost, can be implemented if, for instance, the instant load type is the starting procedure of a dredge pump. The dredge operator decides when to start this large power consumer. This procedure could introduce a small time frame wherein the turbocharger already is assisted before the clutch is closed between the engine and dredge pump.

This preboost approach is applied in the mean value model with four time frames: 1s, 5, 10 and 20 s. As depicted in Figure 6.10, starting with assistance 1s before the load is applied, leads to a small increased load step capability of about 3 - 9%. Starting the assistance 5s in front of the load, results in double the load step capability compared with the baseline case. The preboost times 10 s and 20 s lead to almost the same load step capability which increases from about 20% to 50+% which is 2.5 times higher than the non-assisted engine.

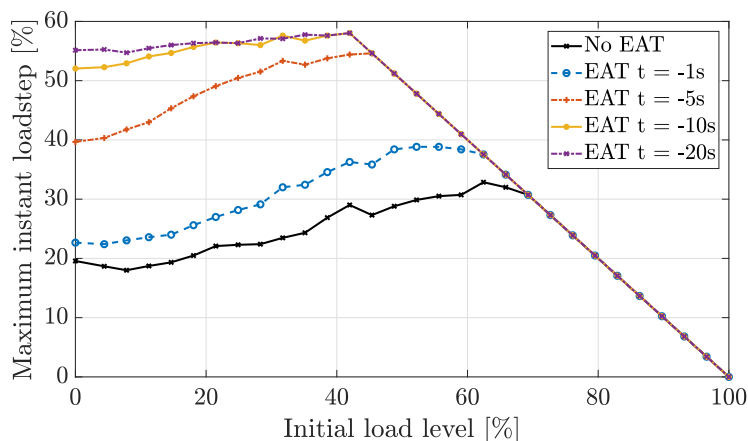


Figure 6.10: Instant load step capability with preboost

The drawback of preboost is the high air excess ratio before the load step is applied to the engine. As shown in Figure 6.11, relative high air excess ratios are reached with preboost. The initial engine load level is 0% for which the air excess ratio response is shown for the maximum load step that can be taken with preboost, as shown in Figure 6.10. In Figure 2.11, the misfire limit is located between , in case of natural gas combustion, probably leads to misfire. However this is not investigated to check if misfire occurs based on the theory discussed in Section 2.3.1.

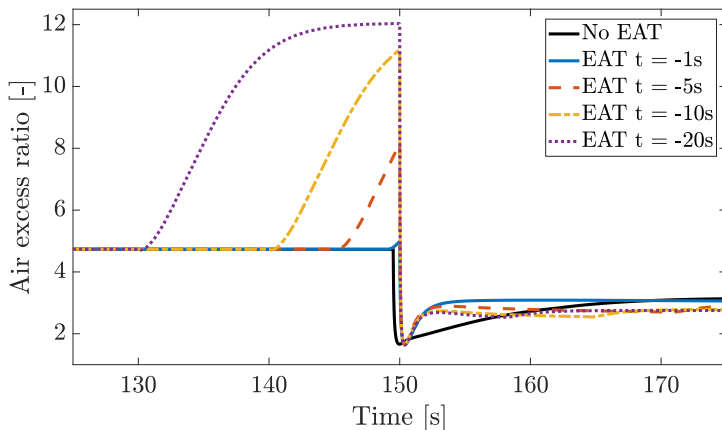


Figure 6.11: Air excess ratio response load step from 0% load with preboost

### 6.4. Loading capability: load ramp

The load ramp is the third loading function investigated in this chapter. The engine load is linearly increased from 0 to 100% load within the shortest time possible without crossing a lower air excess ratio limit. First the results of the non-assisted turbocharged engine are given, thereafter the effect of turbocharger assistance on the load ramp capability will be discussed.

#### 6.4.1. Load ramp without electrical assistance

The lower the acceptable air excess ratio, the faster the load ramp can be taken (Figure 6.12a). The load ramp can be taken within 26 s for  $\lambda = 1.7$ , this time can be reduced up to 15 s for the lower limit  $\lambda = 1.3$  which is below the smoke limit ( $\lambda = 1.7$ ) for Heavy Fuel Oil (HFO). The recovery time needed before the air excess ratio reaches steady state is about 13 - 15 s after the load ramp is finished.

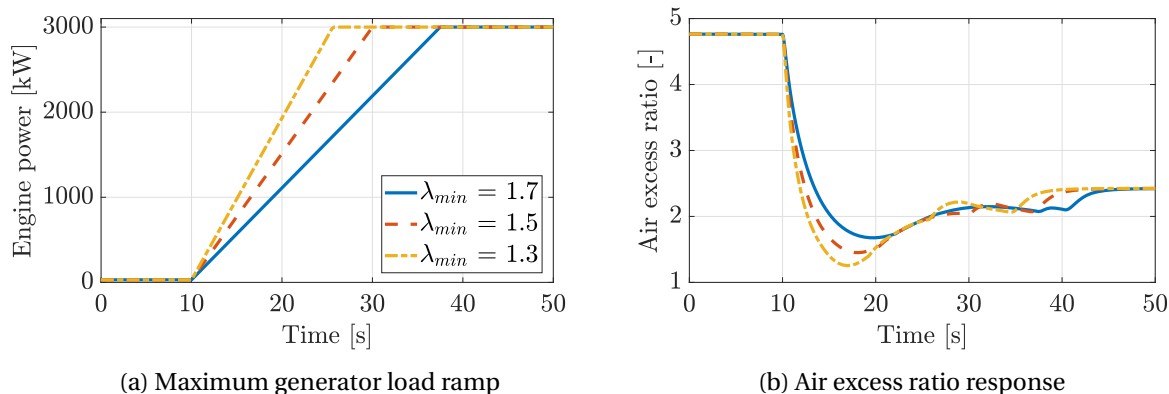


Figure 6.12: Maximum load ramp and air excess ratio for three load ramps with as limit three cases:  $\lambda_{min} = 1.3, 1.5, 1.7$

### 6.4.2. Load ramp with electrical assistance

The time needed to take a load ramp from 0 - 100% can be reduced by assisting the turbocharger (EAT). Three cases are compared, the non-assisted baseline engine, secondly assisting the turbocharger which starts when the load ramp is initiated, and, last, assisting the turbocharger while the system was in turbocompounding mode (ETC) before the load ramp is taken. The lower air excess ratio limit is chosen to be  $\lambda = 1.7$ , which means taking the load ramp without engine smoking. The lowest time needed, to take the load ramp, is obtained when no turbocompounding (ETC) is used in front of the load ramp. When turbocompounding is used, the load step can be taken in a shorter time span too compared with the unassisted case, however more time is needed compared with the solely assisted case (EAT). The time needed to take the ramp load reduces from 28 s for the non-assisted case to 6 s for the assisted case. For initially turbocompounding and thereafter turbocharger assistance (EAT, ETC), 13 s are needed for the load ramp.

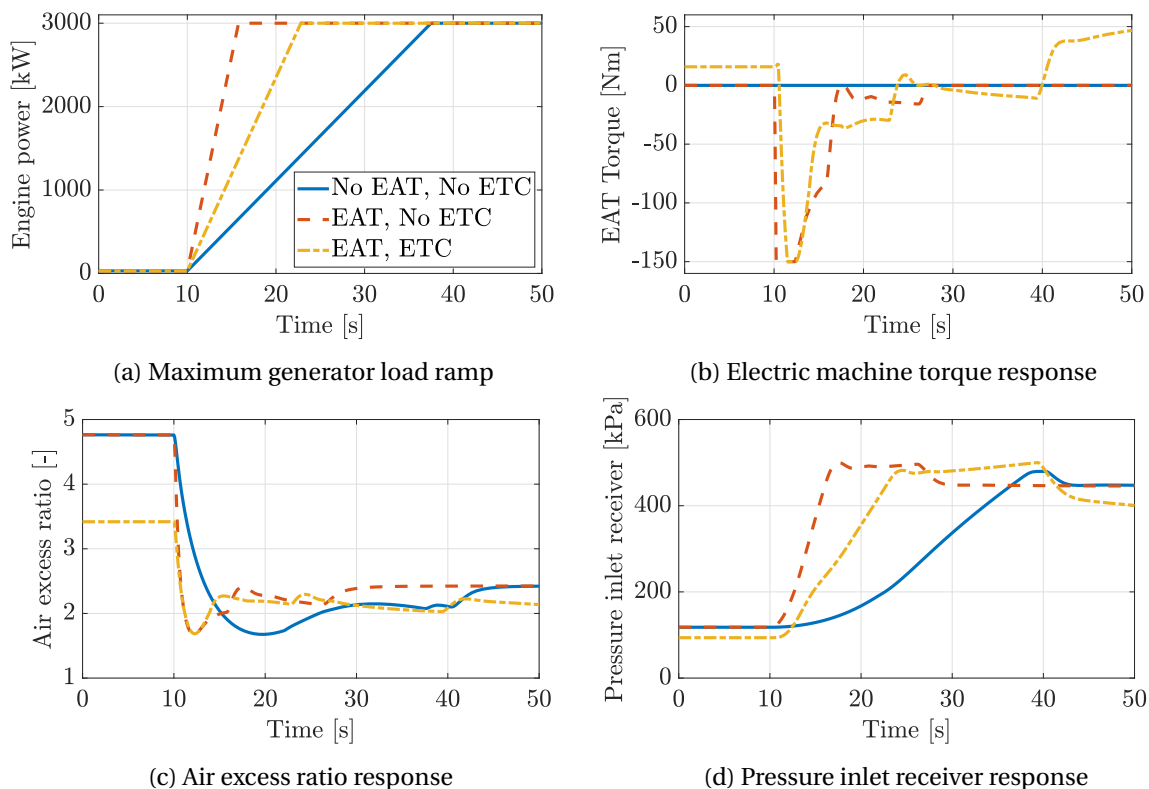


Figure 6.13: Maximum load ramp and air excess ratio for three cases: no EAT and no ETC, EAT and no ETC, EAT and ETC enabled

The quantification of above shown figures is given in Table 6.2. The duration of the load ramp can be reduced with 80% when the turbocharger is assisted, and with 55% for the turbocompounding and assistance case.

Table 6.2: Quantification of three cases for load ramp function

Case	Settling time	Time reduction
-	s	%
No EAT, No ETC	27.7	100
EAT, No ETC	5.9	-79
EAT and ETC	12.9	-54

### 6.5. Loading capability: sinusoidal load

The fourth loading function investigated in this thesis is the sinusoidal load. In reality, generator load fluctuations are present in, for example, the dredge system due to varying slurry densities during dredging operation. Other examples are wind and wave forces. A cyclic loading and unloading function is set as generator load on the engine in the mean value by multiplying a sinusoidal function with a constant load. The system's response to the fluctuating generator loads is analysed for 33 frequencies from 0.001 - 10 Hz to investigate what the effect of turbocharger assistance is on the engine performance. The sinusoidal generator load varies between 70 - 100%, composed of a constant load of 85% and an amplitude of 15% engine load.

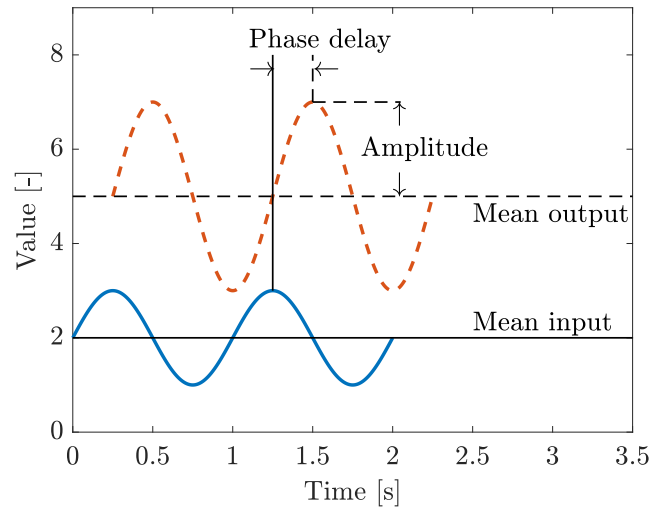


Figure 6.14: Amplitude and phase delay between sinusoidal input load and output parameter of interest

### 6.5.1. Power electric machine

Turbocompounding is possible for cyclic loading up to 0.2 Hz, however for higher frequencies the generator mode cannot be used, as depicted in the most upper sub figure of Figure 6.15. Moreover, for higher frequencies than 0.2 Hz, turbocharger assistance is used to control the air excess ratio as result of the control strategy. For low frequencies, a relative constant turbocompounding power output is obtained, as shown in the amplitude plot (middle sub plot) of Figure 6.15. The turbocharger assistance power varies for higher frequencies with power amplitudes up to 600 kW. The phase plot (lower sub plot of Figure 6.15) shows that movement from turbocompounding to turbocharger assistance as function of the frequency. No turbocharger assistance is needed for low frequencies, however changes from a major turbocompounding and minor assistance to no turbocompounding and solely assistance, quantified with the phase difference between the load and electric machine power response. The higher the turbocharger shaft inertia, the lower the maximum frequency below which turbocompounding is possible.

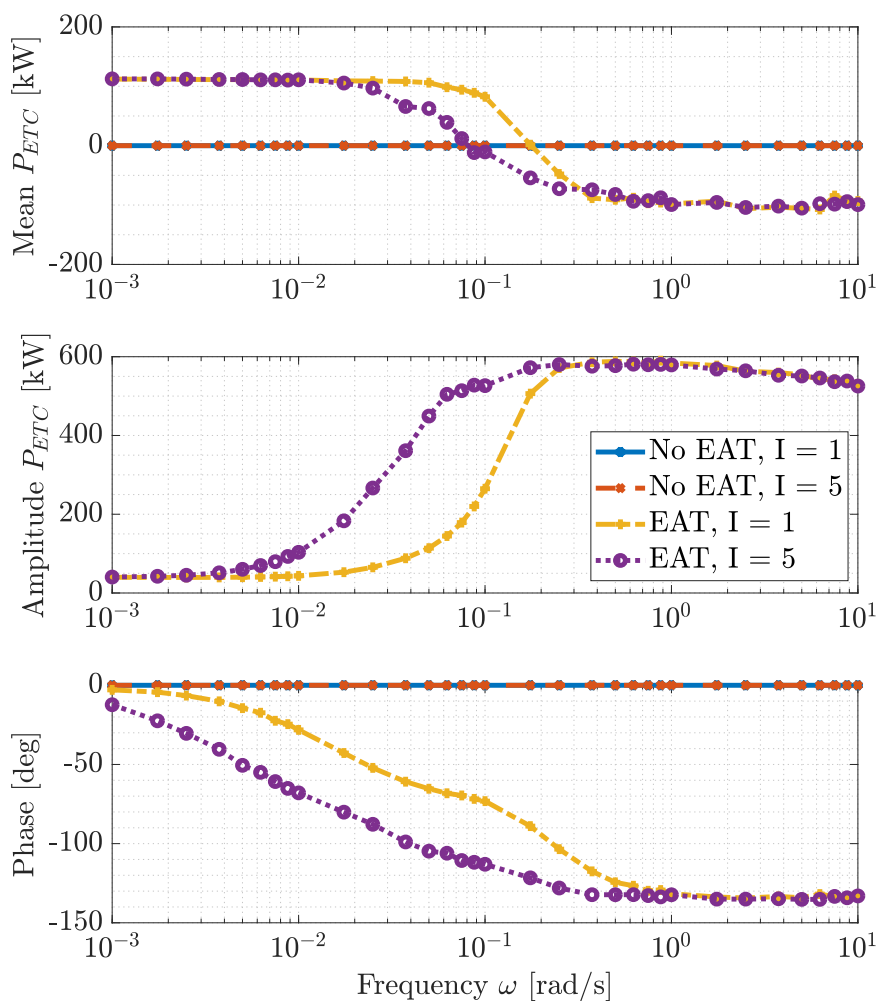


Figure 6.15: Power electric machine response for sinusoidal loads, mean load = 85%, amplitude load = 15%

### 6.5.2. Turbocharger speed

The reduced turbocharger speed for turbocompounding is also recognizable in the upper sub figure of Figure 6.16. For the low frequency range, turbocompounding is successful which leads to a lower mean turbocharger speed, while for higher frequencies, the mean turbocharger speed increases due to the aid of the electric machine. The turbocharger speed amplitude is reduced for the higher turbocharger inertia case (No EAT,  $I = 5$ ) compared to the baseline case (No EAT,  $I = 1$ ). The turbocharger assistance mode increases the speed amplitude for the frequency range of 0.001 - 0.1 Hz, thereafter the load frequency influence on the turbocharger shaft speed is reduced. The effect of turbocharger assistance on the phase between the load and turbocharger response is depicted in the lower sub figure of Figure 6.16. The higher the turbocharger shaft inertia, the lower the frequency for which the phase breaks off. Turbocharger assistance improves the turbocharger speed response up to such manner, that the break off point moves from 0.001 to 0.2 Hz for the low inertia (EAT,  $I = 1$ ) case.

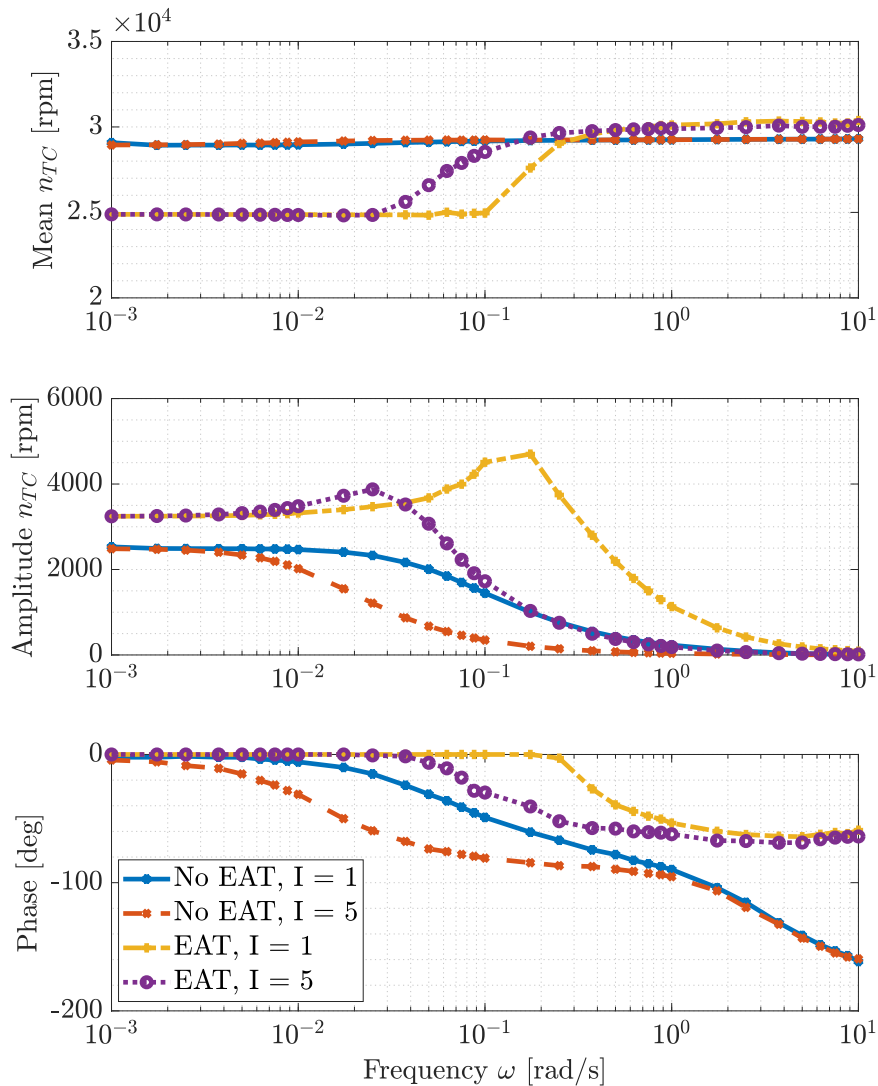


Figure 6.16: Turbocharge speed ( $n_{TC}$ ) response for sinusoidal loads, mean load = 85%, amplitude load = 15%

### 6.5.3. Air excess ratio

The hybrid electric turbocharger in turbocompounding mode tries to keep the actual air excess ratio as close as possible to its desired set point. This is successful for the lower speed range, as can be seen in Figure 6.17. The air excess ratio for the lower frequency range is lowered from  $\lambda = 2.8$  to  $\lambda = 2.0$ , which is the set point of the control strategy. There is no phase between the cyclic load and air excess ratio response for the lower frequency range. Moreover there is no amplitude for the air excess ratio due to turbocompounding. These results show the controllability of the air excess ratio with the hybrid electric turbocharger. An increased turbocharger shaft inertia deteriorates this controllability due to moving the break off to a lower load frequency. For higher frequencies the used control strategy is not sufficient any more to keep the air excess ratio at the desired value, which can be concluded from the amplitude shown in the middle sub figure of Figure 6.17.

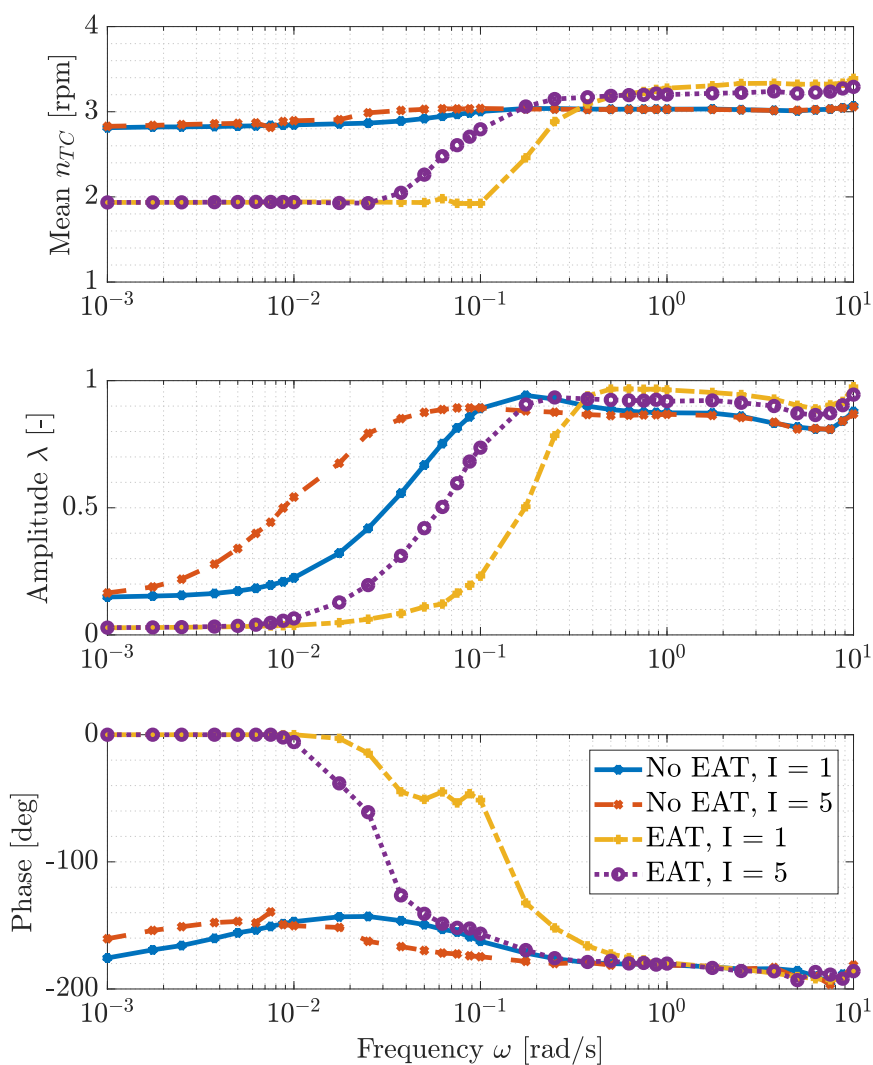


Figure 6.17: Air excess ratio response for sinusoidal loads, mean load = 85%, amplitude load = 15%

## 6.6. Conclusions

Assisting the turbocharger for the four load functions results in:

- a reduced recovery time needed between three consecutive loads steps from 0 to 100% load. The next load step can be taken within a shorter time frame compared to the baseline engine without turbocharger assistance
- no change for the instant load step function. The turbocharger assistance has no effect on the air excess ratio drop just after the sudden load step is taken by the engine. Turbocompounding lowers the instant load step capability because the turbocharger should be first increase the inlet receiver pressure up to the level of the baseline engine, which needs time.
- in a significant instant load step capability when preboost is used. Already speeding up the turbocharger a couple of seconds before the instant load step is taken, increases the load step capability by almost 2 to 2.5 times compared to the baseline engine. However, relative high air excess ratios are found with preboost, which, probably, leads to misfire for natural gas combustion.
- a shorter time needed to take a load ramp from 0 to 100% load. The time needed can be reduced up to 80% when solely turbocharger assistance is used. If the engine is running in turbocompounding mode before the load ramp is taken, the time needed is also reduced.

For cyclic engine loading, turbocompounding can be for load cycle frequencies up to 0.2 Hz. Hybrid electric turbocharging can be successfully used to keep the air excess ratio close to the desired set point value. However for higher frequencies than 0.2 Hz, the air excess ratio starts to break off. The hybrid electric turbocharger does not prevent air excess ratio fluctuations.

## Proposal for Future Research

This chapter is meant to propose a turbocompound system for future research based on the knowledge gathered with this hybrid electric turbocharger research. The benefits and drawbacks of the hybrid electric turbocharging topology are kept in mind while drawing up this topology, as depicted in Figure 7.1.

The system consists of a diesel or dual-fuel engine with a turbocharger that is matched for a lower operating point. The waste gate is replaced with a power turbine, located in parallel to the turbocharger's turbine. Instead of wasting the exhaust gasses into atmosphere with a waste gate, the bypassed exhaust gas is expanded in the power turbine to increase the system efficiency without influencing the operation of the turbocharger's turbine. An electrical driven compressor (supercharger) is placed in front of the turbocharger's compressor, to improve the boost pressure build up and, therefore, reduces the effect of turbocharger lag on the engine power output response. An electric machine is mounted to the driveline or the engine's flywheel to assist the engine for sudden load steps for which the indirect turbocharger assistance is not capable to take them.

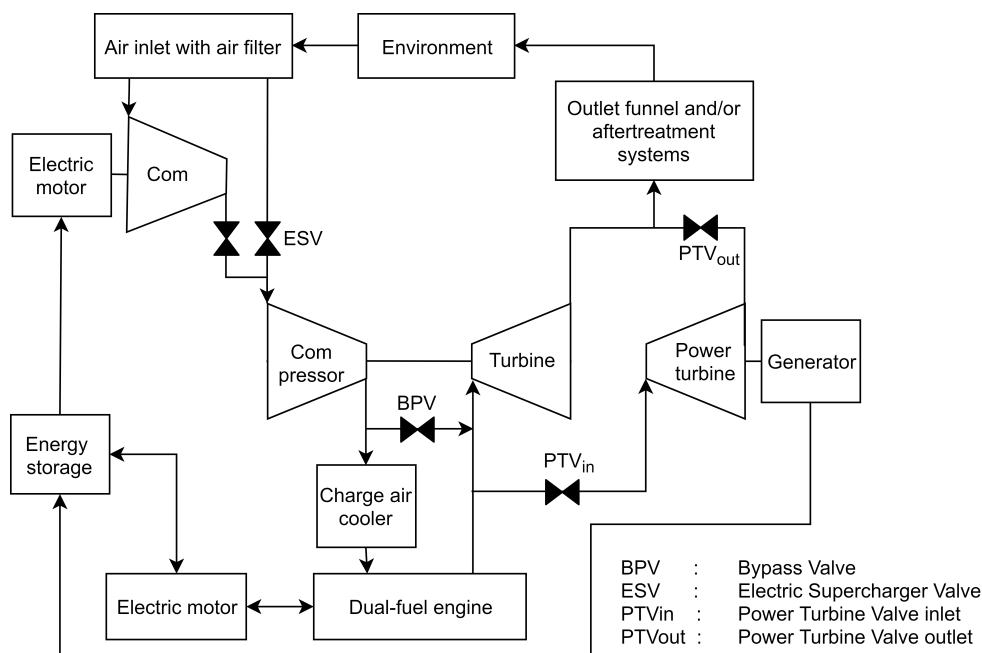
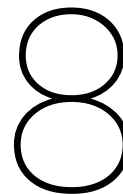


Figure 7.1: Proposed system with low-pressure electric supercharger and parallel located power turbine

The benefits of the proposed topology compared to the hybrid electric turbocharger are:

- The parallel located power turbine does not affect the pressure level of the turbocharger's turbine outlet compared with the hybrid electric turbocharger or due to two stage expansion with two in-line located turbines.

- The power balance of the turbocharger is not affected when the bypassed exhaust gas is expanded in the power turbine. No gas exchange deterioration is expected which also means no increased thermal loading.
- Flywheel/drive train mounted electric machine assists engine to take larger load steps which cannot be reached with the electric supercharger.
- Compressor surge is no issue any more due to the two stage compressor. Placing the electric supercharger between the turbocharger's compressor and the charge air cooler reduces the time needed to build up pressure for the electric supercharger, however the turbocharger's compressor has to pressurize a larger volume which takes more time. The electric supercharger is much less used compared to the engine's turbocharger, therefore a low-pressure electric supercharger is selected to assist the turbocharger. Placing the electric supercharger in parallel with the turbocharger's compressor does not move the operating conditions away from the surge limitation due to an unchanged pressure ratio and, presumably, even a reduced compressor's mass flow.



# Conclusions and Recommendations

## 8.1. Conclusions

The main objective of this thesis was to gain insight into the potential of an hybrid electric turbocharger for enhancing the loading capability of a dual-fuel engine and its potential as waste heat recovery system. In literature, the limitation of compressor surge on the operational envelope and loading capability is not clear. Improved loading capability with turbocharger assistance is shown in multiple researches, however some researchers show or mention the limitation of compressor surge. Moreover, no effects of turbocompounding on the performance of the dual fuel engine or any other engine are shown. To investigate the effect of a hybrid electric turbocharger, a mean-value dual-fuel engine model has been composed by merging the natural gas combustion of an older dual-fuel engine model with a more recent mean-value diesel engine model. This generic mean-value dual-fuel model is matched for the Wärtsilä 6L34DF and validated with independent test bench data. The hybrid electric turbocharger is controlled with a sophisticated control strategy which contains a main feedback air excess ratio controller and eight feed back boundary controllers.

The conclusions are treated in two separate parts: firstly, the conclusions from the results of turbocompounding and, secondly, the conclusions on the loading capability are discussed.

Turbocompounding:

- to increase the system efficiency is limited to the nominal load and speed region. A maximum system efficiency increase of 1.3% can be reached for the Wärtsilä 6L34DF. For lower load and speeds, the system efficiency is deteriorated, turbocompounding should be turned off.
- to increase the system efficiency depends on the engine and turbocharger matching point. It was found that replacing a waste-gated turbocharger with a hybrid electric turbocharger has the highest potential in terms of area of the operating envelope in which turbocompounding is possible, and the gain in system efficiency compared to the non waste-gated dual fuel or diesel engine. Replacing the waste gate with a hybrid electric turbocharger resulted in a system efficiency increase of about 2.3% at nominal load and speed.
- lowers the power available for the compressor leading to a reduced inlet receiver pressure. The latter affects the gas exchange process of the cylinder. The charge air mass and pressure is lower than without turbocompounding resulting in a reduced peak in-cylinder pressure. Moreover, the scavenging mass flow is reduced, due to the lower pressure difference over the inlet and outlet valves.
- increases the thermal loading of the engine, due to the reduced available fresh air in the cylinder and increased quantity of injected fuel. The latter is the result of a decreased engine efficiency. The temperature levels of the engine increase leading to a higher thermal loading of the engine.
- in combination with Advanced Miller Timing lowers the gain in system efficiency while for engines without turbocompounding Advanced Miller Timing results in an improved engine efficiency. Early inlet valve closure timing should be reduced to improve the system efficiency.

Assisting the turbocharger:

- to increase the engine's operating envelope is limited to cases where compressor air mass flow to the engine can be regulated with a bypass valve or blow off valve. An almost constant engine torque output can be obtained what leads to an increased operating envelope area. Without these air regulation valves, the operating envelope is reduced in size for the low to mid engine speed range due to compressor surge. An increased operating envelope leads to reduced engine limits for marine system engineers and therefore gives the possibility to match drive line systems for system efficiency without having compressor surge limitations near the operating line for the engine mid speed range.
- improves the engine recovery after a sudden load step, but does not increase the instant loading capability. No increase of the load step capability is obtained due to the lagging behaviour of the assisted turbocharger. The instant load step can only be increased with preboost (already speeding up the turbocharger before the load is applied to the engine). Preboost leads to relative high air excess ratio before the load is applied which can be a limitation for dual fuel engines running in gas mode due to misfire. The load ramp from idling to nominal load can be done in a shorter period of time with turbocharger assistance enabled.
- shortens the time needed to go from no load to nominal load with three consecutive instant load steps. The recovery time after each load step is reduced, therefore the recovery time needed between two load steps is reduced compared with the non assisted baseline engine.
- reduces the phase up to 180deg between the sinusoidal generator load and the air excess ratio compared to the non assisted case till a certain frequency. Moreover, the amplitude of the air excess ratio is reduced which means a more constant air excess ratio which is an improvement for natural gas combustion. The air excess ratio follows the cyclic load up to a certain frequency, after which its starts to break off, and its response becomes equal to the non assisted system case.

## 8.2. Recommendations

The research shown in this thesis is based upon available and improved models and assumptions needed to draw up project boundaries. In order to enhance the model's predictions, the following recommendations should be carried out in order to investigate the effect of a hybrid electric turbocharger on a marine dual-fuel engine for, especially, natural gas combustion.

- The natural gas combustion model in the Diesel B model, built by Georgescu et al. (2016b), is based upon semi-empirical relationships obtained from a crank angle engine model (Diesel C). The phenomena happening during natural gas combustion should be investigated to build a generic combustion model which can represent the natural gas combustion for, amongst others, the Wärtsilä 6L34DF.
- Implement the proposed effective compression ratio, discussed in Section 4.5.4, to include the pressure loss due to advanced Miller timing into the Diesel B model. More research is needed to Advanced Miller Timing if only an effective compression ratio is sufficient to involve all the effects of a very early closure of the inlet valve.
- After the modification of the Diesel B model to include Advanced Miller Timing, the Diesel B model should be rematched in order to get more accurate predictions of the Wärtsilä 6L34DF Engine data for other engine speeds should be found to compare the model's predictions at low and mid speed range.
- Investigate up to which extend a matching procedure can be composed in order to build an engine matching tool. Loonstijn (2016) has already mentioned the need for a matching tool. The modelling part needed for this thesis, also shows the need for a matching tool to avoid the tedious and time consuming process of matching the Diesel B model with engine data. Step one is to drawn up a procedure to manually match an engine with limited data available. Thereafter, this procedure can be translated into a matching tool by combining the matching procedure with computational power.
- Investigate more advanced control strategies for the hybrid turbocharger's electric machine in order to optimize the system efficiency. A proposal of a control strategy is to use the inlet receiver pressure ( $p_{ir}$ ) instead of the air excess ratio ( $\lambda$ ). For natural gas combustion, both the air excess ratio and inlet receiver pressure feedback control strategies could be insufficient to operate between the knock and misfire limits. Model Predictive Control can be used as control strategy which predicts if knock or misfire could happen with the controller actions.

- 
- Replace the turbocharger shaft torque addition/subtraction with an electric machine model in order to investigate the effect of physical limitations of the electric machine such as peak acceleration as result of the maximum allowable current.
  - Integrate an energy storage into the system to investigate dynamic loading with charging and discharging.
  - Investigate the effect of decoupling the compressor and turbine matching for the system efficiency with turbocompounding. Decouple the sizing and balancing of the compressor and turbine as used in the Diesel B model. Match separately the compressor and turbine with the cylinder model and make use of the electric machine to balance the available power and taken power by the compressor.
  - Determine from engine data the time constant of the governor and fuel pump. In this thesis, fuel is immediately supplied in the cylinder due to high governor controller parameters, while in reality there is a certain time delay. After changing the fuel governor's response, the loading capability with respect to maximum speed drop can be investigated. This should be done for all the four load steps discussed in this thesis.



# Bibliography

- Aghaali, H. and Ångström, H. E. (2015). A review of turbocompounding as a waste heat recovery system for internal combustion engines. *Renewable and Sustainable Energy Reviews*, 49:813–824.
- Arsie, I., Cricchio, A., Pianese, C., Ricciardi, V., and De Cesare, M. (2015). Evaluation of CO<sub>2</sub> reduction in SI engines with Electric Turbo-Compound by dynamic powertrain modelling. *IFAC-PapersOnLine*, 28(15):93–100.
- Banawan, A. A., El Gohary, M. M., and Sadek, I. S. (2010). Environmental and economical benefits of changing from marine diesel oil to natural-gas fuel for short-voyage high-power passenger ships. *Proceedings of the Institution of Mechanical Engineers Part M: Journal of Engineering for the Maritime Environment*, 224(2):103–113.
- Boonen, E.-J. (2009). Advanced waste heat recovery for 4-stroke diesel engines onboard ships. Master's thesis, Delft University of Technology.
- Boretti, A. (2017). F1 style MGU-H applied to the turbocharger of a gasoline hybrid electric passenger car. *Nonlinear Engineering*, 6(4):293–300.
- Bumby, J., Crossland, S., and Carter, J. (2006). Electrically assisted turbochargers: their potential for energy recovery. In *Hybrid Vehicle Conference, IET The Institution of Engineering and Technology*, volume 2006, pages 43–52. IEE.
- Burel, F., Taccani, R., and Zuliani, N. (2013). Improving sustainability of maritime transport through utilization of Liquefied Natural Gas (LNG) for propulsion. *Energy*, 57:412–420.
- Burke, R. D. (2016). A Numerical Study of the Benefits of Electrically Assisted Boosting Systems. *Journal of Engineering for Gas Turbines and Power*, 138(9):092808.
- Chen, H., Goswami, D. Y., and Stefanakos, E. K. (2010). A review of thermodynamic cycles and working fluids for the conversion of low-grade heat. *Renewable and Sustainable Energy Reviews*, 14(9):3059–3067.
- Cho, H. M. and He, B. Q. (2007). Spark ignition natural gas engines-A review. *Energy Conversion and Management*, 48(2):608–618.
- Choi, J. W. and Lee, S. C. (2009). Antiwindup strategy for PI-type speed controller. *IEEE Transactions on Industrial Electronics*, 56(6):2039–2046.
- Christer Wik, S. H. (2010). Utilisation of cylinder air injection as a low load and load acceptance improver on a medium-speed diesel engine. In *CIMAC Congress 2010, Bergen*.
- CIMAC WG17 'Gas Engines' (2011). Transient Response Behaviour of Gas Engines. Technical report, CIMAC, Work group Gas Engines.
- Claudio Christen, D. B. (2013). Imo tier 3: Gas and dual fuel engines as a clean and efficient solution. In *CIMAC Congress Shanghai*. CIMAC.
- Codan, E., Mathey, C., and Rettig, A. (2010). 2-Stage Turbocharging – Flexibility for Engine Optimisation. In *CIMAC Congress 2010*. CIMAC.
- Cui, Y., Hu, Z., Deng, K., and Wang, Q. (2013). Miller-Cycle Regulatable, Two-Stage Turbocharging System Design for Marine Diesel Engines. *Journal of Engineering for Gas Turbines and Power*, 136(2):022201.
- Daugas, C. and Chen, S. K. (2000). The empirical approach in the gas engine development. In *ICE Fall Technical Conference*, volume 35-2. ASME.
- de Ruyck, K. (2010). Simulation of advanced engine room configurations with energy saving concepts. Master's thesis, Delft University of Technology.

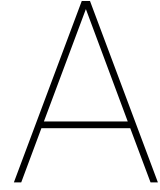
- Dijkstra, C. (2003). Single stage generic turbocharger model, applicable to first principle diesel engine model. Technical report, Delft University of Technology.
- Dijkstra, C. (2004). Description of simulink mean value diesel engine model deii. Technical Report December, Delft University of Technology.
- Dimitriou, P., Burke, R., Zhang, Q., Copeland, C., and Stoffels, H. (2017). Electric Turbocharging for Energy Regeneration and Increased Efficiency at Real Driving Conditions. *Applied Sciences*, 7(4):350.
- Eriksson, L. (2007). Modeling and control of turbocharged SI and DI engines. *Oil and Gas Science and Technology*, 62(4):523–538.
- Geertsma, R. D., Negenborn, R. R., Visser, K., Loonstijn, M. A., and Hopman, J. J. (2017). Pitch control for ships with diesel mechanical and hybrid propulsion: Modelling, validation and performance quantification. *Applied Energy*, 206:1609–1631.
- Georgescu, I., Stapersma, D., and Mestemaker, B. (2016a). Dynamic Behaviour of Gas and Dual-Fuel Engines : Using Models and Simulations to Aid System Integration. *International Council on Combustion Engines (CIMAC) Congress*.
- Georgescu, I., Stapersma, D., Nerheim, L. M., and Mestemaker, B. (2016b). Characterisation of Large Gas and Dual-fuel Engines. *MTZ Industrial*, pages 64–71.
- Ghanbariannaeni, A. and Ghazanfarihashemi, G. (2012). Protecting a centrifugal compressor from surge. *Pipeline & Gas Journal*, 239(3):2–6.
- Giakoumis, E. G. (2016). Review of Some Methods for Improving Transient Response in Automotive Diesel Engines through Various Turbocharging Configurations. *Frontiers in Mechanical Engineering*, 2(4).
- Grimmelius, H., Mesbahi, E., Schulten, P., and Stapersma, D. (2007). The use of diesel engine simulation models in ship propulsion plant design and operation. Technical report, Delft University of Technology (TU Delft), NL; University of Newcastle upon Tyne, GB; Ministry of Defence, NL; Netherlands Defence Academy, Den Helder, NL.
- Guzzella, L. and Onder, C. H. (2010). *Introduction to modeling and control of internal combustion engine systems*. Springer Berlin Heidelberg, Berlin, Heidelberg.
- Hegab, A., La Rocca, A., and Shayler, P. (2017). Towards keeping diesel fuel supply and demand in balance: Dual-fuelling of diesel engines with natural gas. *Renewable and Sustainable Energy Reviews*, 70(July 2016):666–697.
- Heim, K. (2002). Existing and future demands on the turbocharging of modern large two-stroke diesel engines. In *8th Supercharging Conference*.
- Hermann, H. and Prenninger, P. (2007). *Charging the Internal Combustion Engine*. Springer Vienna.
- Hiranandani, V. (2014). Sustainable development in seaports: A multi-case study. *WMU Journal of Maritime Affairs*, 13(1):127–172.
- Hountalas, D., Katsanos, C., Kouremenos, D., and Rogdakis, E. (2007). Study of available exhaust gas heat recovery technologies for HD diesel engine applications. *International Journal of Alternative Propulsion*, 1(2/3):228.
- IMO (2014). Third IMO Greenhouse Gas Study 2014. Technical report, international maritime organization, London.
- Ito, Y. O. K. S. K. S. Y. (2012). Development of new turbocharger technologies for energy efficiency and low emissions. *Mitsubishi Heavy Industries, Ltd, Japan*.
- Jacobs, T. J., Jagmin, C., Williamson, W. J., Filipi, Z. S., Assanis, D. N., and Bryzik, W. (2008). Performance and emission enhancements of a variable geometry turbocharger on a heavy-duty diesel engine. *International Journal of Heavy Vehicle Systems*, 15(2/3/4):170.
- Katrašnik, T., Medica, V., and Trenc, F. (2005). Analysis of the dynamic response improvement of a turbocharged diesel engine driven alternating current generating set. *Energy Conversion and Management*, 46(18-19):2838–2855.

- Katrasnik, T., Rodman, S., Trenc, F., Hribernik, A., and Medica, V. (2003). Improvement of the Dynamic Characteristic of an Automotive Engine by a Turbocharger Assisted by an Electric Motor. *Journal of Engineering for Gas Turbines and Power*, 125(2):590.
- Katrasnik, T., Trenc, F., Medica, V., and Markic, S. (2005). An Analysis of Turbocharged Diesel Engine Dynamic Response Improvement by Electric Assisting Systems. *Journal of Engineering for Gas Turbines and Power*, 127(4):918.
- Klein Woud, H. and Stapersma, D. (2008). *Design of Propulsion and Electric Power Generation Systems*. Imarest.
- Klimstra, J. and Hattar, C. (2006). Performance of Natural-Gas-Fueled Engines Heading Towards Their Optimum. In *International Combustion Engine Division Spring Technical Conference*, volume 2006, pages 1–8. ASME.
- Korakianitis, T., Namasivayam, A. M., and Crookes, R. J. (2011). Natural-gas fueled spark-ignition (SI) and compression-ignition (CI) engine performance and emissions.
- Kumar, S., Kwon, H. T., Choi, K. H., Lim, W., Cho, J. H., Tak, K., and Moon, I. (2011). LNG: An eco-friendly cryogenic fuel for sustainable development. *Applied Energy*, 88(12):4264–4273.
- Loonstijn, M. A. (2016). *A Study on the Effects of Sequential Turbocharged Diesel Engines*. Master thesis, Delft University of Technology.
- Marra, A. M. B. C. E. G. M. (2011). Regulating air emissions from ships: The state of the art on methodologies, technologies and policy options. Technical report, European Commission.
- Meier, E. and Czerwinski, J. (1989). Turbocharging Systems With Control Intervention for Medium Speed Four-Stroke Diesel Engines. *Journal of Engineering for Gas Turbines and Power*, 111:560–569.
- Mestemaker, B. (2014). Wartsila 6l34df engine assessment for application on ihc merwede vessels: Dynamic loading tests with cyclic loading and ramp loading. Technical report, IHC MTI B.V.
- Nwafor, O. M. (2002). Knock characteristics of dual-fuel combustion in diesel engines using natural gas as primary fuel. *Sadhana - Academy Proceedings in Engineering Sciences*, 27(PART 3):375–382.
- Pasini, G., Frigo, S., and Antonelli, M. (2016). Electric Turbo Compounding Applied to a CI Engine: A Numerical Evaluation of Different Layouts. In *ASME 2016 Internal Combustion Engine Fall Technical Conference*, page V001T07A005.
- Rakopoulos, C. D. and Giakoumis, E. G. (2009). *Diesel engine transient operation: Principles of operation and simulation analysis*. Springer London, London.
- Refsgaard, J. C. and Henriksen, H. J. (2004). Modelling guidelines - Terminology and guiding principles. *Advances in Water Resources*, 27(1):71–82.
- Rose, A. T. J. M., Akehurst, S., and Brace, C. J. (2011). Modelling the performance of a continuously variable supercharger drive system. *Proceedings of the Institution of Mechanical Engineers, Part D: Journal of Automobile Engineering*, 225(10):1399–1414.
- Rusman, J. Q. (2018). Charge air configurations for propulsion diesel engines aboard fast naval combatants. Master's thesis, Delft University of Technology.
- Sapra, H., Godjevac, M., Visser, K., Stapersma, D., and Dijkstra, C. (2017). Experimental and simulation-based investigations of marine diesel engine performance against static back pressure. *Applied Energy*, 204:78–92.
- Schulten, P. J. M. (2005). *The interaction between diesel engines, ship and propeller during MANoeuvring*. PhD thesis, Delft University of Technology.
- Semlitsch, B. and Mihăescu, M. (2016). Flow phenomena leading to surge in a centrifugal compressor. *Energy*, 103:572–587.
- Sendyka, B. and Soczowka, J. (2006). Recovery of exhaust gases energy by means of turbocompound. *Heat2Power*, 37(6):1–5.
- Shiraishi, K. and Krishnan, V. (2014). ELECTRO-ASSIST TURBO FOR MARINE TURBOCHARGED DIESEL ENGINES. In *ASME Turbo Expo 2014*, pages 1–7.

- Singh, D. V. and Pedersen, E. (2016). A review of waste heat recovery technologies for maritime applications. *Energy Conversion and Management*, 111:315–328.
- Stapersma, D. (1997). A general model for off-design performance of a single stage turbo machine. KIM-PFS-97-111 A, Delft University of Technology & Netherlands Defence Academy.
- Stapersma, D. (2010a). Diesel Engines Volume 1 Performance Analysis. Technical report, Delft University of Technology.
- Stapersma, D. (2010b). Diesel Engines Volume 2 Turbocharging. Technical report, Delft University of Technology.
- Stapersma, D. (2010c). Diesel Engines Volume 3 Combustion. Technical report, Delft University of Technology.
- Stapersma, D. (2010d). Diesel engines volume 4 emissions and heat transfer. Technical report, Delft University of Technology.
- Stapersma, D. (2010e). Diesel Engines Volume 6 Thermodynamical Principles II April 2010. In *Lecture notes WB4408B*, volume 6. Delft University of Technology, Delft.
- Stapersma, D. (2013). A general model for off-design performance of a single stage turbomachine. KIM-PFS-97-111 D, Delft University of Technology & Netherlands Defence Academy.
- Tavcar, G., Bizjan, F., and Katrasnik, T. (2011). Methods for improving transient response of diesel engines - Influences of different electrically assisted turbocharging topologies. *Proceedings of the Institution of Mechanical Engineers, Part D: Journal of Automobile Engineering*, 225(9):1167–1185.
- Teo, A., Yahya, W., Romagnoli, A., Rajoo, S., and Noor, A. (2015). Effectiveness of Series and Parallel Turbo Compounding on Turbocharged Diesel Engine. *Journal of Mechanical Engineering and Sciences*, 8(June):1448–1459.
- Terdich, N., Martinez-Botas, R. F., Romagnoli, A., and Pesiridis, A. (2013). Mild Hybridization Via Electrification of the Air System: Electrically Assisted and Variable Geometry Turbocharging Impact on an Off-Road Diesel Engine. *Journal of Engineering for Gas Turbines and Power*, 136(3):031703.
- Thimmanoor, S. B. (2018). Organic Rankine cycle as waste heat recovery system for marine application: Screening methodology, modeling and analysis. Master's thesis, Delft University of Technology.
- van Fulpen, A. (2016). Efficient Design of Maritime Chiller Configurations. Master thesis, Delft University of Technology.
- Wärtsilä Engines (2012). Wärtsilä 34DF Product Guide. 2012, page 176.
- White, F. M. (2015). *Fluid Mechanics*. Mcgraw-Hill Education - Europe.
- Winnes, H., Fridell, E., Yaramenka, K., Nelissen, D., Faber, J., and Ahdour, S. (2016). NOx controls for shipping in EU Seas. Technical Report June, CE Delft.
- Yasuaki, I. S. Y. S. K. O. H. J. (2006). Development of the "Hybrid Turbo" an Electrically Assisted Turbocharger. *Mitsubishi Heavy Industries Technical Review*, 43(3):1–5.
- Yoshihisa, S. K. O. (2007). Hybrid Turbocharger with Integrated High Speed Motor- generator. *Review Literature And Arts Of The Americas*, 44(1):1–3.
- Yoshihisa, Ono; Keiichi, S. Y. (2012). Application of a Large Hybrid Turbocharger for Marine Electric-power Generation. *Mitsubishi Heavy Industries technical review*, 49(1):29–33.
- Zammit, J. P., McGhee, M. J., Shayler, P. J., Law, T., and Pegg, I. (2015). The effects of early inlet valve closing and cylinder disablement on fuel economy and emissions of a direct injection diesel engine. *Energy*, 79(C):100–110.
- Zellbeck, H., Friedrich, J., and Berger, C. (1999). Die elektrisch unterstützte Abgasturboaufladung als neues Aufladekonzept. *MTZ Motortechnische Zeitschrift*, 60(6):386–391.

- Zhang, Q., Lu, P., Dimitriou, P., Akehurst, S., Copeland, C., Zangeneh, M., Richards, B., and Fowler, G. (2017). Implementing Full Electric Turbocharging Systems on Highly Boosted Gasoline Engines. *Volume 8: Micro-turbines, Turbochargers and Small Turbomachines; Steam Turbines*, 8:V008T26A032.
- Zulkifli, F. H., Fawzi, M., and Osman, S. A. (2015). A Review on Knock Phenomena in CNG-Diesel Dual Fuel System. *Applied Mechanics and Materials*, 773-774(May):550–554.





## Diesel B parameters

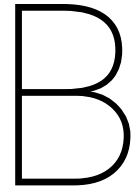
Wärtsilä 6L34DF parameters used in the mean value model are shown below.

CONFIDENTIAL INFORMATION HAS BEEN REMOVED

Table A.1: Dual-fuel engine parameters from project guide (PG)

<b>Diesel engine parameter description</b>	<b>Variable</b>	<b>Value</b>	<b>Source</b>
Ambient pressure	$p_{amb}$	100 kPa	E
Ambient temperature	$T_{amb}$	295 K	E
Bore diameter	$D_B$	0.34 m	PG
Crank angle after TDC, exhaust closure	$\alpha_{EC}$	-	-
Crank angle after TDC, exhaust opening	$\alpha_{EO}$	-	-
Crank angle after TDC, inlet closure	$\alpha_{IC}$	-	-
Crank angle after TDC, inlet opening	$\alpha_{IO}$	-	-
Crank angle variable inlet valve closing	$\alpha_{VIC}$	-	-
Crank rod length	$L_{CR}$	-	-
Diameter exhaust valve	$D_{exh,valve}$	-	-
Diameter inlet valve	$D_{inl,valve}$	-	-
Geometric compression ratio	$\epsilon_c$	-	-
Lower heating value of diesel fuel	$H_{L,diesel}$	42700 kJ/kg	-
Lower heating value of gaseous fuel	$H_{L,gas}$	49710 kJ/kg	-
Maximum cylinder pressure	$p_{max,nom}$	-	-
Nominal engine power	$P_{nom}$	3000 kW	PG
Nominal engine speed	$n_{nom}$	750 rev/min	PG
Nominal exhaust mass flow	$\dot{m}_{exh,nom}$	5.5 kg/s	PG
Nominal spec. fuel consumption	$m_{bsfc,nom}$	190 g/kW h	PG
Number of cylinders	$i_e$	6	PG
Number of inlet valves	$i_{inl,valve}$	2	PG
Number of outlet valves	$i_{out,valve}$	2	PG
Number of revolutions per cycle	$k_e$	2	PG
Stroke length	$L_S$	0.4 m	PG
Temperature after the intercooler	$T_{IR}$	-	-
Temperature exhaust gas in outlet receiver	$T_{IR}$	-	-
Turbocharger speed	$n_{TC}$	-	-





# Compressor map visualisation

This appendix contains the equations used to visualize the compressor map, which is shown multiple times in this report. The visualisation of the compressor map did not exist, or is not available, in the Diesel B version provided to students.

## Goal of visualisation

The purpose of visualising the compressor map is primarily to have a clear figure in which the trajectory of the compressor conditions can be plotted for steady state as well as dynamic/transient simulations. Besides, the influence of various model parameters to the compressor operating conditions can be investigated in visual way instead of only quantitatively with numbers.

The derivation of single stage turbomachine equations is done by StapersmaStapersma (2013). Stapersma has developed a sophisticated turbomachine model which not only covers the prediction of turbomachine behaviour running at nominal conditions, but also covers off-design conditions. Therefore the turbomachine model is integrated into the Diesel B mean-value diesel engine model.

The derivation of the equations governing the compressor model are not given in this thesis. The following compressor equations are shown in order to explain how the visualisation of the compressor map is addressed.

### Input parameters:

- Compressor model shape parameters
- Fluidum parameters
- Inlet conditions (pressure, temperature, mass flow)
- Outlet conditions (pressure, temperature)
- Turbocharger speed

### Required output:

- Compressor map with efficiency as function of pressure ratio and non-dimensional mass flow
- Compressor map with speed as function of pressure ratio and non-dimensional mass flow
- Surge line

StapersmaStapersma (2013) visualised his turbomachine equations into a block diagram (shown in Figure B.1) in order to understand the sequence of the model equations.

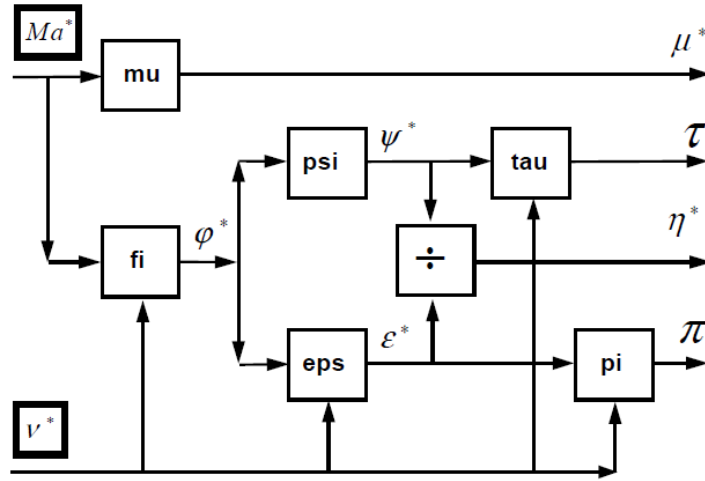


Figure B.1: Block diagram of core model, from Stapersma (2013)

### Equations used to define compressor map

This section covers the turbomachine equations necessary for plotting the compressor map. In the following equations, the superscript "\*" means "relative value", and the subscript "0" means its value for "nominal operating conditions".

$\pi$	Pressure ratio
$\tau$	Temperature ratio
$v^*$	Non-dimensional rotorspeed
$\varphi^*$	Flow coefficient
$Ma^*$	Mach number
$\kappa$	Heat capacity ratio
$\mu^*$	Non-dimensional mass flow
$\psi^*$	Enthalpy coefficient
$\eta^*$	Non-dimensional efficiency

From pressure measurements, the compressor's inlet and outlet pressure levels can be obtained in order to find the compressor's pressure ratio ( $\pi$ ).

$$\pi = \frac{p_{out}}{p_{in}} \quad (B.1)$$

The non-dimensional rotorspeed ( $v^*$ ) follows from the relative rotor speed ( $n^*$ ) and the relative inlet temperature ( $T_{in}^*$ ).

$$n^* = \frac{n}{n_0} \quad T_{in}^* = \frac{T_{in}}{T_{in,0}} \quad (B.2)$$

$$v^* = \frac{n^*}{\sqrt{T_{in}^*}} \quad (B.3)$$

The non-dimensional mass flow ( $\mu^*$ ) can be found with the relative mass flow ( $\dot{m}^*$ ), relative inlet pressure ( $p_{in}^*$ ) and relative inlet temperature ( $T_{in}^*$ ).

$$p_{in}^* = \frac{p_{in}}{p_{in,0}} \quad T_{in}^* = \frac{T_{in}}{T_{in,0}} \quad \dot{m}^* = \frac{\dot{m}}{\dot{m}_0} \quad (B.4)$$

$$\mu^* = \frac{\dot{m}^* \cdot \sqrt{T_{in}^*}}{p_{in}^*} \quad (B.5)$$

The non-dimensional mass flow ( $\mu^*$ ) given above is used to determine the location during simulation in the compressor map. For plotting this compressor map, the following equation is used with varying parameter the Mach number.

$$\mu^* = \frac{Ma^*}{\sqrt{(1-q) + q \cdot Ma^{*2} \left(\frac{k+1}{k-1}\right)}} \quad (\text{B.6})$$

wherein  $q$  is used which can be found with

$$q = \frac{\left(\frac{k-1}{2}\right) \cdot Ma_0^2}{1 + \left(\frac{k-1}{2}\right) \cdot Ma_0^2} \quad (\text{B.7})$$

$$\varphi^* = \frac{1}{v^*} \cdot \frac{Ma^*}{\sqrt{(1-q) + q \cdot Ma^{*2}}} \quad (\text{B.8})$$

The enthalpy coefficient is given as

$$\psi^* = 1 + a \cdot (\varphi^* - 1) \quad (\text{B.9})$$

$$a = 1 - \frac{1}{\Psi_0} \quad b = -x \cdot \frac{1}{\Psi_0} \quad d = -y \cdot \text{sign}(\Psi_0) \quad (\text{B.10})$$

$$\epsilon^* = 1 + a \cdot (\psi^* - 1) + b \cdot (\psi^* - 1)^2 + d \cdot (v^* - 1)^2 \quad (\text{B.11})$$

From the pressure and enthalpy coefficient, the non-dimensional efficiency can be found.

$$\eta_c^* = \frac{\epsilon^*}{\Psi^*} \quad (\text{B.12})$$

$$\eta_c = \eta_{c,0} \cdot \eta_c^* \quad (\text{B.13})$$

Equation (B.15) is used to calculate the pressure ratio ( $\pi$ ) over the compressor using the pressure coefficient ( $\epsilon^*$ ) and non-dimensional rotorspeed ( $v^*$ ). This formula is obtained by rewriting Equation (B.14).

$$\epsilon^* = \frac{1}{v^{*2}} \cdot \left( \frac{\pi^{\frac{k-1}{k}} - 1}{\pi_0^{\frac{k-1}{k}} - 1} \right) \quad (\text{B.14})$$

Rewrite to

$$\pi = \left( 1 + \epsilon^* \cdot v^{*2} \cdot \left( \pi_0^{\frac{k-1}{k}} - 1 \right) \right)^{\frac{k}{k-1}} \quad (\text{B.15})$$

## Surge criterion to determine surge line

The theory behind the surge criterion is given by Dijkstra (2003). Again, the derivation of the surge criterion theory itself is not in this thesis, only the main important equations are briefly given.

The flow coefficient ( $\varphi^*$ ) as function of the pressure coefficient ( $\epsilon^*$ ) and non-dimensional rotorspeed ( $v^*$ ) can be found by filling Equation (B.10) in Equation (B.11) and rewriting it to

$$\varphi^* = \frac{2 \cdot b - a}{2 \cdot b} - \frac{\sqrt{(a^2 - 4 \cdot b \cdot (d(v^{*2} - 2 \cdot v^* + 1) - \epsilon^* + 1))}}{2 \cdot b} \quad (\text{B.16})$$

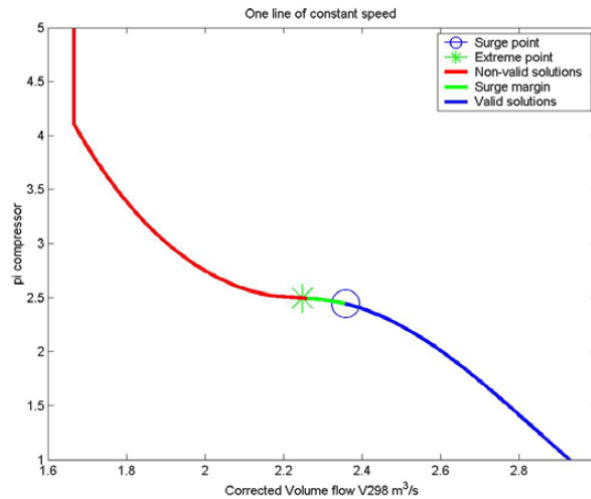


Figure B.2: Line of constant speed with extreme and surge points, from Dijkstra (2003)

The extreme point of Equation (B.18) indicates where surge starts to occur. Figure B.2 shows the line of constant speed. The right side of the extreme point, a dropping pressure ratio ( $\pi$ ) for increasing mass flow, corresponds with the compressor conditions in reality. The behaviour on the left side of the extreme point is non-valid and can be therefore used to indicate the surge region. According to Dijkstra, the compressor starts surging a little earlier in reality which is included by introducing the surge parameter  $f$ .

$$\varphi_{extreme}^* = \frac{2 \cdot b - a}{2 \cdot b} \quad (\text{B.17})$$

$$\varphi_{surge}^* = \varphi_{extreme}^* + f \cdot (1 - \varphi_{extreme}^*) \quad (\text{B.18})$$

## Visualisation of compressor map

All the equations required for setting up the compressor map are given in the previous sections. These equations with model shape parameters (Appendix B) are used with the calculation scheme, as shown in Figure B.1 in a Matlab script wherein several loops are programmed to find the non-dimensional mass flow ( $\mu^*$ ), non-dimensional efficiency ( $\eta^*$ ) and pressure ratio ( $\pi$ ) with as input several non-dimensional rotorspeeds ( $v^*$ ) and Mach numbers ( $Ma$ ).

$Ma$	= 0.4
$n$	= 35371 rpm
$T_{in}$	= 298 K
$k$	= 1.4
$x$	= 3
$y$	= 1
$f$	= 1/3
$\pi_0$	= 4.45
$\Psi_0$	= 0.4
$Ma_0$	= 0.4
$n_0$	= 35371 rpm
$T_{in,0}$	= 298 K
$\eta_{c,0}$	= 0.72
$\eta_{t,0}$	= 0.85

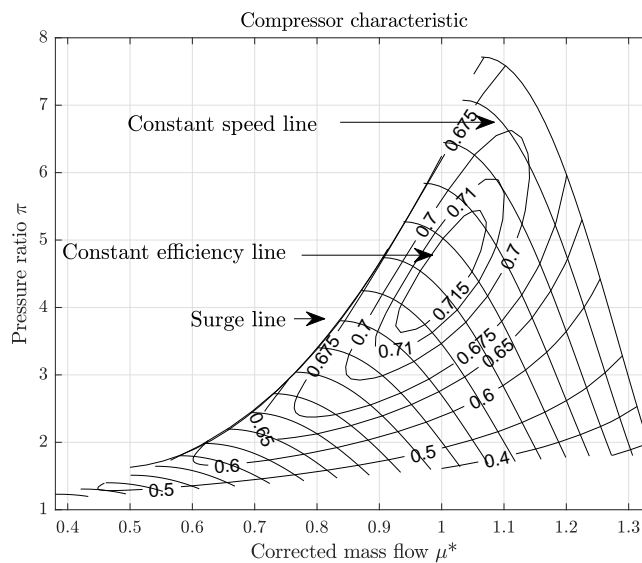


Figure B.3: Visualisation of compressor equations

# C

## Derivation of compressor mass flow and air excess ratio estimation

The first part of this appendix shows the derivation of the compressor air mass flow ( $\dot{m}_{com}$ ). This variable together with the pressure ratio ( $\pi$ ) should be known to find the operational point in the compressor map. The pressure ratio ( $\pi$ ) can be determined by measuring the pressure level at the inlet and outlet of the compressor stage. This appendix will be used to describe the derivation of the compressor mass flow estimation.

The second part of this appendix shows the derivation of the air excess ratio estimation which is used as input for the electrical turbocharger controller.

### Compressor mass flow estimation

The compressor mass flow estimation is shifted to a charge air cooler mass flow estimation in this thesis. The estimation of the mass flow through the compressor for nominal condition as well as off-design conditions is a difficult task which can hardly be done without reproducing the compressor model which is already available in the Diesel B model. In simulations, the compressor mass flow is available from this compressor model, however in reality this is not the case.

On the other hand, pressure sensors are already available at the compressor exit and inlet receiver with as intermediate part the charge air cooler which has a restrictive influence on the air mass flow. This restrictive element of the charge air cooler can be mimicked with an artificial orifice plate. The pressure level measurements together with this artificial orifice plate will be used to determine the compressor's mass flow. It is assumed that the pressure measurements at the compressor outlet and inlet receiver are sufficiently accurate for the mass flow estimation.

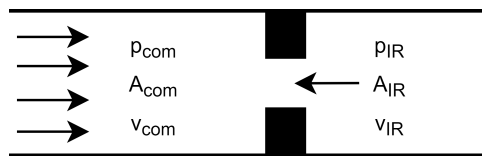


Figure C.1: Overview of used parameters in artificial orifice

### Mass flow through an orifice

The continuity equation (eq. (C.1)) is used together with Bernoulli's equation (eq. (C.2)). The flow is assumed to be steady, incompressible, it has a uniform velocity and constant density. There are no losses and no elevation between the two pressure measurement locations.

Continuity equation:

$$\dot{m} = \rho_{com} \cdot A_{com} \cdot v_{com} = \rho_{IR} \cdot A_{IR} \cdot v_{IR} \quad (C.1)$$

Bernoulli equation with no losses:

$$p_{com} + \frac{1}{2} \cdot \rho \cdot v_{com}^2 + z_{com} = p_{IR} + \frac{1}{2} \cdot \rho \cdot v_{IR}^2 + z_{IR} \quad (C.2)$$

As assumed no elevation,  $z_{com} = z_{IR}$ , and pressure difference to the left delivers

$$p_{com} - p_{IR} = \frac{\rho}{2} (v_{IR}^2 - v_{com}^2) \quad (C.3)$$

Rewriting eq. (C.1) gives,

$$v_{com}^2 = v_{IR}^2 \left( \frac{A_{IR}}{A_{com}} \right)^2 \quad (C.4)$$

Filling in eq. (C.4) into Equation (C.3) gives

$$p_{com} - p_{IR} = \frac{\rho \cdot v_{IR}^2}{2} \left( 1 - \frac{A_{IR}^2}{A_{com}^2} \right) \quad (C.5)$$

Solve eq. (C.5) for  $v_{IR}$  gives

$$v_{IR} = \sqrt{\frac{2(p_{com} - p_{IR})}{\rho \cdot \left( 1 - \frac{A_{IR}^2}{A_{com}^2} \right)}} \quad (C.6)$$

With the velocity at the second point ( $v_{IR}$ ) and the continuity equation (eq. (C.1)), the mass flow through the charge air cooler can be found.

$$\dot{m} = \rho \cdot A_{IR} \cdot \sqrt{\frac{2(p_{com} - p_{IR})}{\rho \cdot \left( 1 - \frac{A_{IR}^2}{A_{com}^2} \right)}} \quad (C.7)$$

Rearranging eq. (C.7) gives a term which contains the orifice dimensions, and a term wherein the pressure difference is used. Because an artificial orifice is used to determine a mass flow in a real system, the "dimension term" in eq. (C.9) does not change. The reader must keep in mind that this is not true for the mass flow calculation of an orifice in reality where losses are present. The derivation of the orifice equations could be continued by introducing a discharge coefficient ( $C_d$ ) which is a function of the Vena Contracta and the Reynolds number, however for a compressor mass flow approximation extending the equations was not necessary. If in future higher accuracy should be obtained, the reader is forwarded to White (2015).

$$\dot{m} = \underbrace{\frac{A_{IR}}{\sqrt{1 - \frac{A_{IR}^2}{A_{com}^2}}}}_{\text{Dimension term}} \cdot \sqrt{2 \cdot \rho (p_{com} - p_{IR})} \quad (C.8)$$

The "Dimension term" in eq. (C.9) is replaced by a resistive element " $R_{CAC}$ ".

$$\dot{m} = R_{CAC} \cdot \sqrt{2 \cdot \rho (p_{com} - p_{IR})} \quad (C.9)$$

### Comparison of estimated compressor mass flow and product data

The value of the resistive element can be found with the compressor mass flow at nominal operation conditions and the pressure difference over the charge air cooler.

$$\begin{aligned} \text{W6L34DF} &\Rightarrow R_{CAC} = 0.058 \\ \text{STA12V280(WG)} &\Rightarrow R_{CAC} = 0.00443 \end{aligned}$$

Table C.1 shows the compressor mass flows for 4 engine loads at nominal speed from product data and simulations. It could be questionable if this compressor mass flow estimation can be done in reality due to lower quality pressure measurements and a time delay while in the model an accurate pressure level is immediately available. However, this question is out of scope of this thesis.

Table C.1: Compressor mass flow estimation vs product data

Engine load [%]	Diesel B			Estimation	Deviation [%]
	$p_{com}$ [kPa]	$p_{IR}$ [kPa]	Diesel B $\dot{m}_{com}$ [kg/s]	Estimated $\dot{m}_{com}$ [kg/s]	
100	445	440	5.69	5.68	0.18
75	366	363	4.70	4.69	0.32
50	281	278	3.59	3.58	0.31
25	193	191	2.40	2.39	0.25

## Air excess ratio estimation

The air excess ratio ( $\lambda$ ) should be estimated for the control strategy used in this thesis. A simplified gas exchange model is used for which the derivations are discussed below.

The air excess ratio ( $\lambda$ ) is defined as:

$$\lambda = \frac{m_{ca}}{m_{a,min}} \quad (C.10)$$

$$m_{a,min} = \sigma \cdot m_f \quad (C.11)$$

The pseudo air excess ratio can be determined as follows:

$$\lambda^* = \frac{\dot{m}_{fresh}}{\dot{m}_{fuel}} \quad (C.12)$$

For ideal scavenging no fouling due to retained flue gasses, the trapped mass is equal to the fresh mass:

$$m_1 = m_{fresh} = m_{ca} \quad (C.13)$$

In this case the pseudo air excess ratio is equal to the air excess ratio:

$$\lambda^* = \lambda \quad (C.14)$$

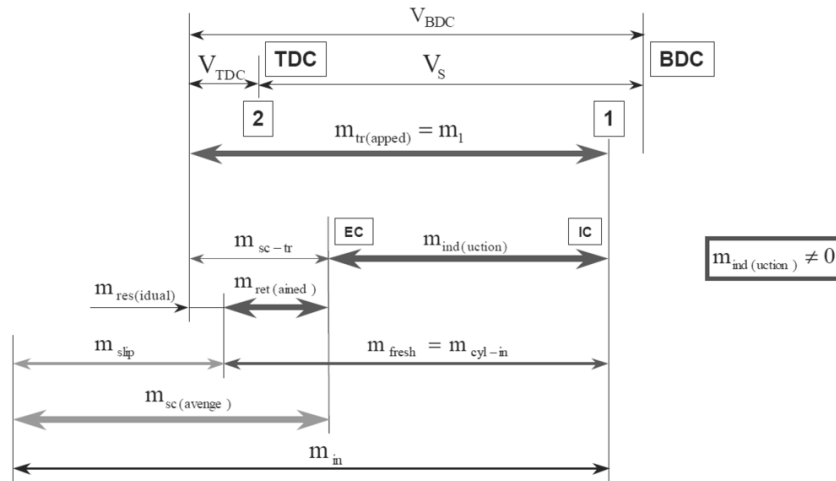


Figure C.2: Partition of mass flows at the inlet of a 4-stroke engine, from Stapersma (2010b)

Turbocharged with positive pressure difference: almost complete fresh air, therefore:

$$m_{fresh} = m_{ind} + m_{ret} \approx m_1 \quad (C.15)$$

The volumetric efficiency can be calculated with geometric cylinder parameters:

$$\eta_{vol} = \frac{V_{IC} - V_{EC}}{V_S} \quad (C.16)$$

The filling efficiency is defined as follows:

$$\eta_{fill} = \eta_{vol} \cdot \frac{T_c}{T_{ind}} \quad (C.17)$$

Assume no heat transfer when cold fresh air flows into the cylinder via the hot ducting and valves, i.e. ( $T_c = T_{ind}$ ).

$$\eta_{fill} \approx \eta_{vol} \quad (C.18)$$

The induction in-cylinder mass for one cylinder can be determined with the inlet flow parameters and filling efficiency:

$$m_{ind} = \eta_{fill} \cdot \frac{p_{IR} \cdot V_S}{R_{IR} \cdot T_{IR}} \quad (C.19)$$

From mass to mass flow for all the cylinders:

$$\dot{m}_{ind} = m_{ind} \cdot \frac{N \cdot i}{k} \quad (C.20)$$

Merging together delivers the induction mass flow:

$$\dot{m}_{ind} = (V_{IC} - V_{EC}) \cdot \frac{p_{IR}}{R_{IR} \cdot T_{IR}} \cdot \frac{N \cdot i}{k} \quad (C.21)$$

Secondly, the retained mass from the scavenging mass should be found with:

$$m_{ret} = \eta_{ret} \cdot m_{sc-tr} \quad (C.22)$$

The scavenge mass partition can be found with:

$$m_{sc-tr} = \frac{p_{IR} \cdot V_{EC}}{R_{IR} \cdot T_{IR}} \quad (C.23)$$

From retained mass to retained mass flow:

$$\dot{m}_{ret} = m_{ret} \cdot \frac{N \cdot i}{k} \quad (C.24)$$

Combining above given equations, leads to the retained mass flow:

$$\dot{m}_{ret} = \eta_{ret} \cdot \frac{p_{IR} \cdot V_{EC}}{R_{IR} \cdot T_{IR}} \cdot \frac{N \cdot i}{k} \quad (C.25)$$

Again, the fresh mass can be determined with above equations:

$$\dot{m}_{fresh} = \dot{m}_{ind} + \dot{m}_{ret} \quad (C.26)$$

Delivers finally:

$$\dot{m}_{fresh} = ((V_{IC} - V_{EC}) + (\eta_{ret} \cdot V_{EC})) \cdot \left( \frac{p_{IR}}{R_{IR} \cdot T_{IR}} \cdot \frac{N \cdot i}{k} \right) \quad (C.27)$$

The fuel input can be found with the nominal fuel mass flow ( $\dot{m}_{nom, fuel}$ ) and fuel rack ratio ( $x$ )

$$\dot{m}_{fuel} = x \cdot \dot{m}_{nom, fuel} \quad (C.28)$$

Combining these equations delivers finally the equation to estimate the air excess ratio ( $\lambda$ ):

$$\lambda_{estimate} = \frac{((V_{IC} - V_{EC}) + (\eta_{ret} \cdot V_{EC})) \cdot \left( \frac{p_{IR}}{R_{IR} \cdot T_{IR}} \cdot \frac{N \cdot i}{k} \right)}{x \cdot \dot{m}_{nom, fuel}} \quad (C.29)$$

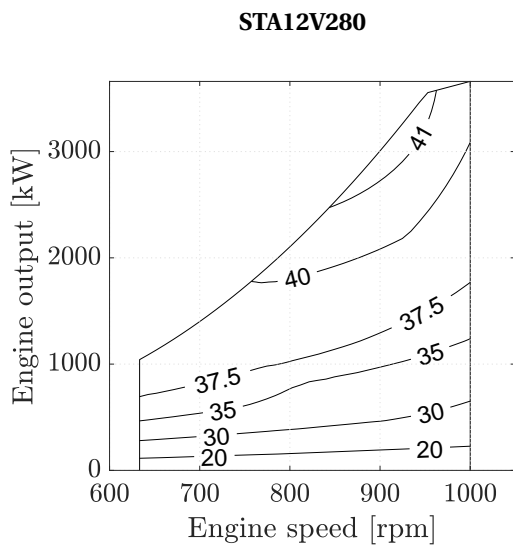
Table C.2 shows the results for the air excess ratio calculation in the Diesel B model compared with the air excess ratio estimation derived in this Appendix. As can be seen, the steady-state deviation is negligible.

Table C.2: Comparison Diesel B and estimated air excess ratio for four engine loads at nominal speed

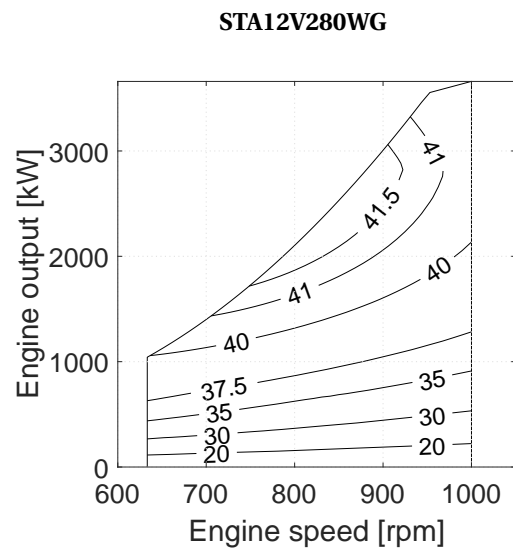
Engine load [%]	$\lambda_{estimate}$ [-]	$\lambda_{DieselB}$ [-]	Deviation [%]
100	2.424	2.425	0.04
75	2.595	2.597	0.08
50	2.807	2.813	0.2
25	3.127	3.16	1

# D

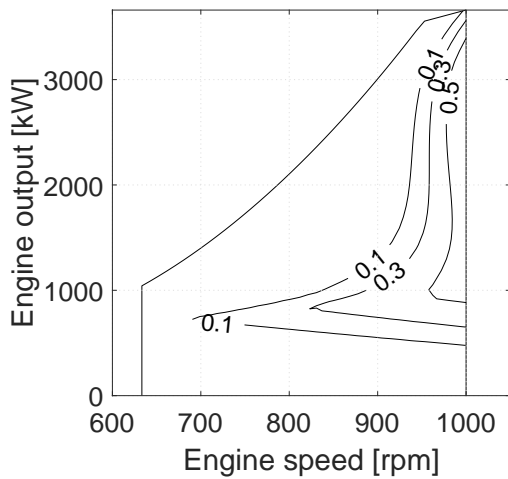
## Figures STA12V280 & STA12V280WG



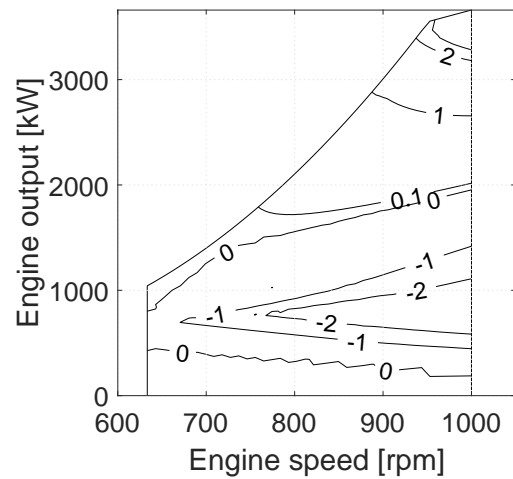
(a) Engine efficiency [%]



(a) Engine efficiency [%]



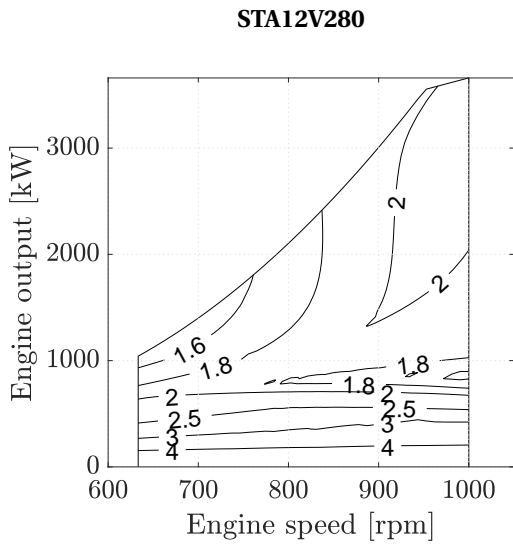
(b) System efficiency increase



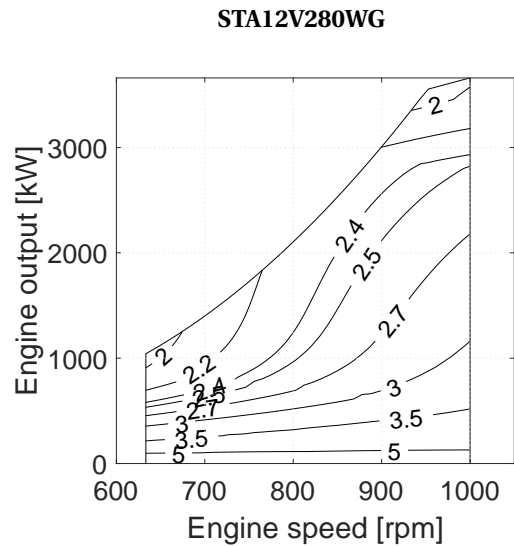
(b) System efficiency increase

Figure D.1: STA12V280 engine efficiency (a) and system efficiency increase with turbocompounding (b)

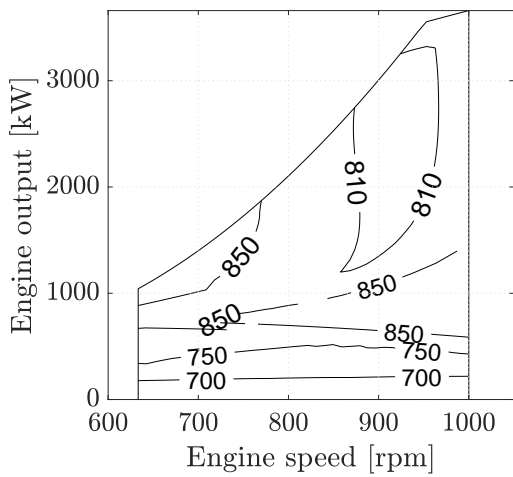
Figure D.2: STA12V280WG engine efficiency (a) and system efficiency increase with turbocompounding (b)



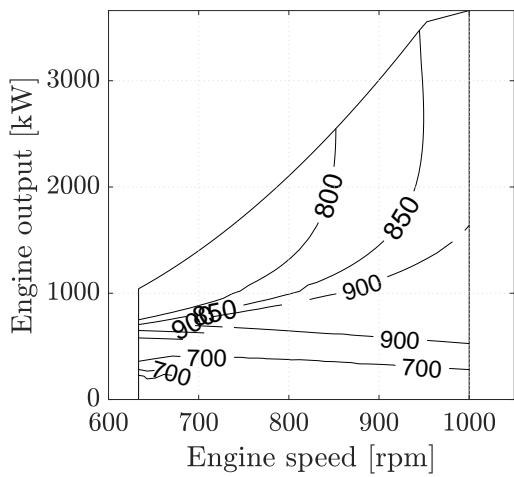
(a) Air excess ratio  $\lambda$  [-]



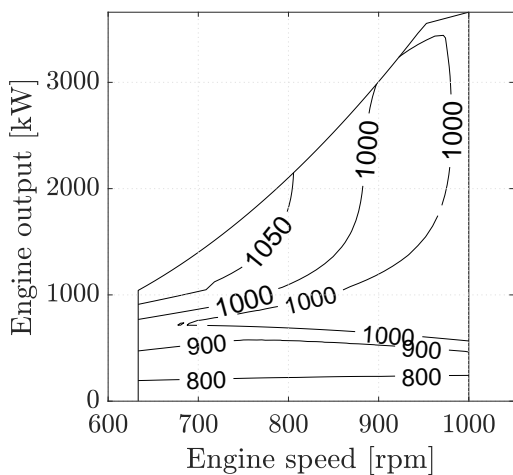
(a) Air excess ratio  $\lambda$  [-]



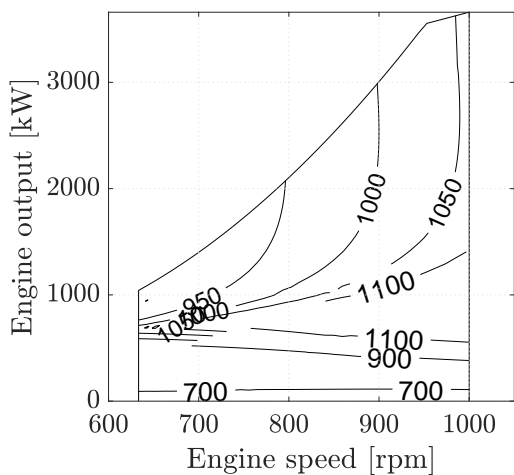
(b) Temperature outlet receiver  $\lambda$  [K]



(b) Temperature outlet receiver  $\lambda$  [K]



(c) Temperature exhaust valve [K]



(c) Temperature exhaust valve [K]

Figure D.3: STA12V280 air excess ratio  $\lambda$  (a), temperature outlet receiver (b) and temperature exhaust valve (c)

Figure D.4: STA12V280WG air excess ratio  $\lambda$  (a), temperature outlet receiver (b) and temperature exhaust valve (c)